NASA Technical Paper 3049

1990

Calibration of the 13- by 13-Inch Adaptive Wall Test Section for the Langley 0.3-Meter Transonic Cryogenic Tunnel

Raymond E. Mineck
and Acquilla S. Hill
Langley Research Center
Hampton, Virginia

National Aeronautics and Space Administration
Office of Management
Scientific and Technical Information Division

Summary

A 13- by 13-in. adaptive solid-wall test section has been installed in the circuit of the Langley 0.3-Meter Transonic Cryogenic Tunnel in place of the 8- by 24-in. slotted-wall test section. This new test section is configured for two-dimensional airfoil testing. The top and bottom walls are flexible and movable, whereas the sidewalls are rigid and fixed. The test section has a turntable to support airfoil models, a survey mechanism to probe the model wake, and provision for a sidewall boundary-layer control system. The wall adaptation strategy employed requires the test section wall shapes associated with uniform test section Mach number distributions. Calibration tests with the test section empty were performed with the top and bottom walls linearly diverged to approach a nearly uniform Mach number distribution. Pressure distributions were measured in the contraction section, the test section, and the high-speed diffuser over a Mach number range from 0.20 to 0.95 and a Reynolds number range from 10×10^6 to 100×10^6 per foot. The fluctuations in the sidewall static pressure measurements are significantly lower in the adaptive solid-wall test section than in the slotted-wall test section used previously.

Introduction

The artificial constraint of wind-tunnel test section walls on the flow field about an airfoil model introduces errors in the simulation of "free air" conditions. Corrections for test section wall interference can be applied to wind-tunnel test data after the test. (See ref. 1.) Test section wall interference can be reduced by using an adaptive wall test section. Adaptive wall test sections have been in use as far back as the 1940's at the National Physical Laboratory in England. (See ref. 2.) Modern adaptive wall test sections were put on a sound technical footing by Sears in reference 3. He demonstrated that wall interference can be eliminated by matching two independent flow field parameters on a control surface. The matching is accomplished in different ways depending on the type of adaptive wall test section. (See ref. 3.) The flow field parameters at the control surface can be modified by varying the wall porosity, the plenum pressure behind a porous wall, or the shape of a solid wall. The NASA Langley 0.3-Meter Transonic Cryogenic Tunnel (0.3-m TCT) uses the adaptive solid-wall test section concept.

The adaptive wall test section design for the 0.3-m TCT is based on work done at the University of Southampton in England. (See ref. 4.) The new test section was installed in the tunnel circuit in 1985 replacing the 8- by 24-in. slotted-wall test section. This report presents a description of the adaptive wall test section, the instrumentation and techniques used during the calibration, and the results from the calibration tests.

Symbols and Abbreviations

A	cross-sectional area, ft^2
BLC	boundary-layer control
D	diameter
GN_2	gaseous nitrogen
H	boundary-layer shape factor
i.d.	inside diameter
LN_2	liquid nitrogen
M_l	local Mach number
M_∞	free-stream Mach number
ΔM	deviation of local Mach number from reference value
o.d.	outside diameter
p_t	stagnation pressure, psi
$\bar{p}$	average static pressure, psi
Δp	root-mean-square deviation of pressure from average static pressure, psi
R	unit Reynolds number per foot
sta.	station measured from center of turntable, positive in streamwise direction
T_t	stagnation temperature, K
TCT	transonic cryogenic tunnel
x	horizontal distance measured from center of turntable, positive downstream, in.
z	vertical distance measured from center of turntable, positive up, in.; or wall displacement, positive outward, in.
δ	average wall divergence angle, positive outward, deg.
δ^*	boundary-layer displacement thickness, in.
θ	orientation of rows of orifices on turntable
σ_M	standard deviation of Mach number from linear curve fit

$\frac{dM_l}{dx}$	longitudinal Mach number gradient, in^{-1}
$\frac{dz}{dx}$	local wall slope

0.3-Meter Transonic Cryogenic Tunnel

The Langley 0.3-Meter Transonic Cryogenic Tunnel (0.3-m TCT) is a fan-driven, cryogenic pressure tunnel that uses gaseous nitrogen (GN_2) as a test gas. It is capable of operating at stagnation temperatures from 327 K (130°F) to about 80 K (-316°F) and at stagnation pressures from 1.2 to 6.0 atm (17.6 to 88.0 psia). The test section Mach number range is from 0.20 to 0.95. From 1976 until 1985, the 0.3-m TCT was frequently used to study airfoil aerodynamic characteristics at high Reynolds numbers. During that time, the tunnel had an 8- by 24-in. test section with slotted top and bottom walls. Details of the development of the 0.3-m TCT and the slotted-wall test section may be found in reference 5.

The adaptive wall test section replaced the 8- by 24-in. slotted-wall test section in 1985. During the installation of the new test section, the tunnel circuit was modified to improve the tunnel operating characteristics. A new contraction section was installed because the adaptive wall test section had a different cross section. A longer high-speed diffuser was installed to reduce flow separation in the diffuser. (See ref. 5.) Figure 1 shows the layout of the tunnel circuit with the 13- by 13-in. adaptive wall test section installed. A photograph of the upper leg of the tunnel circuit is presented in figure 2. Details of the adaptive wall test section, the new contraction section, and the new high-speed diffuser are presented in reference 6. An overview is presented below.

Adaptive Wall Test Section

The layout of the adaptive wall test section with the left sidewall of the plenum removed is presented in figure 3. A photograph of the interior of the plenum is shown in figure 4. All structural components of the test section are aluminum. The test section is configured for two-dimensional airfoil testing with the model supported by two turntables. The angle-of-attack drive system, located outside the plenum, rotates the turntables. A total pressure rake traverses vertically at one of three positions downstream of the model.

Details of the flow region of the test section are presented in figure 5. The test section is 13 in. by 13 in. at the entrance. All four walls are solid. The sidewalls are rigid and fixed with no divergence. The top and bottom walls are flexible and movable. The stainless steel, flexible walls are anchored to the upstream bulkhead of the test section. Each wall is 71.70 in. long. The usable portion of the test section extends from station -29.75 to station 25.05. Eighteen independent jacks control the shape of this portion of each flexible wall. The jack stations for the top and bottom walls, listed in chart A, are the same for both walls. The nonuniform jack spacing provides finer control of the wall shape in the regions above and below the model. The shape of the fully adapted flexible walls depends on the model lift and blockage. A transition region is needed between the end of the usable test section (station 25.05) and the fixed-angle, high-speed diffuser section (station 40.95). (See fig. 5.) The walls are bent outward at the end of the usable test section. With the walls undeflected, the outward bend is 4.1°. This portion of each flexible wall is controlled by three jacks. The downstream end of each flexible wall is held at an angle of 4.1° by a sliding joint. The angle of the joint matches the divergence angle of the first piece of the high-speed diffuser. The jacks are numbered from upstream to downstream. The first jack on the top flexible wall is number 1 and the first jack on the bottom flexible wall is number 22. A static pressure orifice is located at each jack station at the midspan position of each flexible wall. In addition, a static pressure orifice is located in the top and bottom of the opening in the upstream bulkhead of the test section at the midspan position. The static pressure orifice locations for the top and bottom walls in the test section are listed in table 1.

Chart A

Jack	x station, in.	Jack	x station, in.
1, 22	-26.00	11, 32	1.25
2, 23	-20.25	12, 33	2.75
3, 24	-15.25	13, 34	4.75
4, 25	-11.25	14, 35	6.75
5, 26	-8.25	15, 36	8.75
6, 27	-6.25	16, 37	11.75
7, 28	-4.75	17, 38	15.75
8, 29	-3.25	18, 39	20.75
9, 30	-1.75	19, 40	[a]25.75
10, 31	-.25	20, 41	[a]30.75
		21, 42	[a]36.75

[a]Transition between test section and diffuser.

A turntable in each sidewall can support a two-dimensional airfoil model. The center of the

turntable was used as the reference position for determining the distances to the various components in the tunnel. Custom model mounting blocks were used to adapt each airfoil model to the turntables as shown in figure 6. For most of the test section calibration, the model turntables were replaced with solid turntables with static pressure orifices arranged in a horizontal row and in a vertical column as shown in figure 7. These orifice locations are listed in table 1. For these tests, the calibration turntables were fixed with the horizontal row aligned with the flow direction.

Static pressure orifices were installed on the test section sidewall for the calibration and tunnel operations as shown in figure 7. A horizontal row of static pressure orifices was installed along the centerline of the right sidewall. The locations of these orifices are listed in table 1. Columns of static pressure orifices are located on both sidewalls at station –26.75. The orifices are located at ±4.00 and ±2.00 in. from the centerline on the left wall and ±6.00, ±4.00, ±2.00, and 0 in. from the centerline on the right wall. These orifices were used to measure the static pressure for the Mach number calculations during the shakedown tests and to provide a reference for the static pressure instrumentation. The pressures measured from the orifices located at ±6.00 in. were influenced by the flexible wall movement and the flow in the test section corner. Hence, the measurements from these orifices were excluded from the calibration. Three columns of static pressure orifices are located on the right sidewall roughly opposite the three possible tip locations of the wake rake probes at stations 10.75, 15.75, and 20.75. The eight orifices in each column are located at ±4.00, ±3.00, ±2.00, and ±1.00 in. from the centerline.

During part of the calibration, the right model turntable was used instead of the calibration turntable. A 15-tube, boundary-layer total pressure rake was mounted in the model mounting block. A sketch of the rake is presented in figure 8 and a photograph in figure 9. The tip of the rake tubes was located at station –1.25.

The test section photograph in figure 4 shows a rake drive system that translates the wake rake support block. The support block has provisions for mounting a wake rake at one of three stations on the left sidewall (12.50, 17.50, or 22.50) as shown in figure 5. Figures 10 and 11 show details of the wake rake and its installation in the center position. The rake has six total pressure probes and three static pressure probes. This rake was installed at the forward position for some of the calibration tests.

A sidewall boundary-layer control (BLC) system may be used with the adaptive wall test section. The system was retained from the previous 8- by 24-in. slotted-wall test section. Details of the BLC system as used in the previous test section may be found in reference 7. When the BLC system is used, porous plates are installed on the sidewalls upstream of the turntables as shown in figure 5. Each porous plate measures 14 in. by 7 in. and is centered 14.25 in. upstream of the center of the turntable. Ductwork connects the backside of the porous plate to the BLC system. Pressures below the test section static pressure are applied to the nonflow side of the plate to remove all or part of the sidewall boundary layer. The system operates in either an active or passive mode. In the passive mode, the backside of the porous plates is vented to the atmosphere through a flow control valve. The mass removal rate is limited by the difference between the test section static pressure and the atmospheric pressure. In the active mode, a compressor is connected to the backside of the porous plates. The compressor exhaust is injected back into the tunnel circuit downstream of the test section as shown in figures 1 and 2. The mass removal rate is limited by the compressor capability. For these calibration tests, the BLC system was not used and the porous plates were replaced with solid plates. Pressure orifices were installed in the solid plate on the right side to provide additional pressure measurements on the right sidewall as shown in figure 7.

Modified Contraction Section

The contraction section for the adaptive wall test section is split into two components as shown in figures 1 and 12. The first component changes the cross section from a circle to a 16-sided polygon to an 8-sided polygon. The second component changes the 8-sided polygon into a square. The contraction ratio is 10.7:1, based on the nominal 13- by 13-in. cross section of the test section. Eight instrument mounting blocks are available for installing probes to measure total temperature and total pressure at station –105.53. Two total pressure probes, located at about 4 o'clock and 10 o'clock when looking upstream, are manifolded together to provide the total pressure for the Mach number calculations. The probes, made from 0.125-in. o.d. tubing, extend 6.00 in. into the stream from the sidewall and 2.00 in. upstream. Static pressure orifices are installed in the walls of both contraction section components. The measured orifice locations are presented in chart B. The screen section, located upstream of the contraction section, is 48 in. in diameter. It supports three 40-mesh (per

inch) screens made with 0.0065-in-diameter Monel metal wire to reduce the turbulence.

Chart B

x station, in.	x station, in.
−106.2	−76.0
−102.2	−62.4
−98.2	−52.2
−94.7	−48.2
−90.9	−42.1
−87.0	−38.2
−83.2	−34.1
−79.7	

Modified High-Speed Diffuser

The new high-speed diffuser consists of three sections as shown in figure 1. The first section, shown in figure 13, is 24 in. long and changes the cross section from a rectangle to a circle. The design of the section provides a nearly constant cross-sectional area distribution. The second section is 60 in. long with a circular cross section and a divergence angle of 1.2°. The third section is 110.5 in. long with a circular cross section and a divergence angle of 3.0°. The divergence angles in the diffuser were kept small in an effort to prevent flow separation for the expected test conditions. The third section has four ports for reinjection of gaseous nitrogen when the active sidewall boundary-layer control system is in use. The static pressure orifice locations on the high-speed diffuser are listed in chart C.

Chart C

x station, in.	x station, in.
45.4	102.3
49.4	108.3
53.4	114.3
57.4	120.3
61.4	138.4
71.3	156.4
78.2	174.4
84.2	192.4
90.2	210.4
96.2	228.4

Instrumentation

Two types of transducers are used for the pressure measurements to obtain accurate values over the large range of tunnel test pressures. They are quartz Bourdon tube transducers and variable-capacitance transducers. The four quartz transducers measure the total and static pressures for the calculation of the Mach number in the test section and reference pressures for the differential total and static pressure measurements. Since the quartz transducers measure differential pressure, each is referenced to a vacuum to function as an absolute pressure device. The analog output from each of these transducers is converted to digital form by dedicated digital voltmeters.

The variable-capacitance transducers are used for the research measurements. These transducers also measure differential pressure. Each transducer is connected to a reference pressure that is measured by one of the above quartz pressure transducers. An autoranging signal conditioner with seven ranges is dedicated to each transducer. The autoranging capability keeps the analog output signal at a high level even when the transducer is operating at the low end of its range. The analog output signal and the gain from the signal conditioner are converted to digital form by the data acquisition system of the tunnel described in reference 5. During the calibration tests, dedicated variable-capacitance transducers were used for the static pressure measurements on the left and right turntables and the left and right sidewalls. Five variable-capacitance transducers were used with scanning valves to measure the static pressures on the test section top wall, the test section bottom wall, the contraction section, the high-speed diffuser, and the boundary-layer rake.

The tunnel stagnation temperature is measured with a platinum resistance thermometer located at station −105.53. The analog signal from this transducer is converted to digital form by a dedicated digital voltmeter.

Description of Calibration Tests

The calibration tests were divided into two parts. During the first part, test procedures were developed and the boundary-layer measurements on the test section sidewall were recorded. The development of test procedures involved identifying the orifices to be used for the measurement of the free-stream static pressure, the test parameters to be varied, and the type of shape to be used for the top and bottom walls during the calibration. The type of wall shapes that were considered were straight and parallel, straight and linearly diverged, and nonlinear (adapted). During the second part, detailed static

pressure measurements from the test section, the contraction section, and the high-speed diffuser were recorded.

Part 1: Development of Test Procedures

The location in the test section of the free-stream static pressure measurement was chosen using guidelines similar to those used to select the location in a conventional tunnel. The measurement for the free-stream static pressure should not be influenced by the presence of a model or the movement of the flexible walls. Different combinations of static pressure orifices in the test section were evaluated. The pressures from the orifices located on both sidewalls at station −26.75 (see fig. 7) were influenced by the flexible wall movement and did not reflect free-stream conditions. An orifice, located in the top of the opening for the flow in the upstream bulkhead of the test section at station −31.25, was used to measure the free-stream static pressure for all results reported herein.

The test parameters generally used by the research staff of the 0.3-m TCT are normally the Mach number and Reynolds number. The parameters used for tunnel control are the stagnation pressure, stagnation temperature, and fan speed. The calibration was expected to depend primarily on the Mach number and Reynolds number and not on the combination of the stagnation temperature and pressure used to obtain the particular Mach number and Reynolds number. The local Mach number distributions in the contraction section, test section, and high-speed diffuser were measured for a constant unit Reynolds number of 20×10^6 per foot but with different combinations of stagnation temperature and pressure. The results, presented in figure 14 for Mach numbers of 0.50 and 0.75, show that there is no measurable effect of temperature or pressure on the local Mach number distribution. The small differences at the beginning of the contraction section are probably due to small errors in the measured static pressures leading to large errors in the very low local Mach number. The differences are not attributable to the temperature or pressure but to the scatter associated with measurement noise. Since the calibration measurements depend primarily on the Mach number and Reynolds number, these variables were selected as the test parameters for the calibration.

The wall adaptation software was based on the software developed at the University of Southampton in England and reported in reference 8. The software uses the wall shape that produces a uniform Mach number distribution for its initialization. A library of wall shapes for different free-stream Mach numbers and Reynolds numbers is required. Three different types of wall shapes were evaluated: straight and parallel, straight and linearly diverged, and nonlinear (adapted). Typical results for these three types are presented in figure 15 at a Mach number of 0.70 and a unit Reynolds number of 10×10^6 per foot. The boundary-layer buildup on the test section walls leads to a longitudinal Mach number gradient along the test section. Results for the walls set to 0-in. displacement (straight, parallel walls) clearly show the gradient (fig. 15(a)). The wake rake was installed in the forward position (station 12.50) when these measurements were taken. This explains the sudden increase in the local Mach number near that station. The right sidewall Mach number generally increases smoothly. The sidewalls are thick and rigid and have a flat, smooth surface. A smooth increase in the Mach number would be expected.

The Mach numbers along the top and bottom walls tend to have a lot of scatter. The top and bottom walls are thin and flexible. The surface is smooth, but problems with the current wall-attachment system can lead to a wavy surface. In the current arrangement, plates are bolted between the wall-movement drive rods and the backside of the flexible wall. Small misalignments between the drive rods and the wall attachment can lead to large moments at the wall attachment. The moment generated at each wall-attachment location results in an "S" shape or waves in the wall displacement between the jacks. Additional details are presented in reference 6. Waves in the wall can lead to scatter in the measured pressure and the calculated Mach number distributions on the flexible walls. Problems associated with the installation of the orifices in the thin wall or unsteadiness in the flow coupled with the asynchronous measurements from the scanning valves can also be a cause of the scatter. A sufficiently long settling time was used after stepping to each port to eliminate insufficient dwell time as the cause of the scatter.

The first solution to improve the longitudinal Mach number distribution was to diverge the top and bottom walls linearly. The divergence required to eliminate the gradient was estimated from calculations of the growth of the displacement thickness of a turbulent boundary layer at selected Mach numbers and unit Reynolds numbers. Results with the walls linearly diverged are shown in figure 15(b). Note that positive wall displacement has been defined as positive outward to compare the top and bottom wall displacements directly. The variation of the local Mach number from the free-stream Mach number is much smaller for the linearly diverged walls in figure 15(b) than for the parallel walls in figure 15(a). As before, the scatter in the local Mach number for the sidewalls is less than that for the top and bottom walls, and

the Mach number deviation increases sharply near the wake rake. During research operations, the wall adaptation algorithm would adapt for the wake rake blockage at whatever position it was installed. The detailed calibration pressure measurements should be obtained with the wake rake removed.

The next solution to improve the Mach number distribution was to allow the wall adaptation algorithm to determine the flexible wall shape. Only one iteration of the algorithm was used. This led to the partially adapted results of figure 15(c). Note that the wall displacement is not monotonically increasing and that there is still some scatter in the Mach number distribution. Near the wake rake, the Mach number deviation on the top and bottom walls is much smaller after one iteration of the adaptation algorithm. The wall shapes that correspond to a uniform Mach number distribution at various Mach numbers and Reynolds numbers are used as initial conditions by the wall adaptation algorithm when a model is present. The wall shape that corresponds to a uniform Mach number distribution is defined as an "aerodynamically straight wall." The adaptation process computes a curved wall shape to eliminate the lift and blockage interference from whatever is present in the test section. The required wall shape that must be set by the jacks is the sum of the aerodynamically straight wall shape and curved wall shape from the adaptation process.

Shakedown tests with an airfoil model initially used the partially adapted results as the aerodynamically straight wall shape. For many moderate test conditions, the required wall shapes could not be achieved because the load required to position the wall exceeded the capability of the wall positioning hardware. The linearly diverging walls, such as those shown in figure 15(b), were then used as the aerodynamically straight wall shape during additional shakedown tests. These subsequent tests demonstrated that the linearly diverging shapes allow testing with a model. The linearly diverging wall shapes were selected for use in the calibration.

The boundary-layer characteristics on the test section sidewall at the model are needed to correct airfoil results for sidewall interference. A boundary-layer rake was installed just downstream of the center of the right turntable. The boundary-layer thickness exceeded the rake height for some of the test conditions. A technique, described in reference 9, was developed to extrapolate the rake measurements to the free stream and to compute the desired boundary-layer characteristics.

Part 2: Calibration Pressure Measurements

The second part of the calibration tests determined the test section Mach number distribution using the linearly diverged walls. The linear divergence was selected by the adaptive wall test section operator before acquiring the test section calibration data. The selected wall divergence generally increased with Mach number and unit Reynolds number. The tests were conducted at six unit Reynolds numbers per foot: 10×10^6, 20×10^6, 40×10^6, 60×10^6, 80×10^6, and 100×10^6. At each unit Reynolds number, the Mach number was varied from 0.20 to 0.95. Some of the Mach numbers could not be achieved because they were outside the tunnel operating envelope. The wake rake was removed from the test section for these tests.

The tunnel can operate at high pressure and low temperature where the test gas behavior measurably departs from that of an ideal gas. Therefore, all results presented herein have been corrected for the real gas effects using the procedure of reference 10.

Presentation of Results

The wall static pressure measurements are presented as plots of the local Mach number distribution as a function of the longitudinal position for the streamwise rows of orifices in figures 16 to 19 and as a function of vertical position for the vertical columns of orifices in figure 19. Detailed plots of the test section wall shape and the Mach number deviation from the free-stream value are also presented for each combination of Mach number and Reynolds number tested in figures 20 to 25. An index to the results is presented in the following table:

Results and Discussion

Mach Number Distributions on Top and Bottom Walls

The longitudinal Mach number distributions on the centerline of the flexible walls are presented in figure 16 for the top wall and in figure 17 for the bottom wall. The walls were linearly diverged and the wake rake was removed. The average wall divergence angle δ was set as a function of both the Mach number and the Reynolds number. The measured wall divergence is listed in table 2. For Mach numbers of 0.70 and below, the local Mach number distribution is relatively flat up to the location of the 4.1° bend in the walls. There is a small gradient and scatter in the Mach number, both of which increase with Mach number. At a Mach number of 0.95 and $R = 20 \times 10^6$ per foot, the wall divergence was not sufficient to prevent a rapid increase in the Mach number that was terminated by a shock in the front part of the test section. Increasing the divergence at $R = 60 \times 10^6$ per foot reduced the Mach number gradient and eliminated the shock.

At the higher Mach numbers (generally 0.75 and above), there are noticeable oscillations in the longitudinal Mach number distribution. These oscillations occur near stations –8.00 and 19.25 where the thickness of the flexible walls changes. They appear at all the Reynolds numbers and become more severe as the Mach number increases. Since most airfoil testing occurs at or below a Mach number of 0.80, the oscillations in the Mach number distribution should not significantly impact airfoil tests.

The local Mach number decreases over the rear part of the test section. The flexible walls bend outward 4.1° at station 25.05. Three jacks set the wall contour between the bend and the end of each flexible wall. These three jacks were set to reduce the wall deflection linearly to 0 at the end of the flexible wall. The flow area increases with downstream distance although there is an increase in the local wall curvature near the bend. The local Mach number just downstream of the bend at station 25.75 is higher than the Mach number measured just upstream. As the flow accelerates around the bend, the local Mach number increases. The outward displacement of the first jack in this diverging section should be adjusted to eliminate the increase in the Mach number.

Mach Number Distributions on Sidewall and Turntable

The longitudinal Mach number distributions on the right sidewall and turntable are presented in figure 18. Unlike the top and bottom wall results, the sidewall results have a smaller longitudinal gradient and much less scatter. The sign and size of the gradient were determined by the linear divergence. The small gradient in the Mach number can be eliminated by adjusting the linear divergence of the top and bottom walls.

The local Mach number distributions along the horizontal and vertical rows of orifices on the left turntable are presented in figure 19. The measurements on the left and right turntables were selected for further analysis since they are not affected by the surface waviness problems associated with the top and bottom flexible walls. A linear least-squares curve fit was applied to the local Mach number distributions on the left and right turntables. From the curve fit, the longitudinal Mach number gradient dM_l/dx and the standard deviation of the results from the curve fit σ_M were determined. The standard deviation was computed using the difference from the linear curve fit rather than the mean because the gradient could be eliminated by the proper selection of the divergence of the top and bottom walls.

The results of the curve fit are presented in table 2 along with the wall divergence for each Mach number and Reynolds number. The longitudinal gradient and scatter in the Mach number are larger on the left turntable than on the right turntable. The distribution in the vertical direction is flat with similar scatter. The standard deviation of the Mach number on the left wall is almost always higher than that on the right wall. For Mach numbers less than or equal to 0.80, the largest average of the standard deviations of the Mach number on the two turntables is 0.0021. The standard deviation is smallest at a Mach number of about 0.50 and increases rapidly for Mach numbers above 0.80. There are small longitudinal gradients in the Mach number. Using the average of the Mach number gradients, the change in Mach number along an airfoil model with a 10-in. chord is less than 0.0036 for Mach numbers less than or equal to 0.80. Thus, the flow field in the model region, as measured on the left and right turntables, has small longitudinal gradients and small standard deviations in the local Mach number. These levels will not limit airfoil testing at Mach numbers up to 0.80. The longitudinal gradient should be reduced by adjusting the top and bottom wall divergence. These refined shapes would be used by the wall adaptation process to set the wall shape for tests with models and to define more accurately the reference wall shape needed to compute any residual top and bottom wall interference.

Test Section Wall Shape and Mach Number Distribution

The longitudinal Mach number distribution in the test section is dependent on the shape of the top and

bottom flexible walls. The flexible wall shape and the deviation of the local Mach number from the free-stream Mach number are presented in figures 20 to 25. The wake rake was removed for these tests. As noted above, the deviation of the sidewall Mach numbers is smaller and has less scatter than the top and bottom walls. The scatter increases dramatically for the Mach numbers above 0.80. Any gradients remaining can be eliminated by changing the linear divergence of the walls slightly.

Mach Number Distributions in Contraction Section

The longitudinal Mach number distributions on the wall of the contraction section are presented in figure 26. In general, the Mach number smoothly increases through the contraction with a small overshoot at station −38.20. There is some scatter at the beginning of the contraction section where small errors in the measured pressure lead to large errors in the Mach number. It should be noted that the desired Mach number is reached near station −38.20 providing a run of about 7 in. at a constant Mach number before the flexible walls are reached.

Mach Number Distributions in High-Speed Diffuser

The longitudinal Mach number distributions on the wall of the three sections of the high-speed diffuser are presented in figure 27. The rear portion of the flexible wall in the test section (from station 25.05 to station 40.95) diverges outward 4.1° so that the cross-sectional area at the end of the test section (station 40.95) is larger than the area at the end of the contraction section where the free-stream Mach number is measured. The local Mach number decreases downstream of the 4.1° bend. Thus, the local Mach number at the entrance to the high-speed diffuser is less than the free-stream Mach number. The largest measured local Mach number on the wall of the first diffuser section occurs at station 61.40 where the computed cross-sectional area (shown in fig. 13) is minimum. At the higher Mach numbers, there is a significant decrease in the local Mach number near station 50.00. The local Mach number distributions in the second and third sections of the diffuser show a smooth decrease in the local Mach number with no indication of separation.

Boundary-Layer Characteristics on Test Section Sidewall

The test section boundary-layer characteristics were determined from the total pressure measurements obtained from the rake mounted to the right turntable. The method of reference 9 was used to compute the boundary-layer displacement thickness and the shape factor, and the results are presented in figures 28(a) and 28(b). The boundary-layer displacement thickness increases with the Mach number and generally decreases with the Reynolds number. The shape factor also increases with the Mach number, but the decrease with Reynolds number is very small.

Fluctuating Pressure Distribution on Test Section Sidewall

After the tunnel calibration was complete, William B. Igoe of the NASA Langley Research Center took fluctuating pressure measurements on the sidewall. These measurements, which were taken as part of the requirements for a proposed doctoral dissertation to be submitted to the George Washington University, are presented in figure 29. These results are compared with similar measurements from the 8- by 24-in. test section that were reported in reference 11. The fluctuating pressures have been reduced to about one-half the level found in the 8- by 24-in. slotted-wall test section.

Concluding Remarks

An adaptive wall test section has been installed in the circuit of the Langley 0.3-Meter Transonic Cryogenic Tunnel. The flexible wall shape and the longitudinal Mach number distribution have been measured on the test section walls at Mach numbers from 0.20 to 0.95 and Reynolds numbers from 10×10^6 to 100×10^6 per foot. Linearly diverging the test section walls reduced the longitudinal gradient in the Mach number. The local Mach number on the flexible top and bottom walls showed a larger gradient and more scatter than on the sidewalls. The new high-speed diffuser shows no signs of separation in that part of the circuit. The sidewall fluctuating pressure has been reduced to about one-half the level measured in the previous 8- by 24-in. slotted-wall test section.

NASA Langley Research Center
Hampton, VA 23665-5225
September 28, 1990

References

1. Mokry, M.; Chan, Y. Y.; and Jones, D. J.: *Two-Dimensional Wind Tunnel Wall Interference.* AGARD-AG-281, Nov. 1983.
2. *Fluid Dynamics Panel Working Group 12 on Adaptive Wind Tunnel Walls: Technology & Applications.* AGARD-AR-269, Apr. 1990.
3. Sears, W. R.: Self-Correcting Wind Tunnels. *Aeronaut. J.*, vol. 78, no. 758/759, Feb./Mar. 1974, pp. 80–89.

4. Wolf, S. W. D.: *Self Streamlining Wind Tunnel - Further Low Speed Testing and Final Design Studies for the Transonic Facility.* NASA CR-158900, 1978.
5. Ladson, Charles L.; and Ray, Edward J.: *Evolution, Calibration, and Operational Characteristics of the Two-Dimensional Test Section of the Langley 0.3-Meter Transonic Cryogenic Tunnel.* NASA TP-2749, 1987.
6. Mineck, Raymond E.: *Hardware and Operating Features of the Adaptive Wall Test Section for the Langley 0.3-Meter Transonic Cryogenic Tunnel.* NASA TM-4114, 1989.
7. Johnson, Charles B.; Murthy, A. V.; and Ray, Edward J.: *A Description of the Active and Passive Sidewall-Boundary-Layer Removal Systems of the 0.3-Meter Transonic Cryogenic Tunnel.* NASA TM-87764, 1986.
8. Wolf, Stephen W. D.; and Goodyer, Michael J.: *Predictive Wall Adjustment Strategy for Two-Dimensional Flexible Walled Adaptive Wind Tunnel - A Detailed Description of the First One-Step Method.* NASA CR-181635, 1988.
9. Murthy, A. V.: *Calculation of Sidewall Boundary-Layer Parameters From Rake Measurements for the Langley 0.3-Meter Transonic Cryogenic Tunnel.* NASA CR-178241, 1987.
10. Adcock, Jerry B.: *Real-Gas Effects Associated With One-Dimensional Transonic Flow of Cryogenic Nitrogen.* NASA TN D-8274, 1976.
11. Johnson, C. B.; Johnson, W. G., Jr.; and Stainback, P. C.: *A Summary of Reynolds Number Effects on Some Recent Tests in the Langley 0.3-Meter Transonic Cryogenic Tunnel.* SAE Tech. Paper Ser. 861765, Oct. 1986.

Table 1. Static Pressure Orifice Locations in Test Section

(a) Top and bottom wall

x station (on centerline), in.
−31.25
−26.00
−20.25
−15.25
−11.25
−8.25
−6.25
−4.75
−3.25
−1.75
−0.25
1.25
2.75
4.75
6.75
8.75
11.75
15.75
20.75
25.75
30.75
36.75

(b) Right sidewall (horizontal row)

x station, in.	z station, in.
−26.75	0
−24.75	↓
−22.75	
−20.75	
−17.25	
−15.25	
−13.25	
−11.25	
10.45	
12.45	
14.45	
16.45	
18.45	
20.45	
22.45	
24.45	

(c) Turntable

x station, in.	z station, in.
Horizontal row	
−7.00	0
−6.00	↓
−5.00	
−4.00	
−3.00	
−2.00	
−1.00	
0.00	
1.00	
2.00	
3.00	
4.00	
5.00	
6.00	
7.00	
Vertical column	
0	6.00
↓	5.00
	4.00
	3.00
	2.00
	1.00
	−1.00
	−2.00
	−3.00
	−4.00
	−5.00
	−6.00

(d) Right sidewall (vertical columns)

x station, in.	z station, in.
Downstream of test section entrance	
−26.75	6.00
↓	4.00
	2.00
	−2.00
	−4.00
	−6.00
Opposite rake front position	
10.75	4.00
↓	3.00
	2.00
	1.00
	−1.00
	−2.00
	−3.00
	−4.00
Opposite rake center position	
15.75	4.00
↓	3.00
	2.00
	1.00
	−1.00
	−2.00
	−3.00
	−4.00
Opposite rake aft position	
20.75	4.00
↓	3.00
	2.00
	1.00
	−1.00
	−2.00
	−3.00
	−4.00

Table 2. Mach Number Gradient and Standard Deviation

$R \times 10^{-6}$, ft^{-1}	M_∞	$\sigma_M \times 10^3$		$\frac{dM_l}{dx} \times 10^3$, in^{-1}		$\frac{dz}{dx} \times 10^3$		δ, deg
		Right	Left	Right	Left	Top	Bottom	Top
10	0.201	1.46	2.10	−0.046	0.348	0.81	0.82	0.05
20	0.201	1.49	2.32	−0.053	0.355	0.98	0.95	0.06
↓	.500	.95	1.48	.075	.267	1.88	1.82	.11
	.600	1.04	1.57	.194	.350	1.84	1.80	.11
	.701	1.41	1.70	.333	.475	1.83	1.83	.10
	.751	1.43	1.82	.182	.325	2.73	2.71	.16
	.802	1.55	1.94	.301	.420	2.71	2.70	.16
	.799	1.56	1.94	.266	.392	2.80	2.83	.16
	.851	1.68	2.05	.006	.118	3.57	3.61	.20
	.900	2.39	2.41	.129	.233	3.48	3.55	.20
	.946	3.49	3.25	.189	.258	3.48	3.57	.20
40	0.500	0.99	1.47	0.075	0.277	1.89	1.84	0.11
↓	.601	1.06	1.59	.130	.284	2.09	2.00	.12
	.700	1.40	1.80	.178	.305	1.94	1.95	.11
	.750	1.54	2.10	.125	.320	2.72	2.68	.16
	.803	1.70	2.27	.252	.440	2.64	2.61	.15
	.850	1.78	2.33	−.170	.020	3.61	3.64	.21
	.901	1.83	2.86	−.216	.007	3.55	3.59	.20
60	0.503	1.01	1.66	0.078	0.289	1.84	1.92	0.11
↓	.598	1.15	1.81	.130	.302	1.88	1.79	.11
	.702	1.56	2.04	.126	.292	2.08	2.13	.12
	.750	1.63	2.13	.084	.293	2.63	2.69	.15
	.801	1.83	2.34	.180	.396	2.58	2.66	.15
	.853	1.98	2.44	−.114	.117	3.63	3.55	.21
	.902	2.46	2.64	−.173	.088	3.63	3.56	.21
	.955	2.90	2.99	−.154	.087	3.62	3.61	.21
80	0.501	1.04	1.80	0.090	0.302	1.93	1.92	0.11
↓	.601	1.29	1.92	.133	.320	2.09	1.99	.12
	.705	1.73	2.13	.154	.335	1.96	1.98	.11
	.750	1.54	2.34	.007	.230	2.59	2.57	.15
	.800	1.74	2.46	.040	.270	2.61	2.64	.15
	.851	2.25	2.53	−.244	−.010	3.60	3.54	.21
	.902	2.43	2.82	−.347	−.092	3.59	3.55	.21
100	0.702	1.65	2.09	−0.034	0.180	1.88	1.82	0.11
↓	.753	1.48	2.40	−.156	.074	2.67	2.73	.15
	.803	1.57	2.51	−.167	.051	2.69	2.75	.15
	.852	1.75	2.70	−.518	−.314	3.57	3.62	.20
	.902	2.07	2.82	−.702	−.527	3.24	3.61	.20

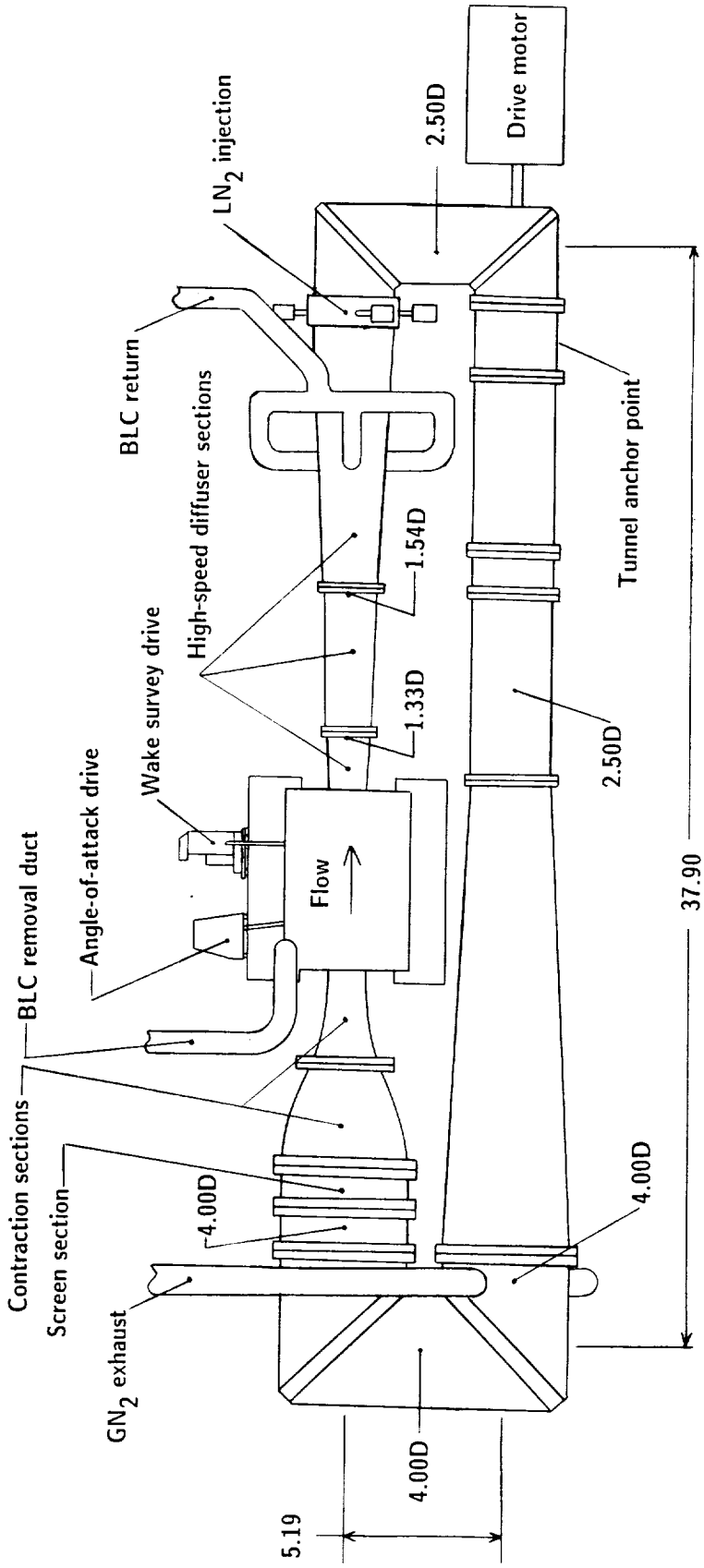

Figure 1. Sketch of the 0.3-m TCT with 13- by 13-in. adaptive wall test section. All dimensions are given in feet.

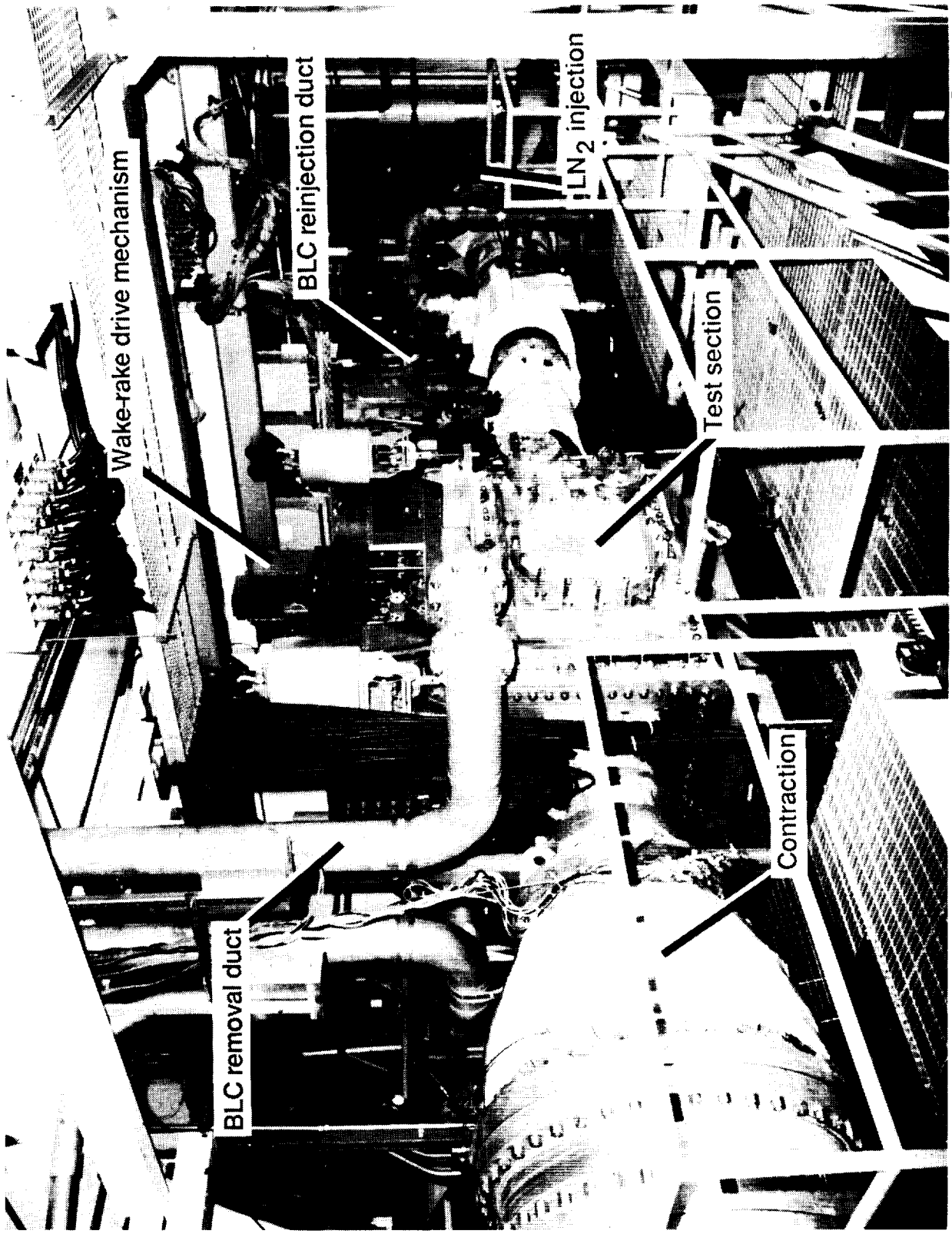

Figure 2. Upper leg of the Langley 0.3-Meter Transonic Cryogenic Tunnel with 13- by 13-in. adaptive wall test section.

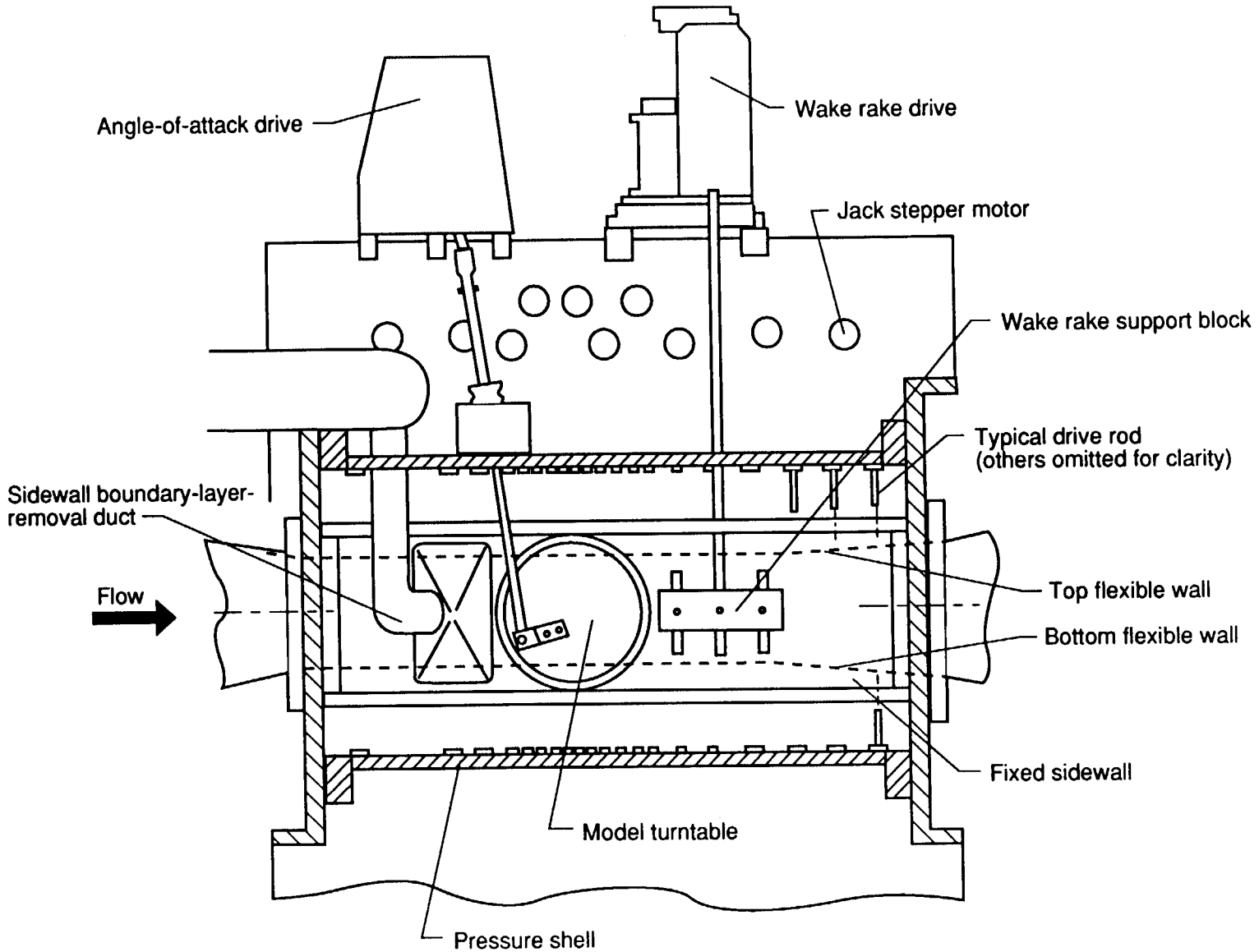

Figure 3. Layout of 13- by 13-in. adaptive wall test section with plenum sidewall removed.

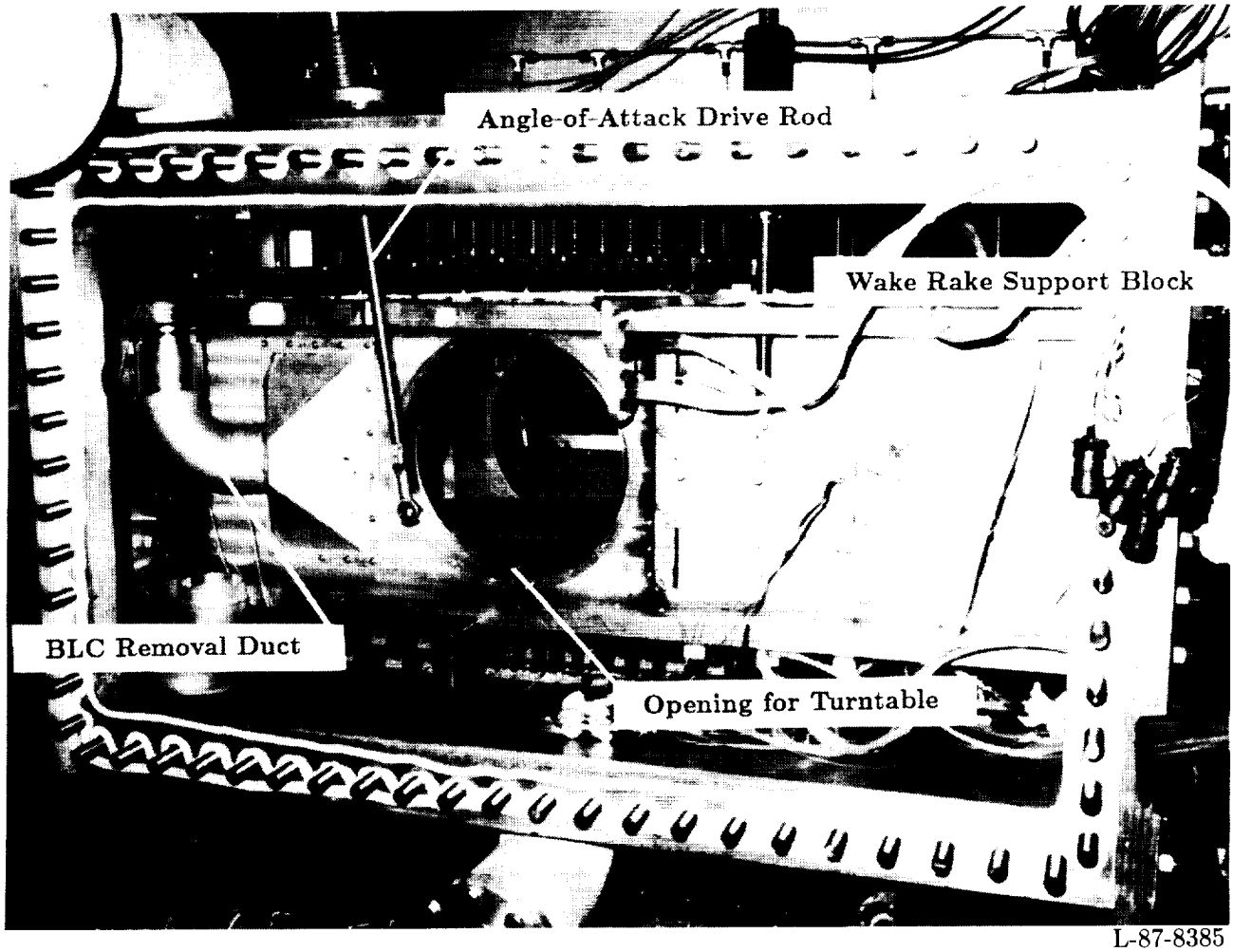

Figure 4. Photograph of flow region of adaptive wall test section with plenum sidewall removed.

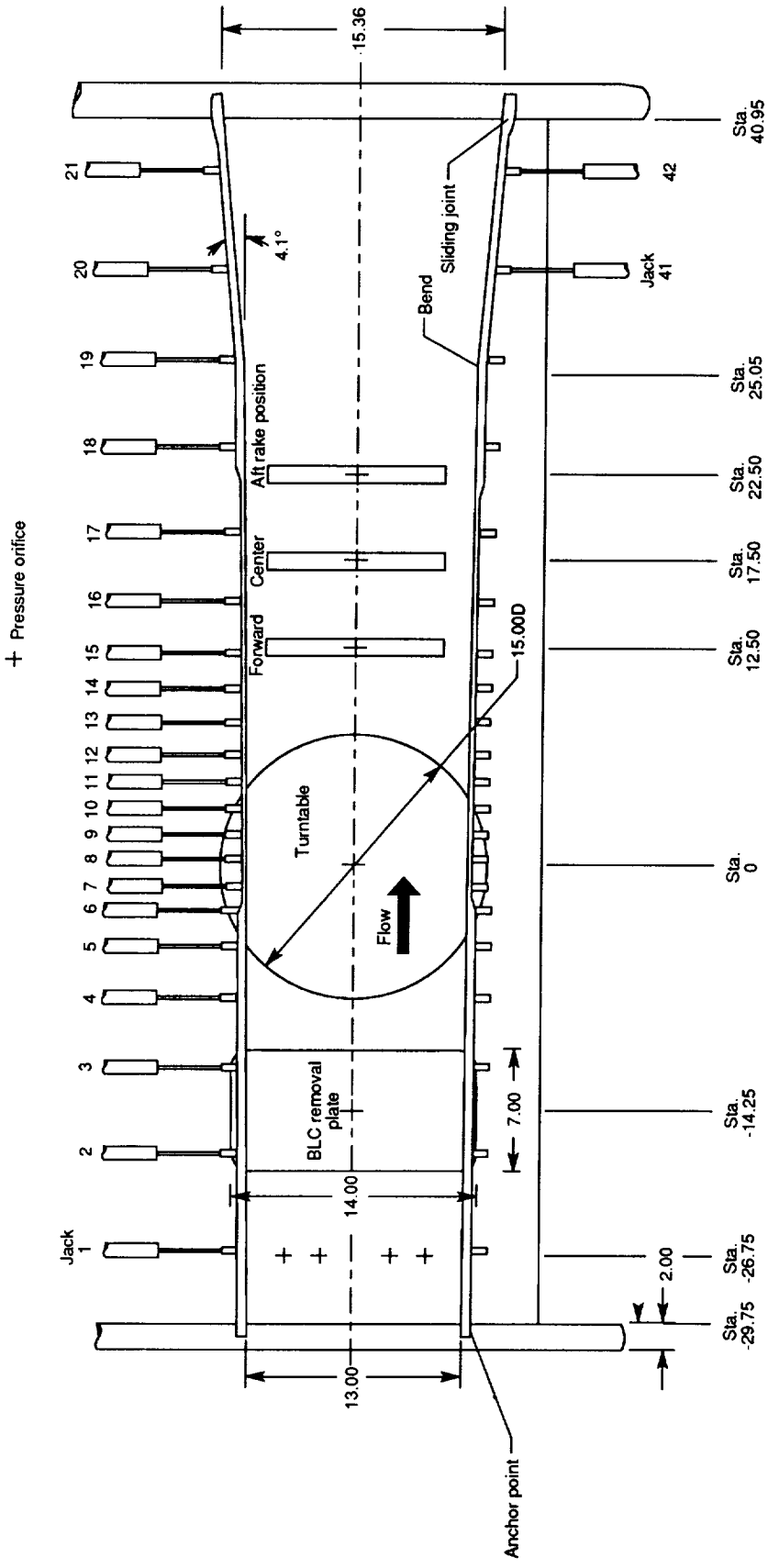

Figure 5. Details of flow region of 13- by 13-in. adaptive wall test section. All dimensions are given in inches. (Note that some lower wall jacks are omitted for clarity.)

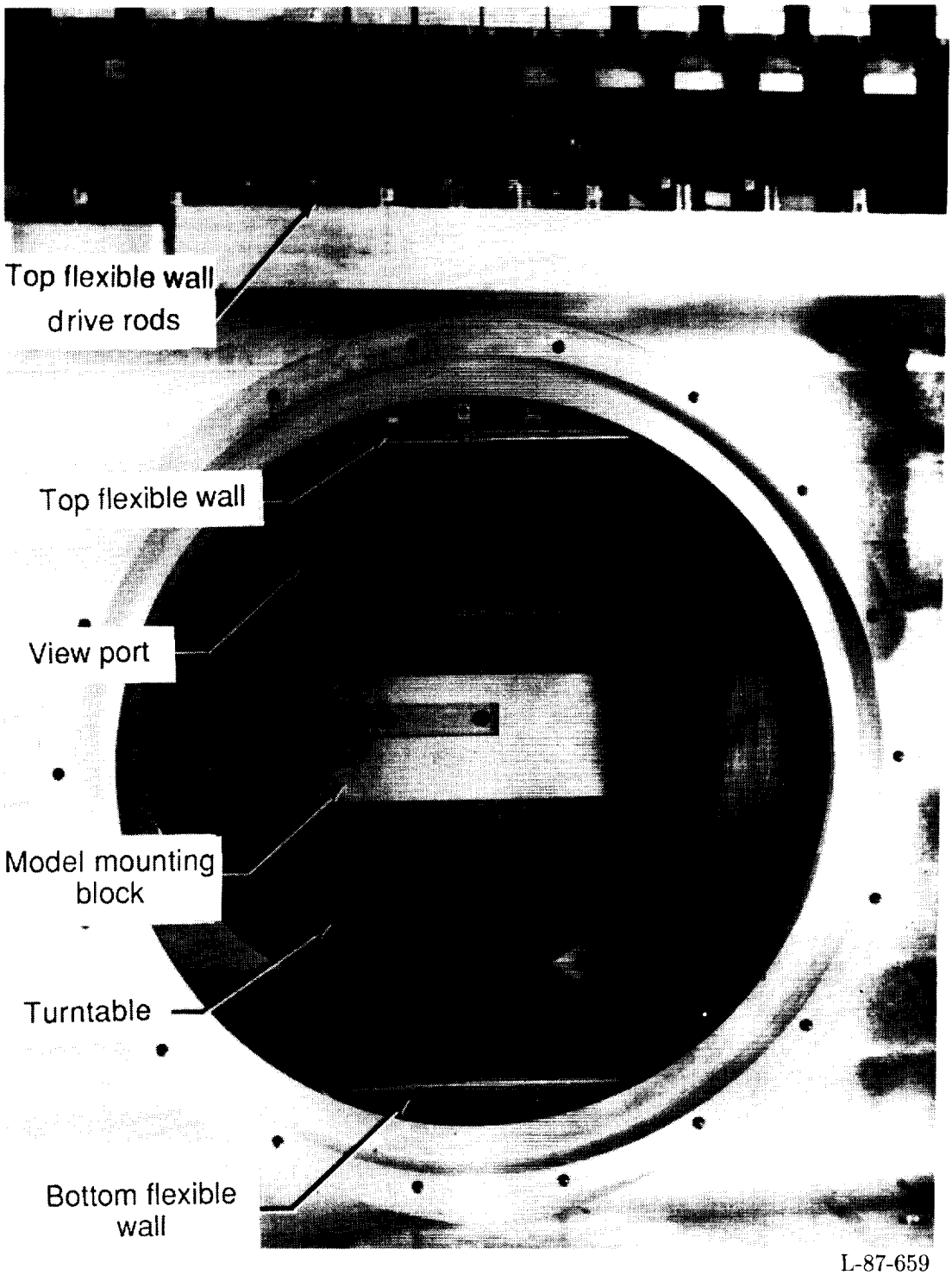

L-87-659

Figure 6. Photograph of region where model is installed.

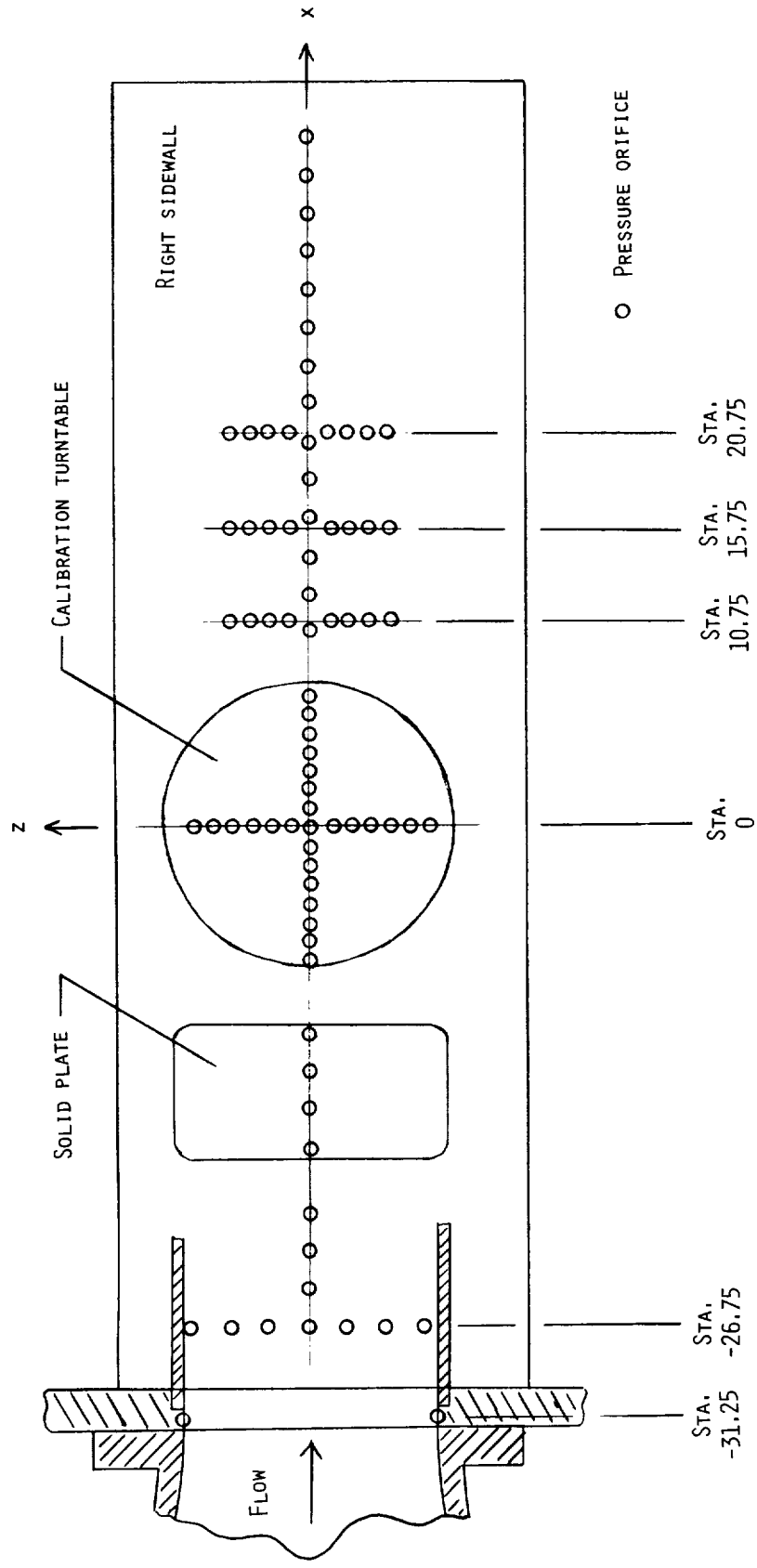

Figure 7. Static pressure orifice locations in test section. All dimensions are given in inches.

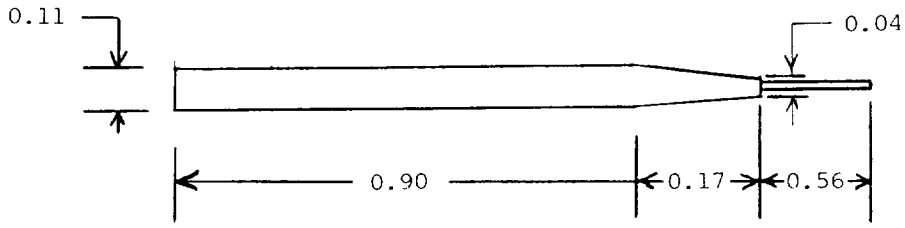

(a) Side view.

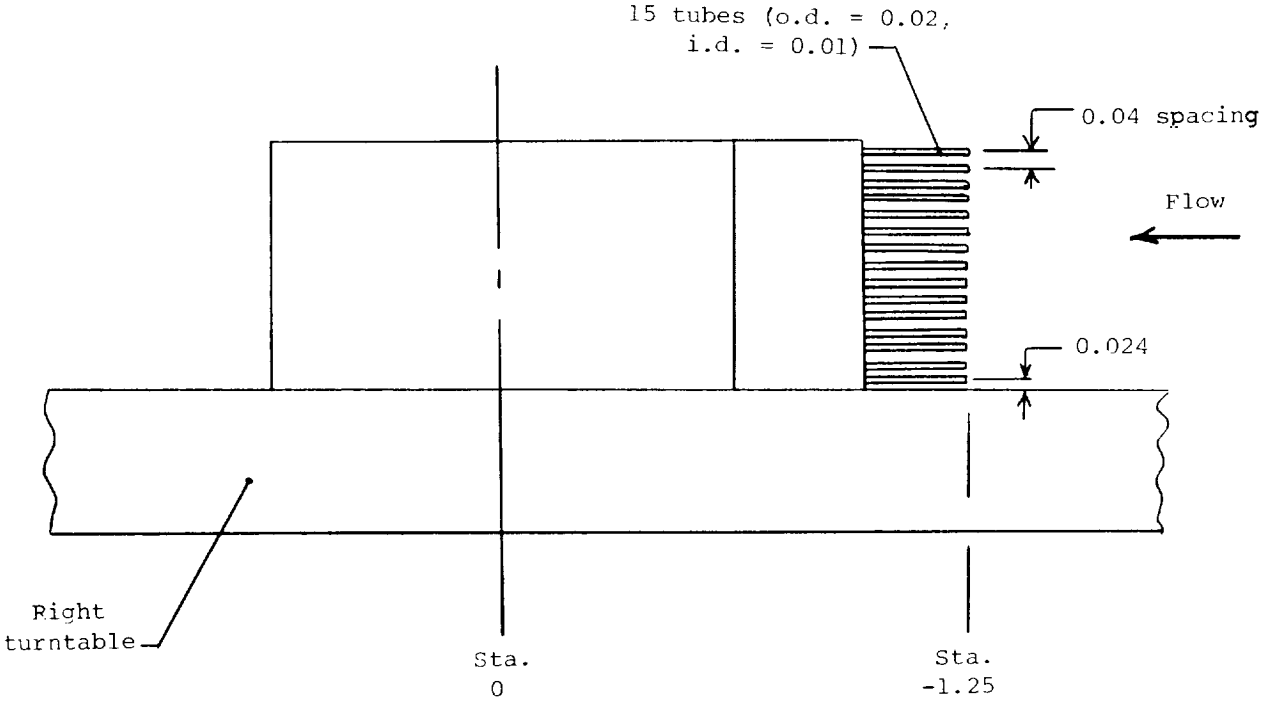

(b) Top view.

Figure 8. Sketches of boundary-layer total pressure rake. All dimensions are given in inches.

L-82-8981

Figure 9. Photograph of boundary-layer total pressure rake.

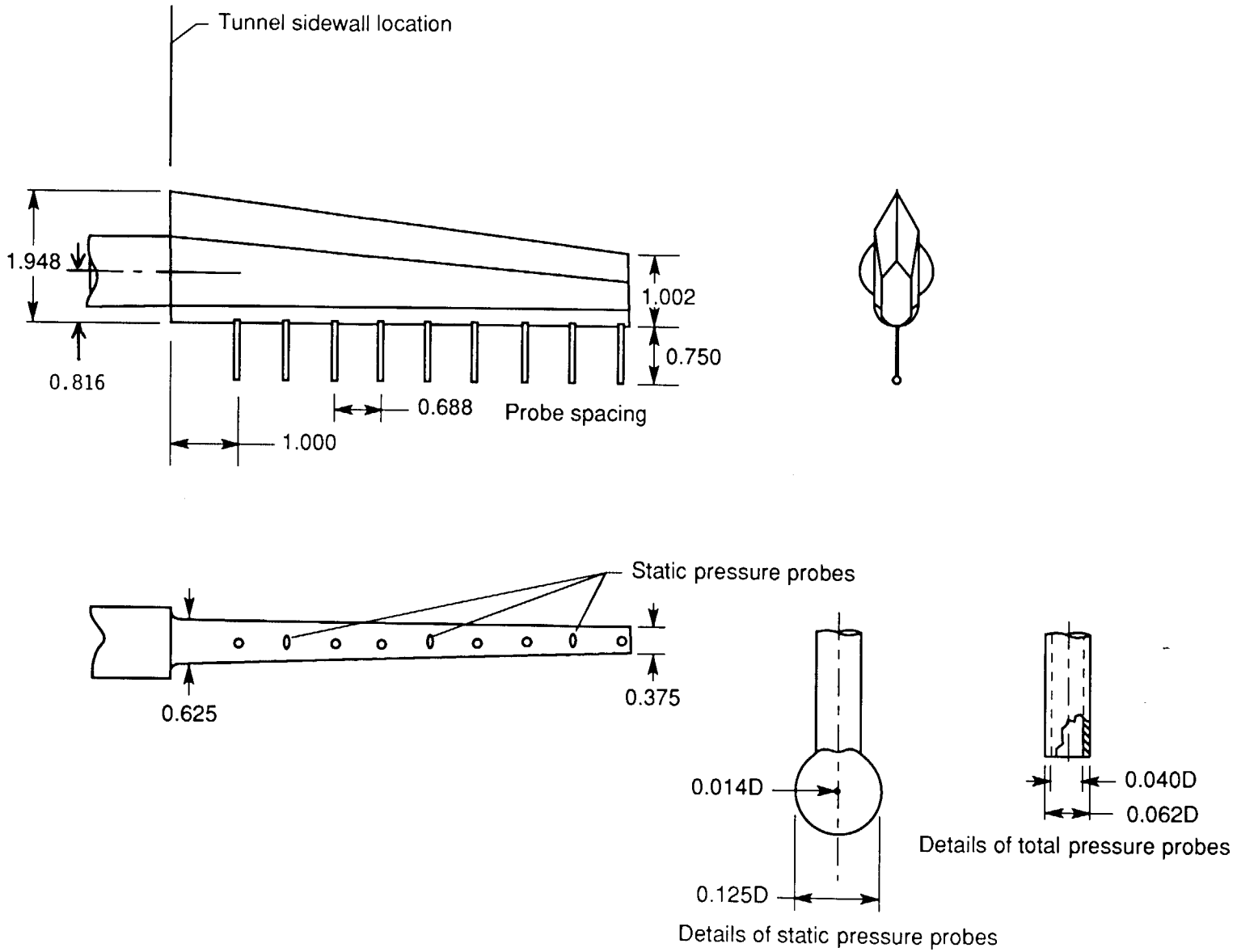

Figure 10. Sketch of wake survey probe. All dimensions are given in inches.

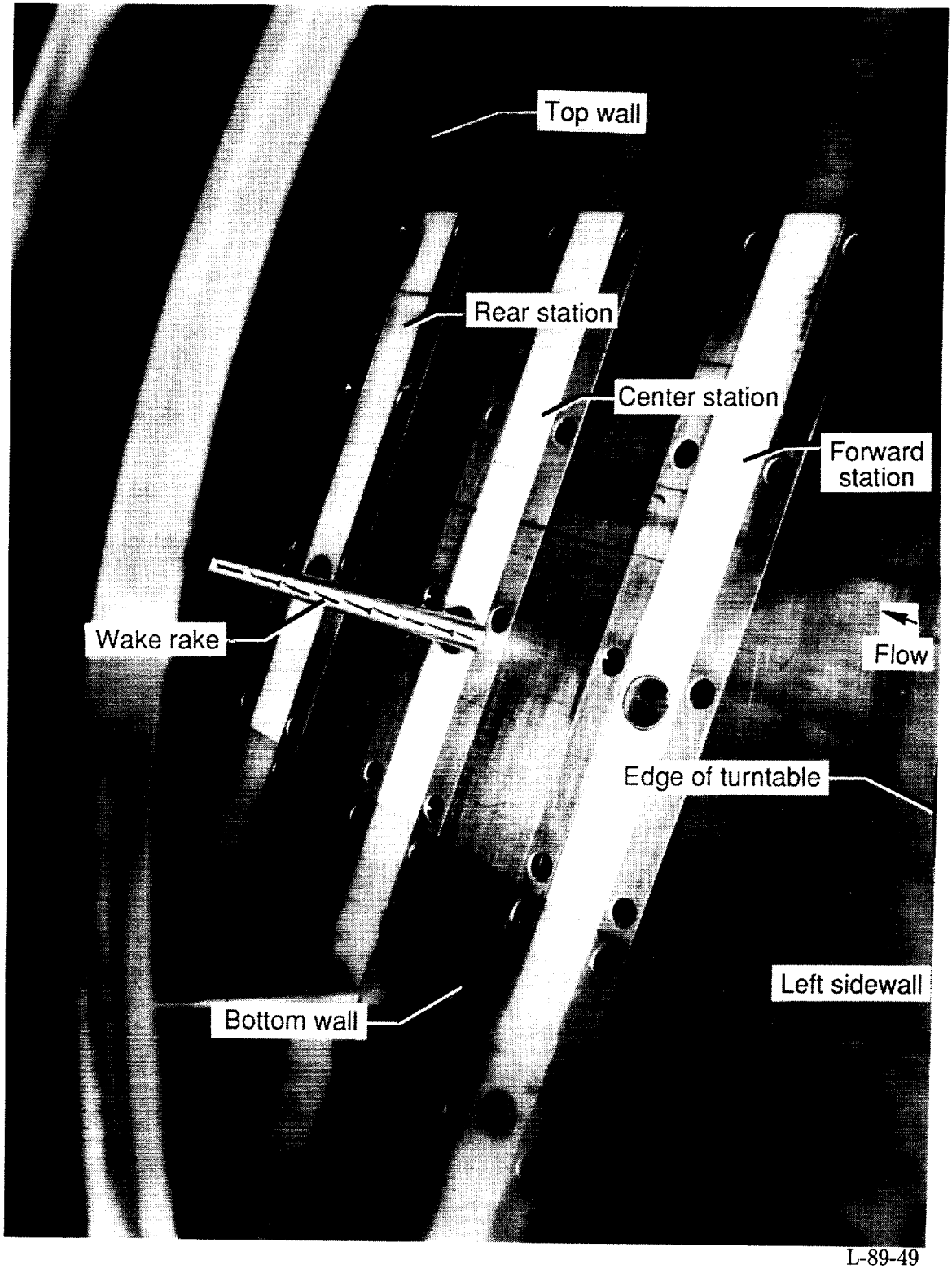

L-89-49

Figure 11. Photograph of wake survey probe mounted in center survey station.

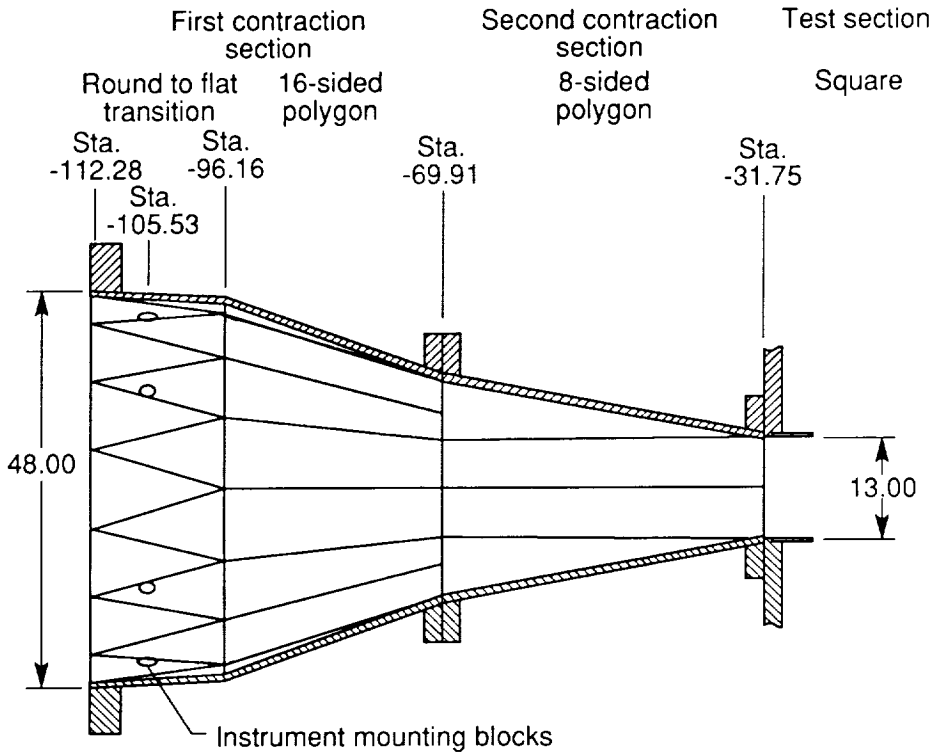

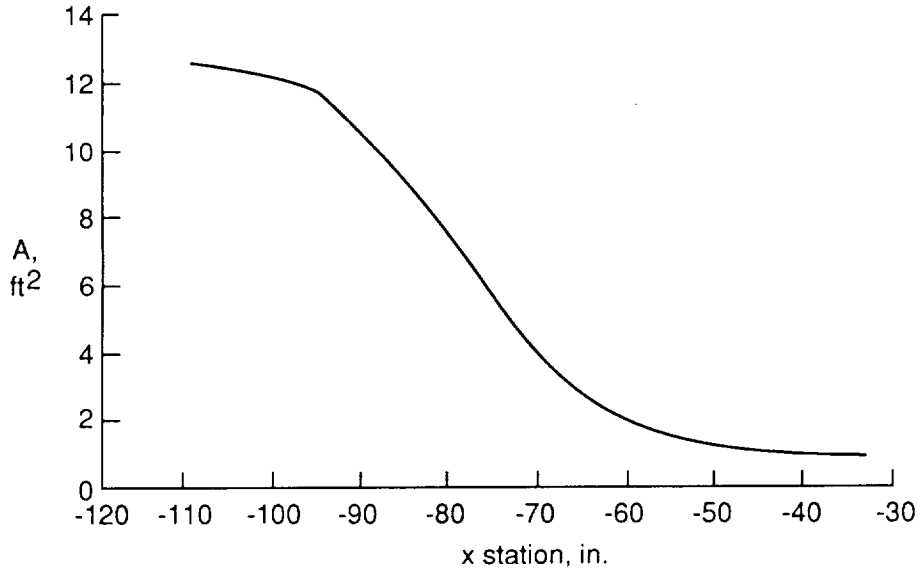

Figure 12. Details of contraction section. All dimensions are given in inches. (Note that x stations in sketch and area distribution are aligned.)

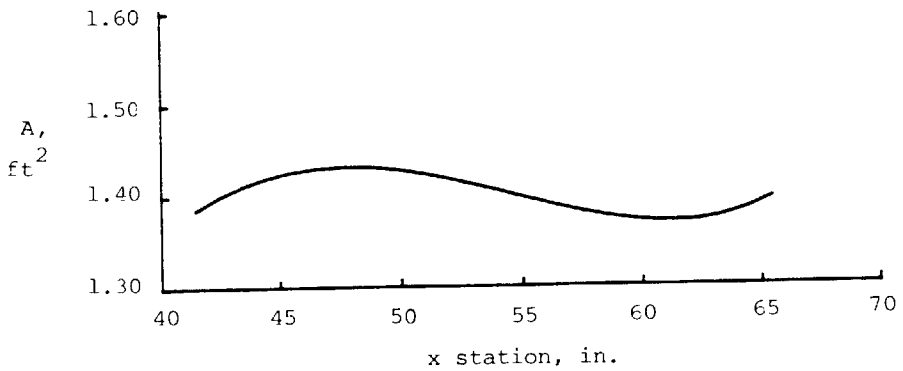

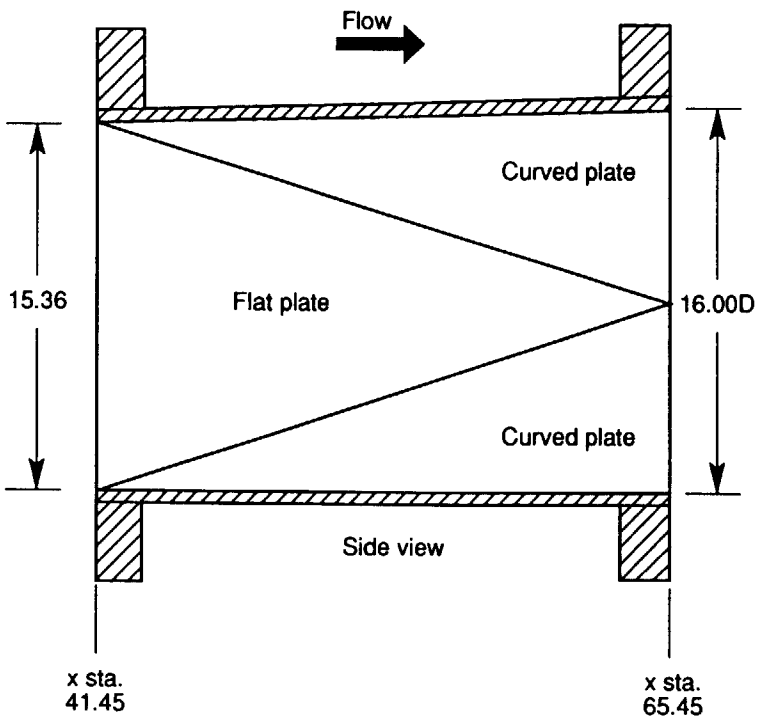

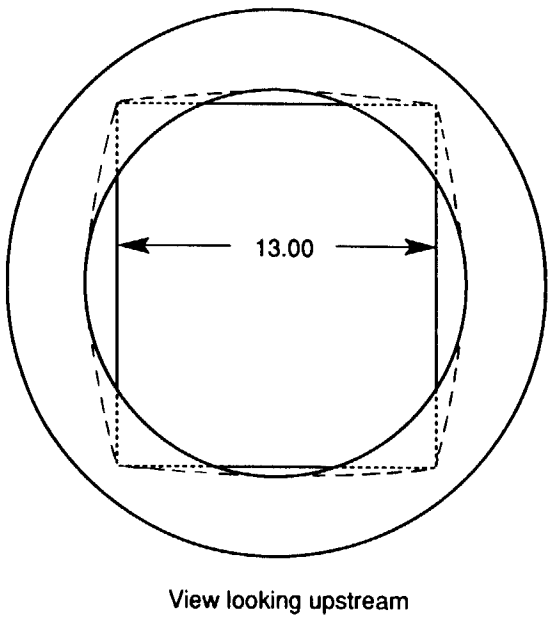

Figure 13. Details of first section of high-speed diffuser. Dimensions are given in inches except where noted.

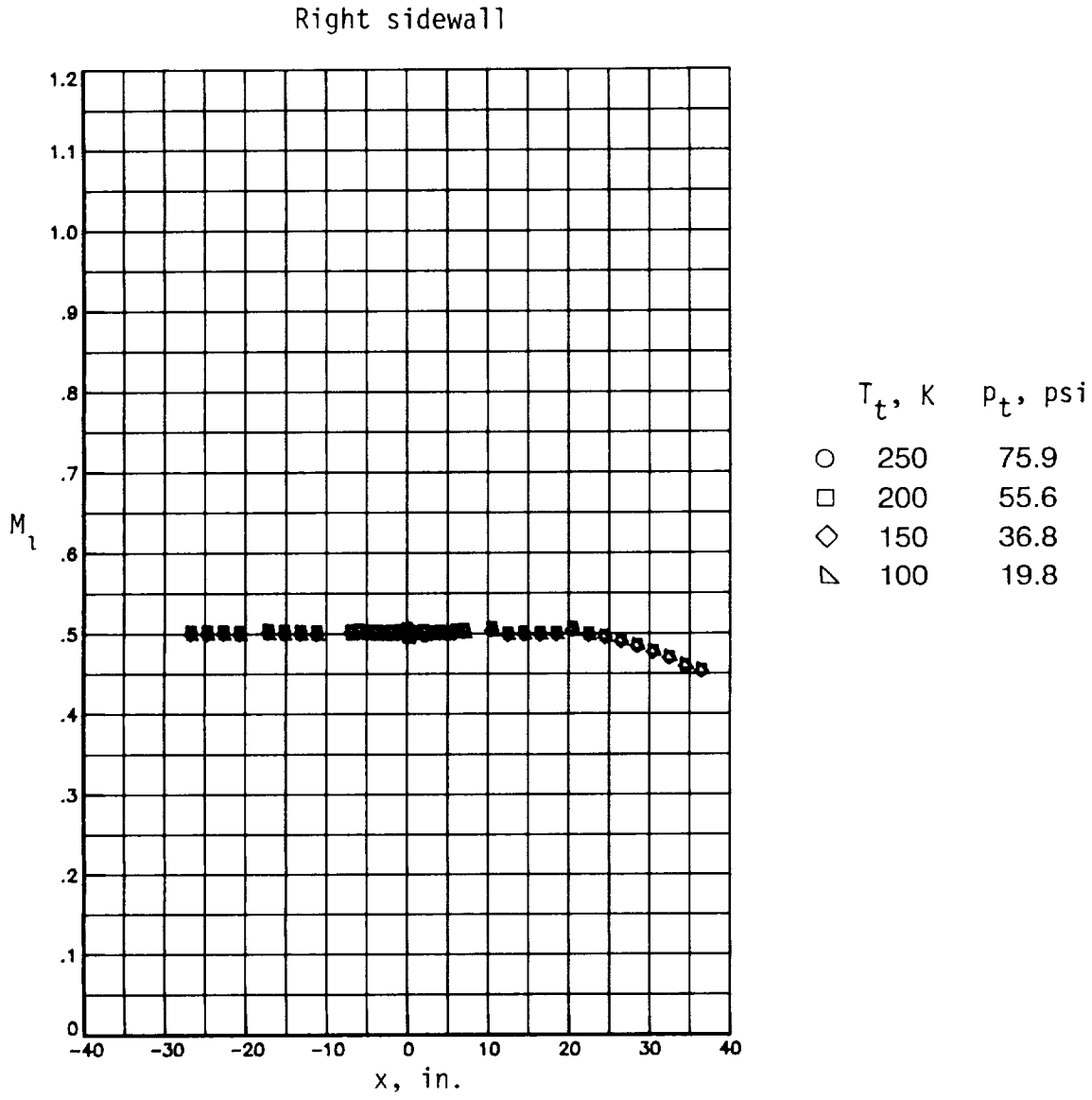

(a) $M_\infty = 0.50$.

Figure 14. Effect of temperature and pressure on local Mach number distribution in test section, contraction section, and high-speed diffuser for $R = 20 \times 10^6$ per foot.

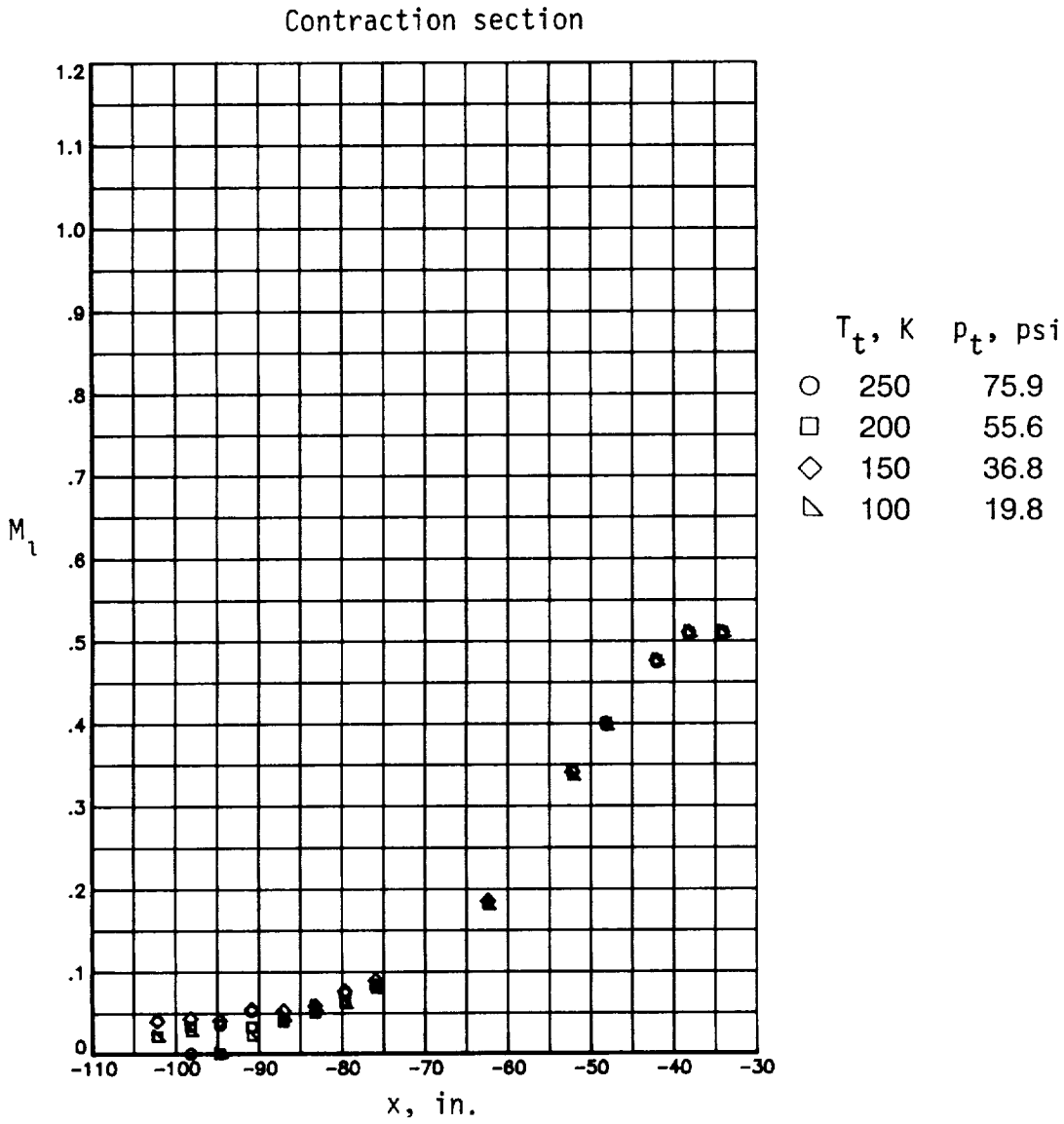

(a) Continued.

Figure 14. Continued.

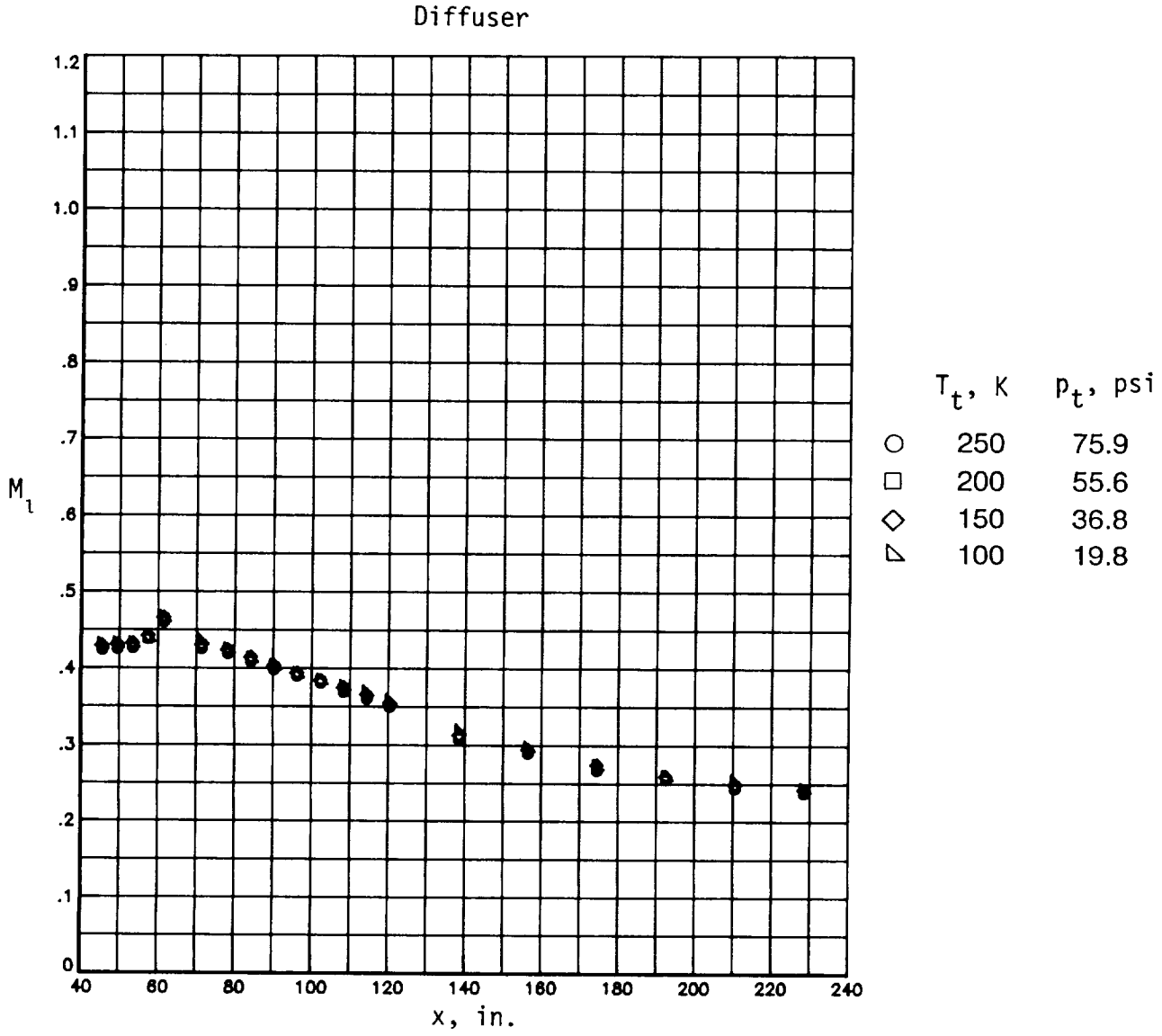

(a) Concluded.

Figure 14. Continued.

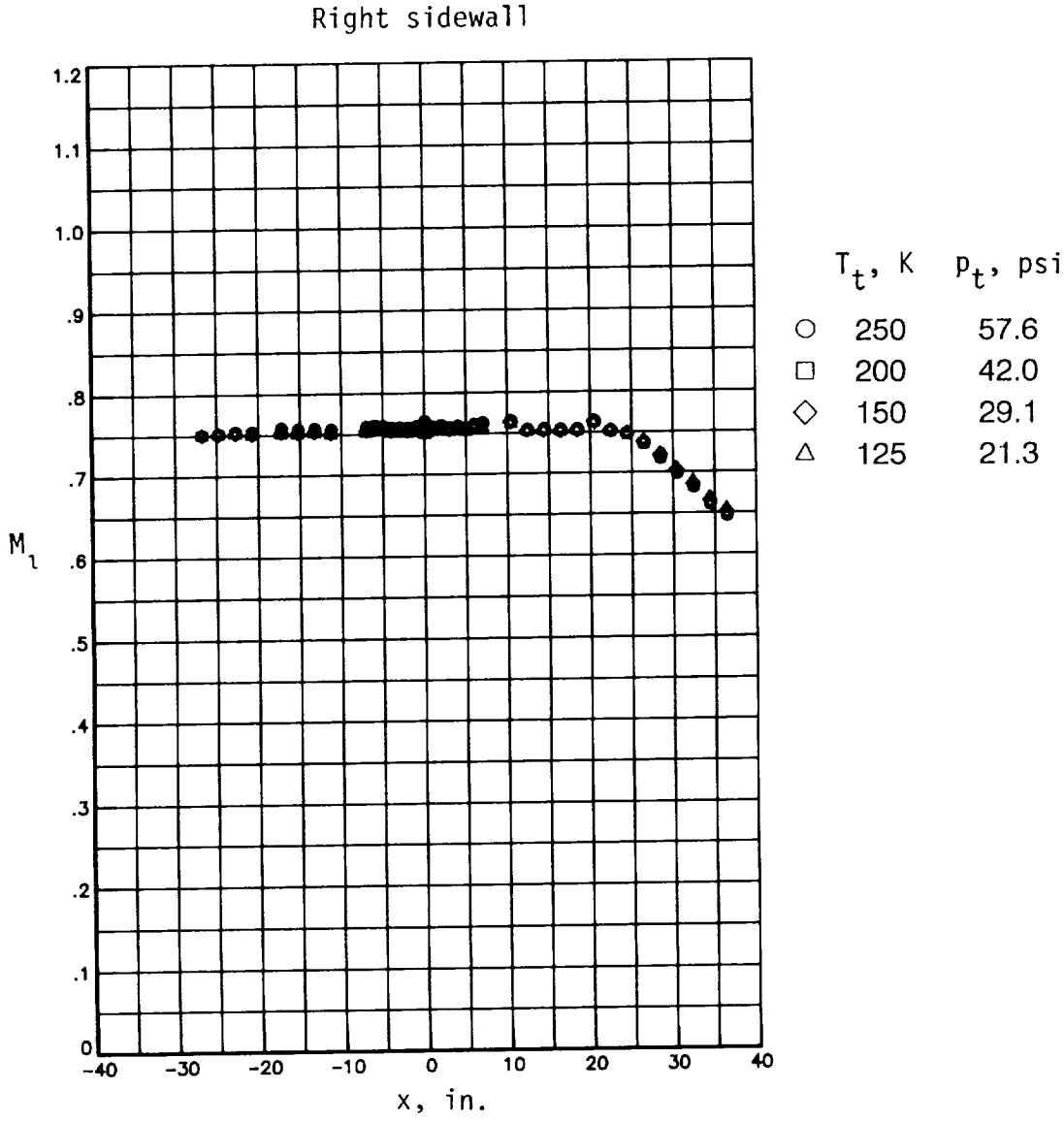

(b) $M_\infty = 0.75$.

Figure 14. Continued.

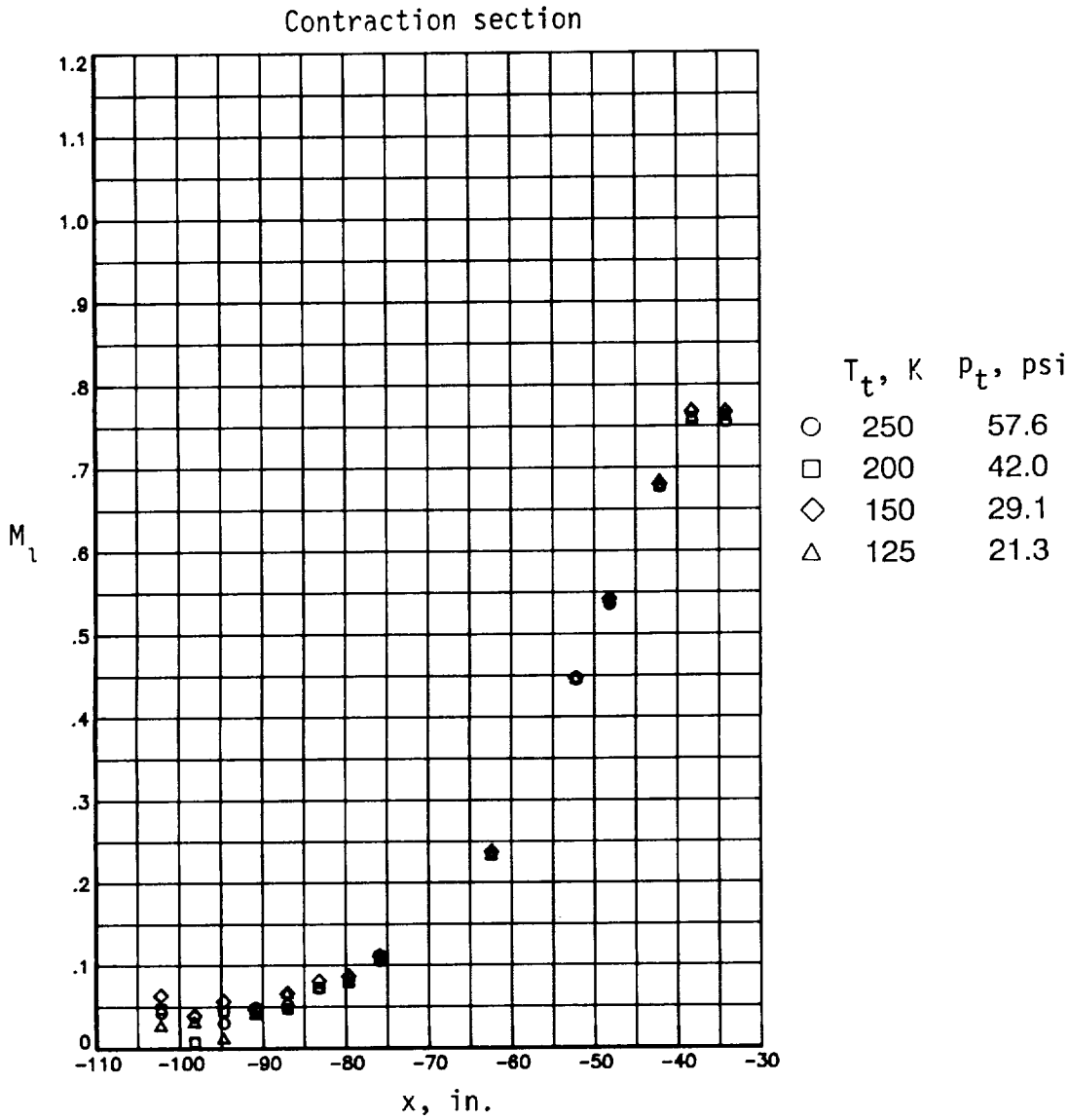

(b) Continued.

Figure 14. Continued.

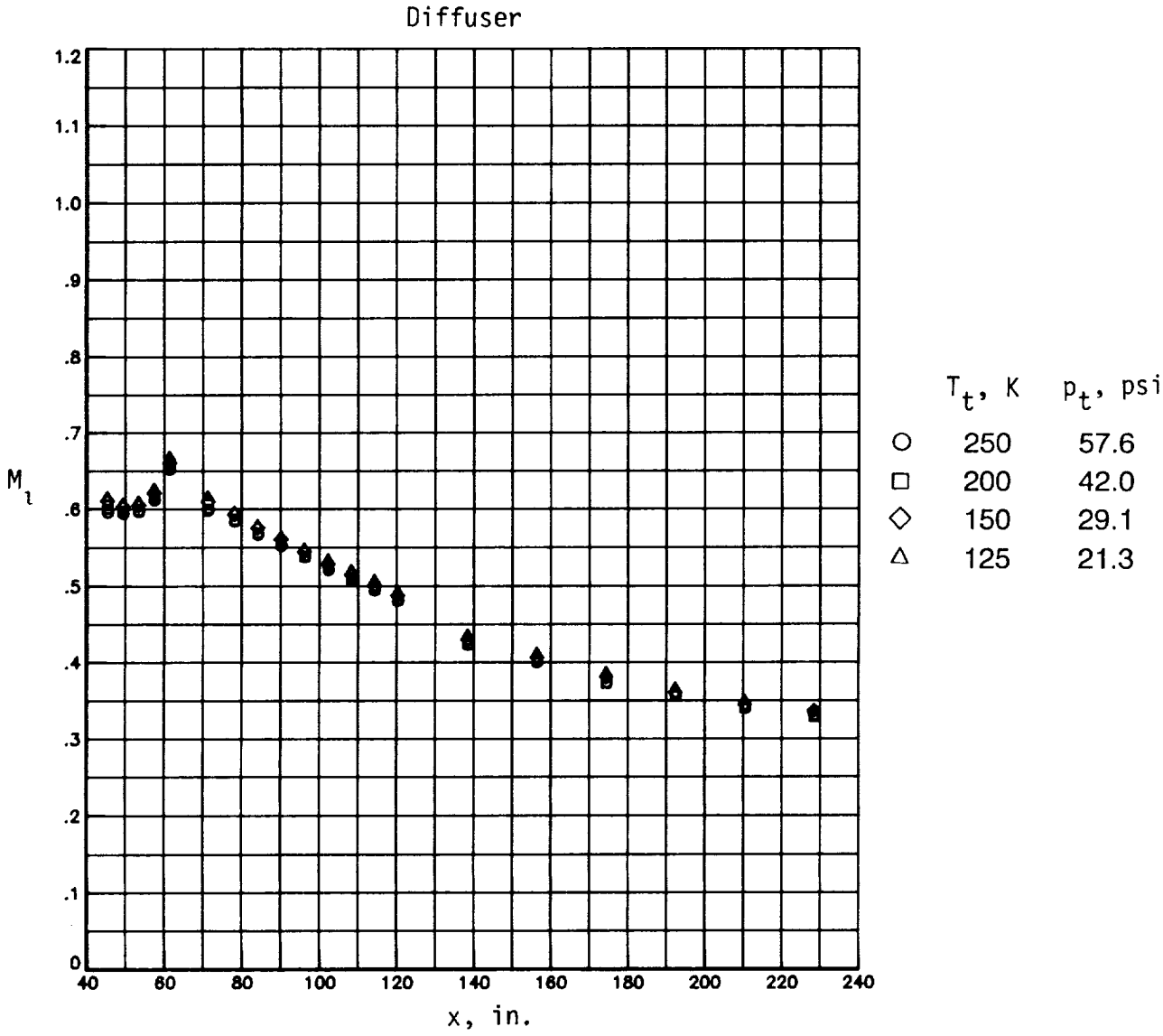

(b) Concluded.

Figure 14. Concluded.

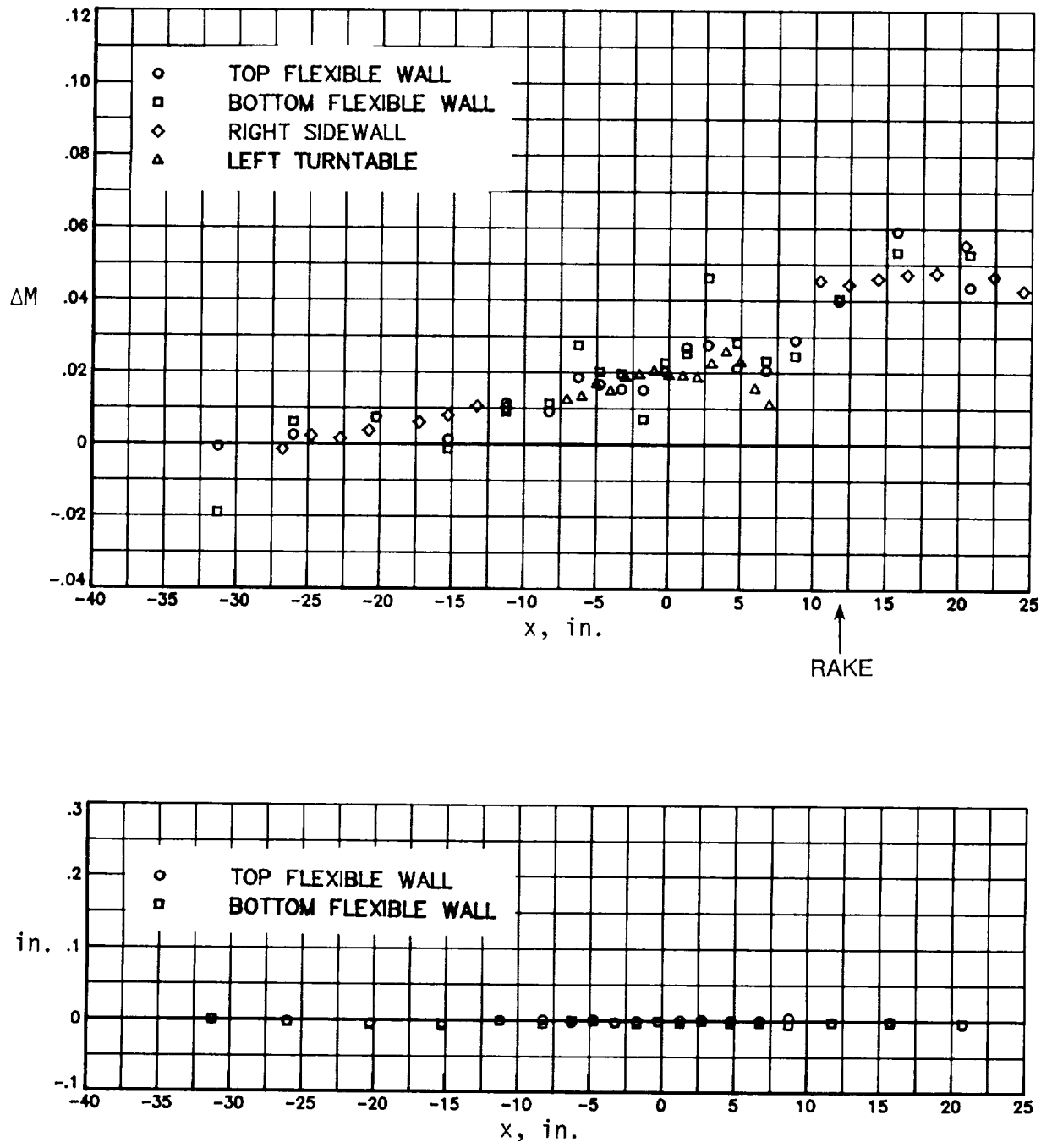

(a) Straight, parallel walls.

Figure 15. Effect of flexible wall shape on Mach number distribution in test section for $R = 10 \times 10^6$ per foot and $M_\infty = 0.70$.

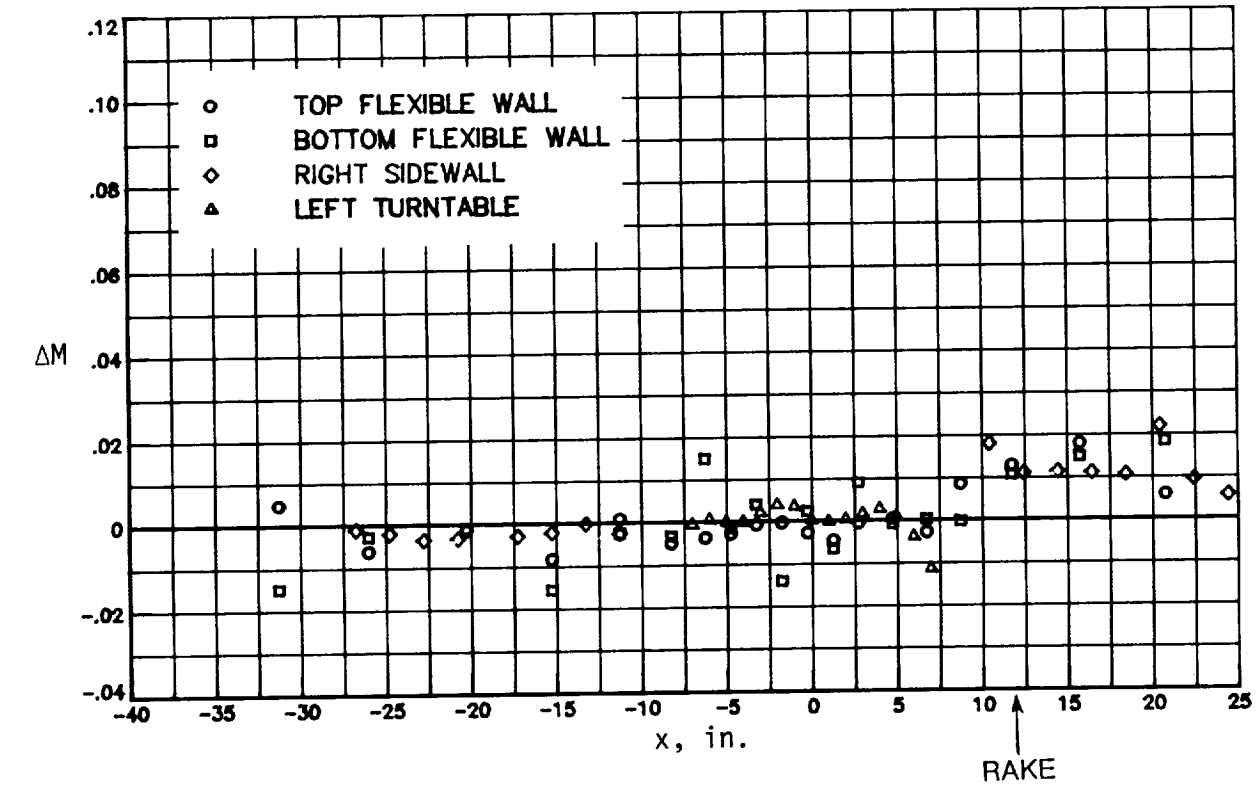

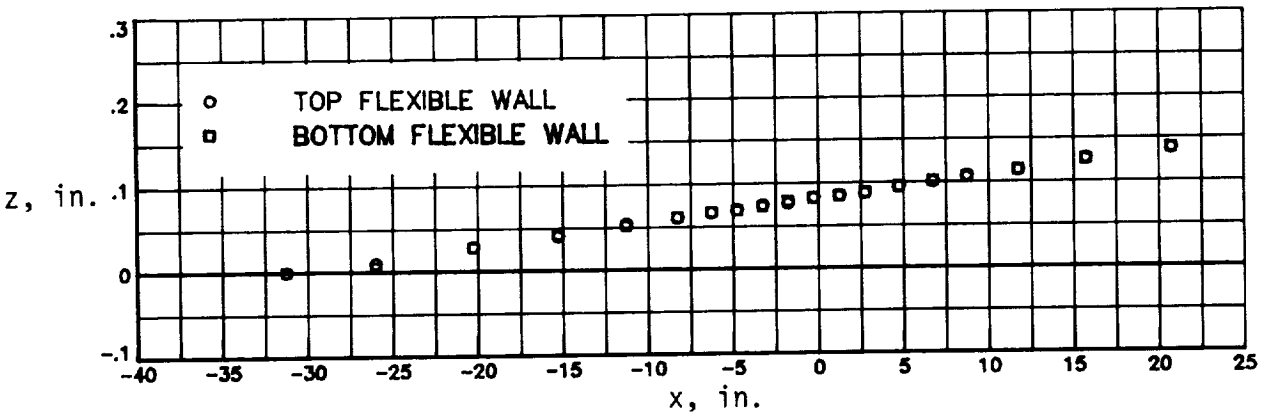

(b) Linearly diverged walls.

Figure 15. Continued.

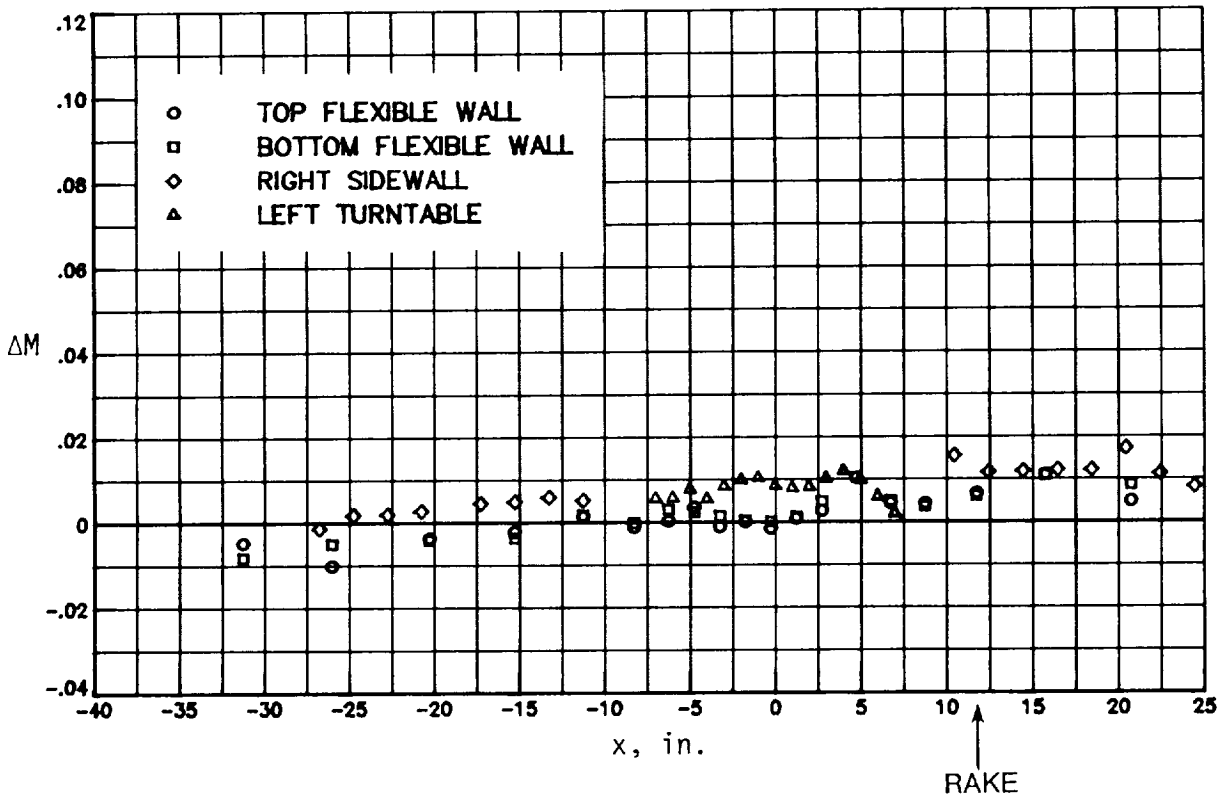

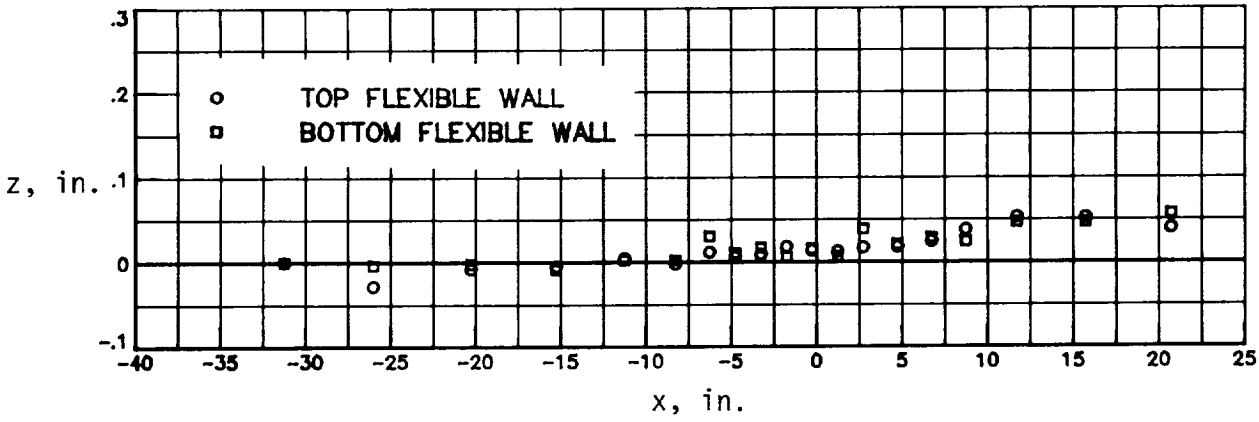

(c) Partially adapted walls.

Figure 15. Concluded.

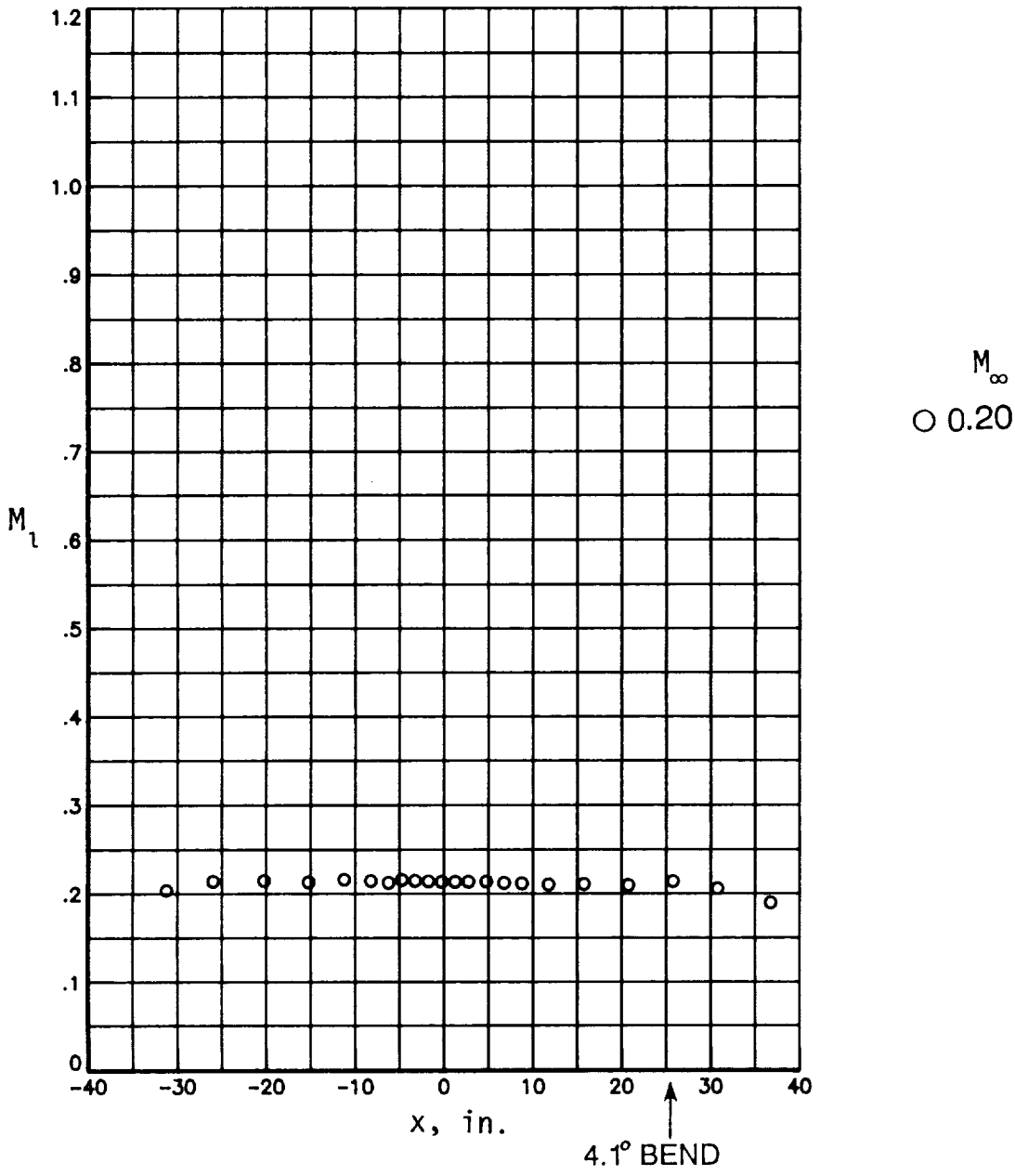

(a) $R = 10 \times 10^6$ per foot.

Figure 16. Local Mach number distributions on top flexible wall with linear divergence.

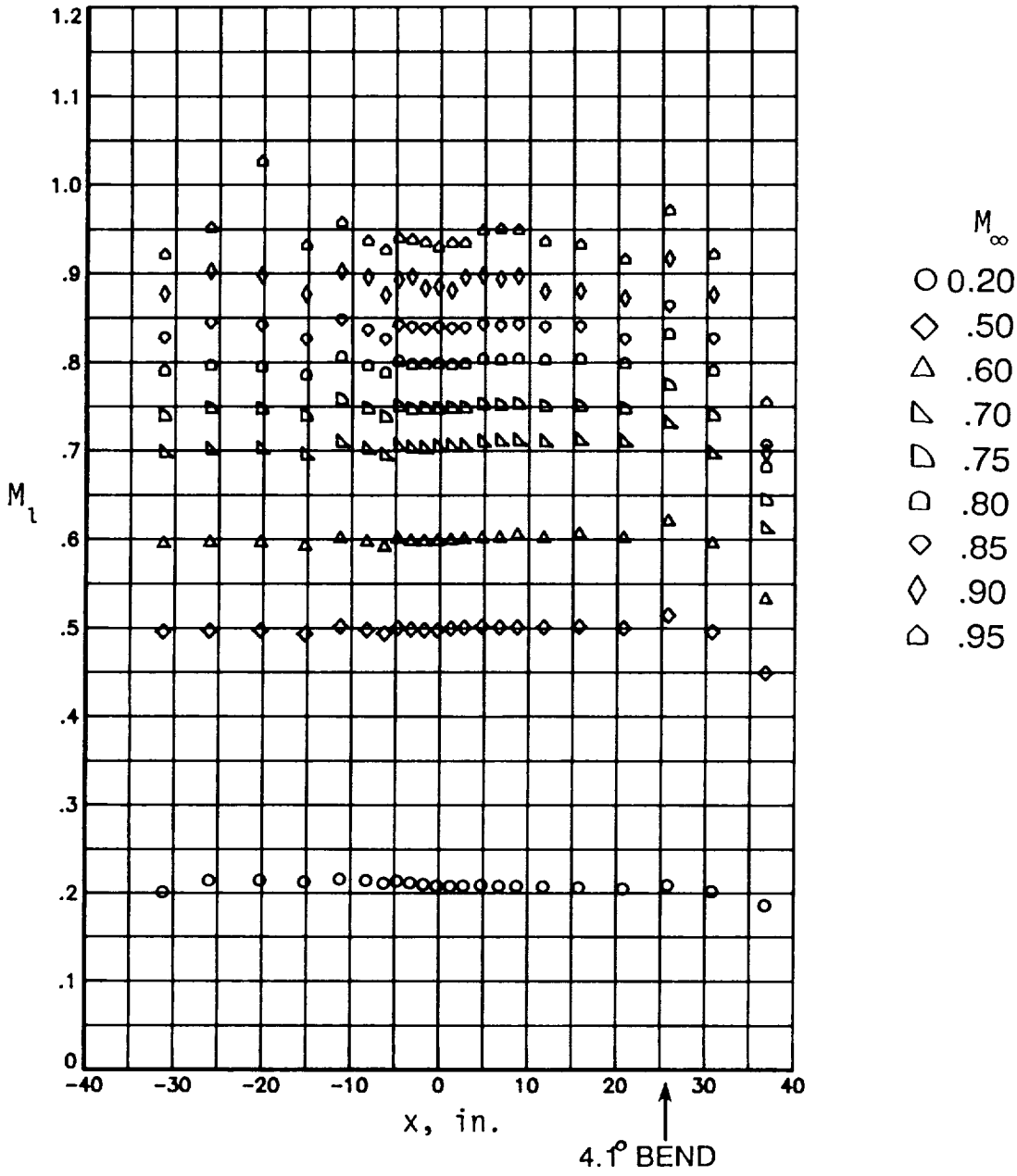

(b) $R = 20 \times 10^6$ per foot.

Figure 16. Continued.

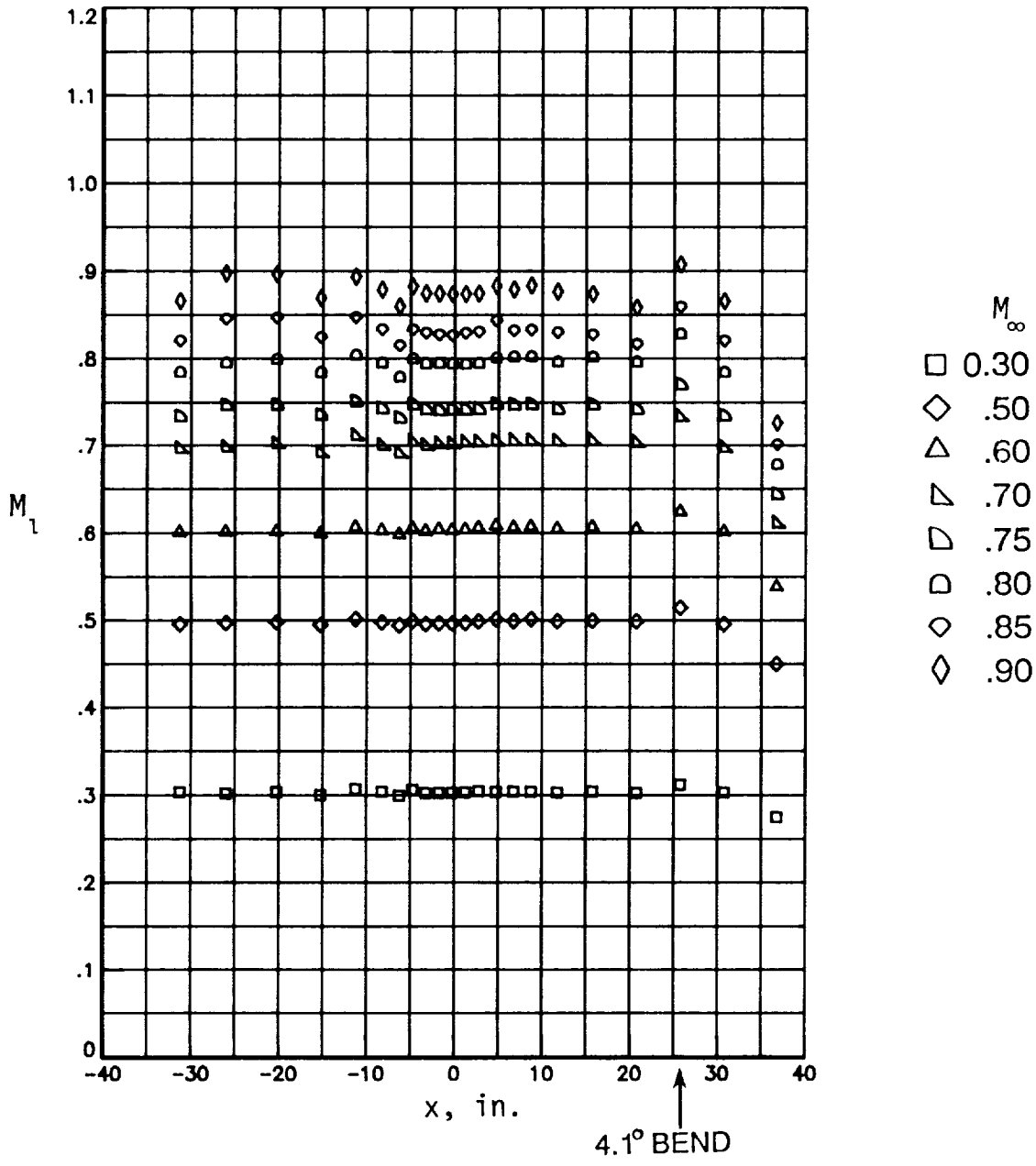

(c) $R = 40 \times 10^6$ per foot.

Figure 16. Continued.

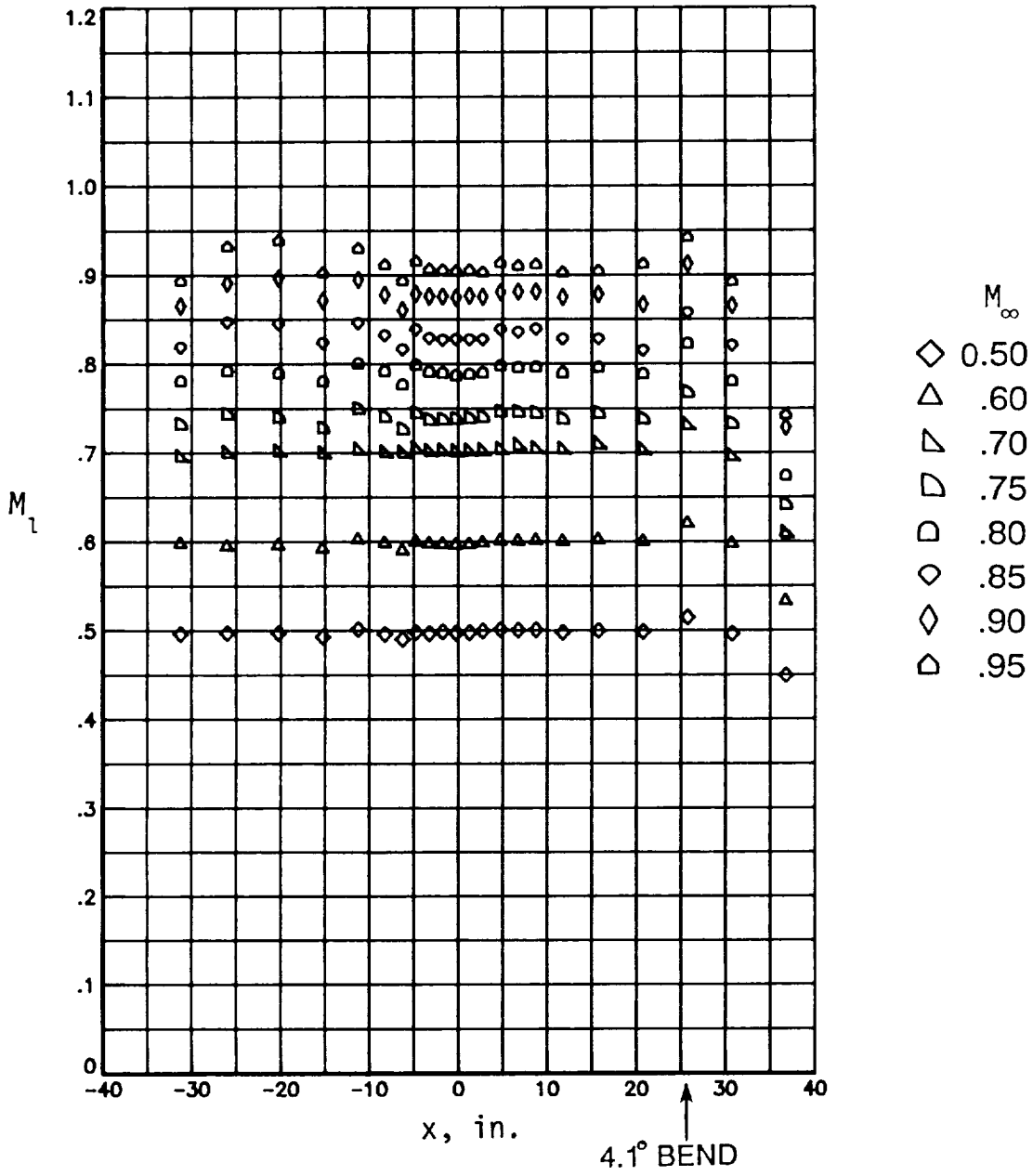

(d) $R = 60 \times 10^6$ per foot.

Figure 16. Continued.

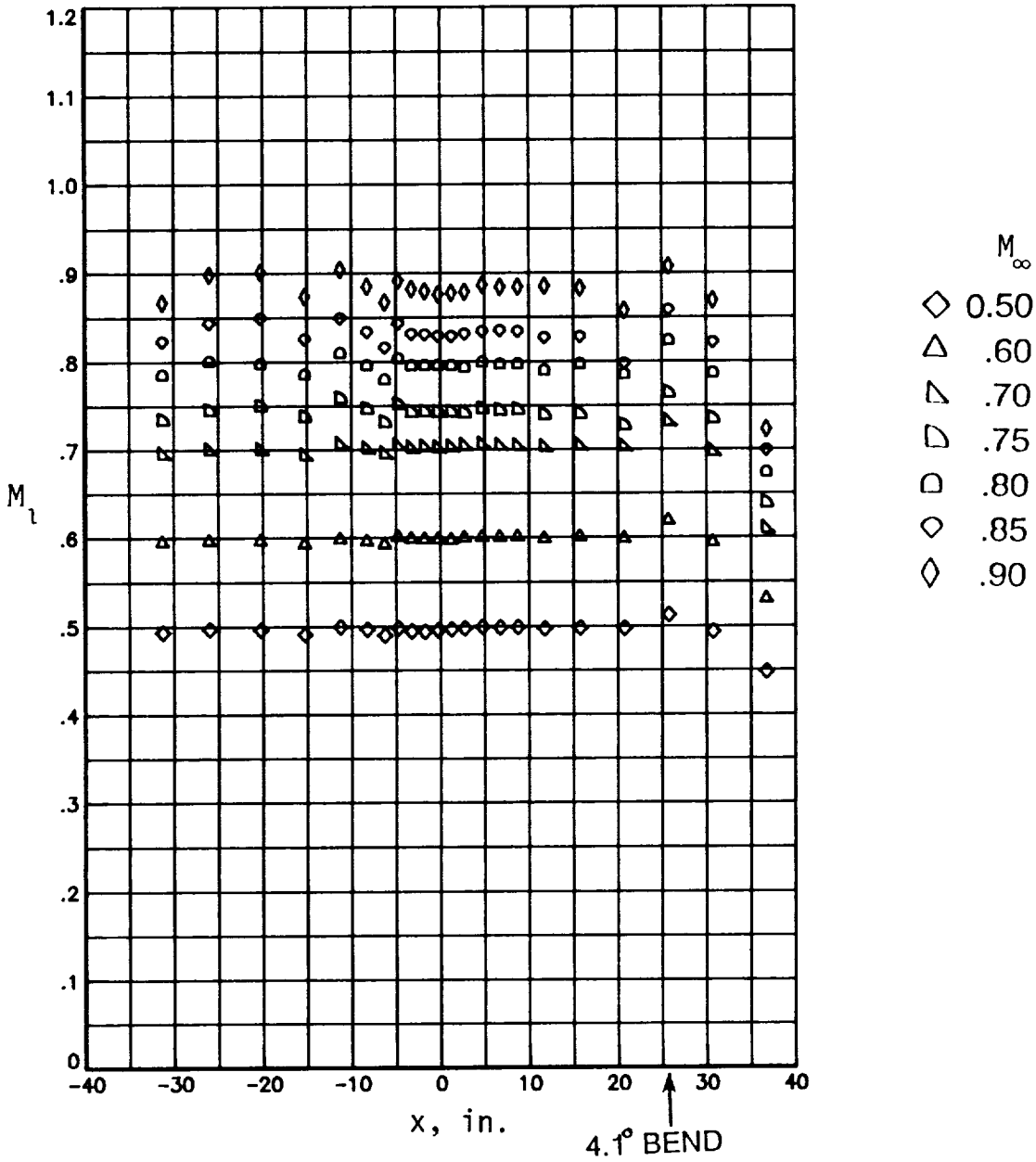

(e) $R = 80 \times 10^6$ per foot.

Figure 16. Continued.

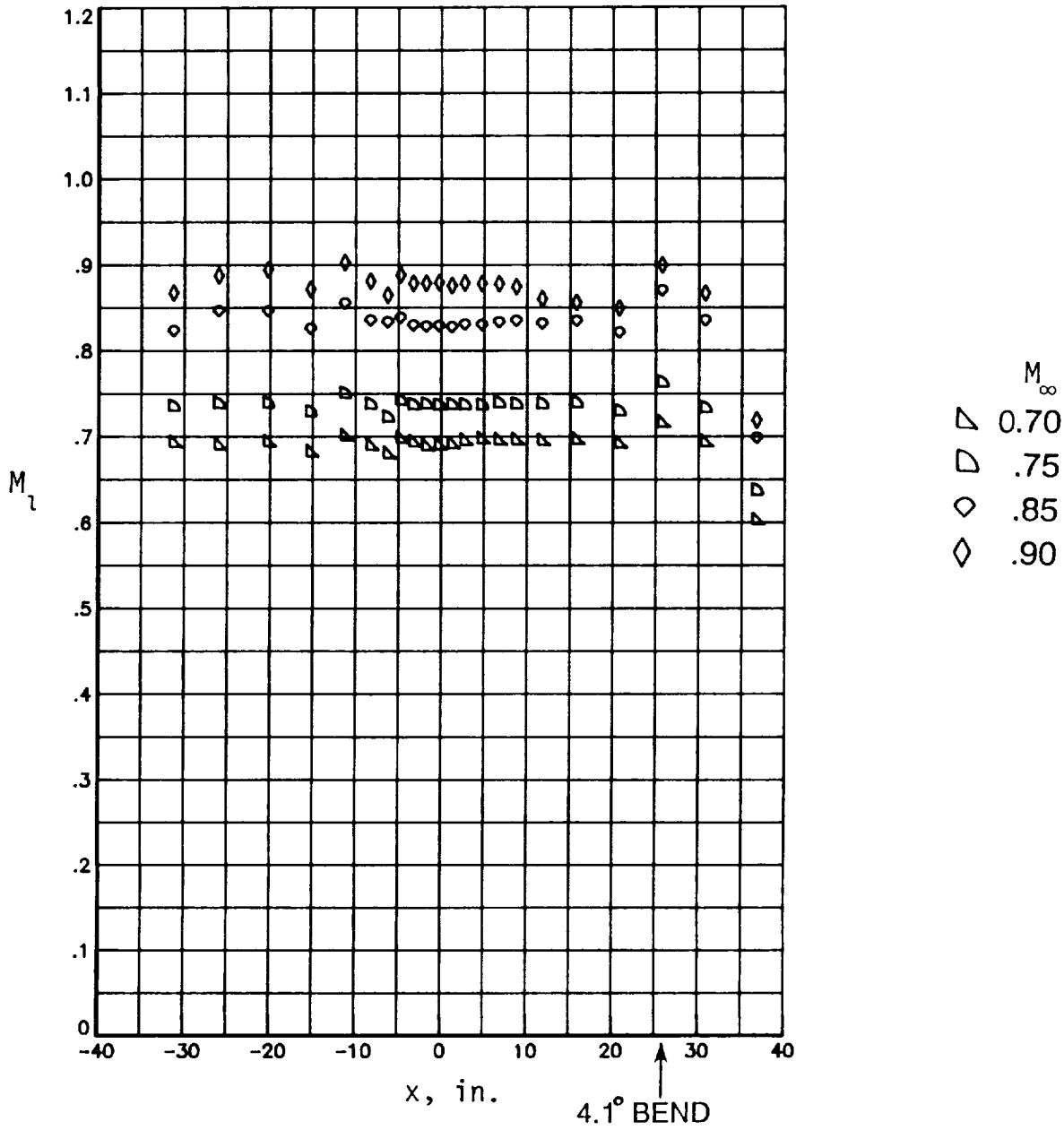

(f) $R = 100 \times 10^6$ per foot.

Figure 16. Concluded.

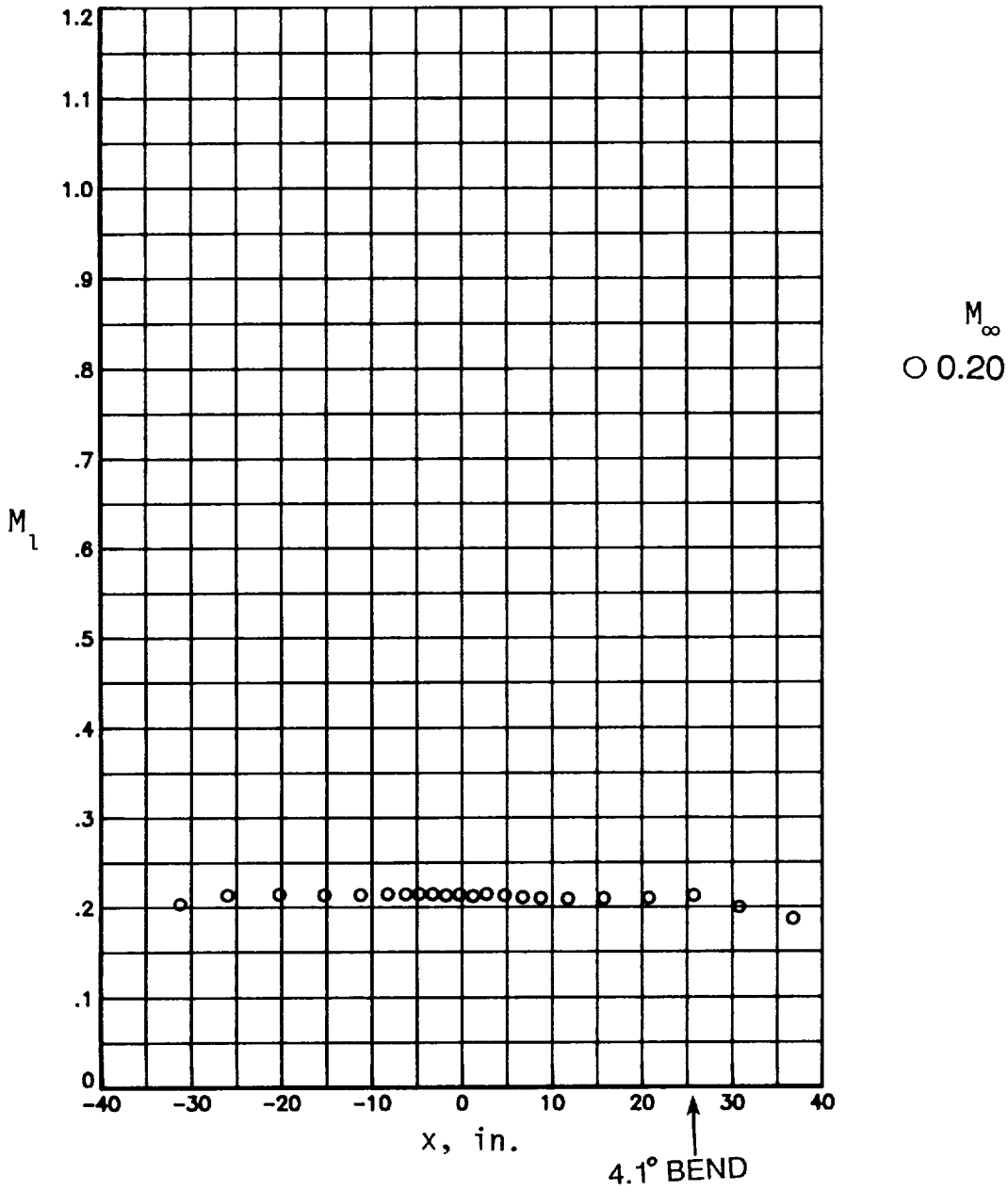

(a) $R = 10 \times 10^6$ per foot.

Figure 17. Local Mach number distributions on bottom flexible wall with linear divergence.

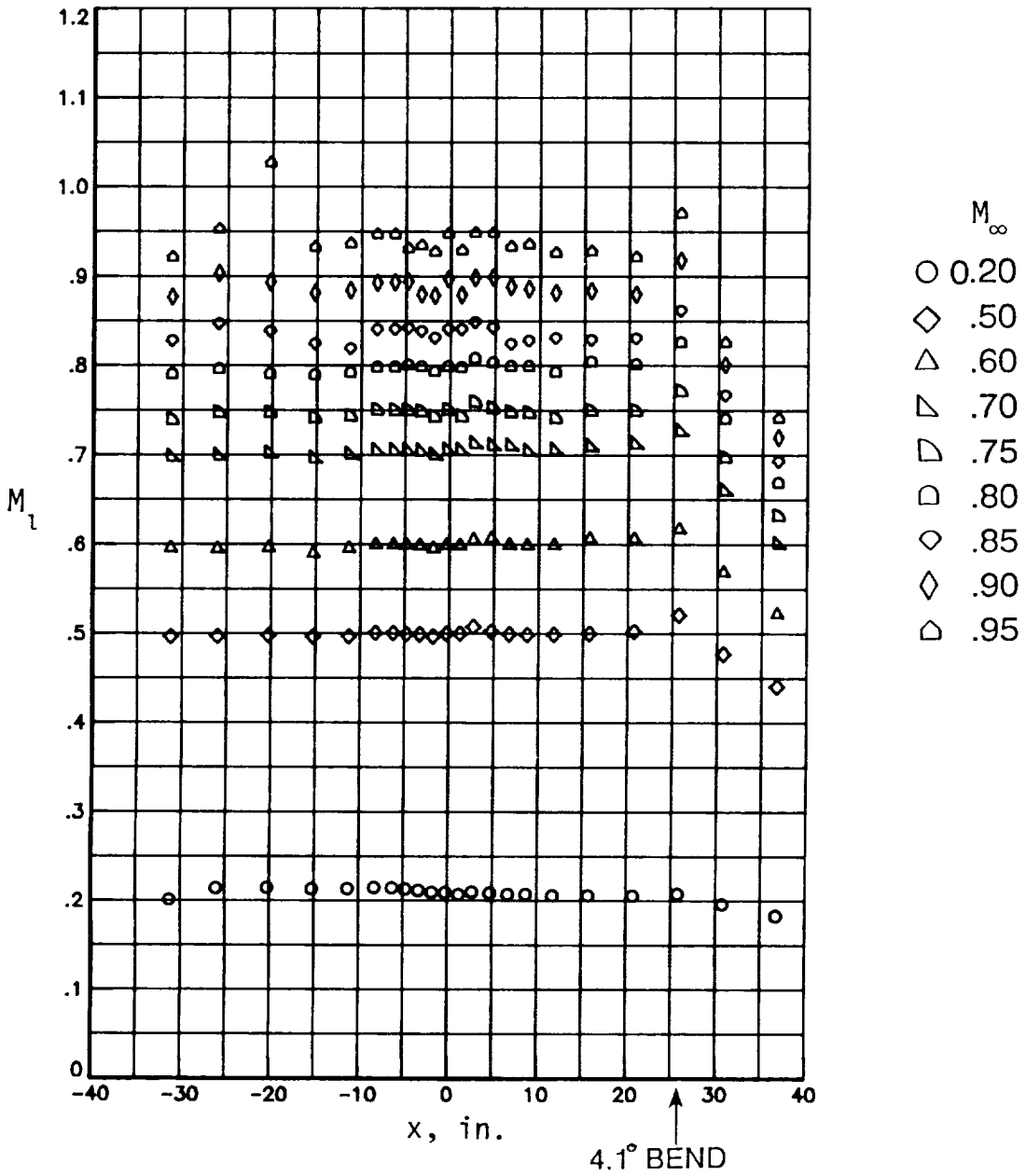

(b) $R = 20 \times 10^6$ per foot.

Figure 17. Continued.

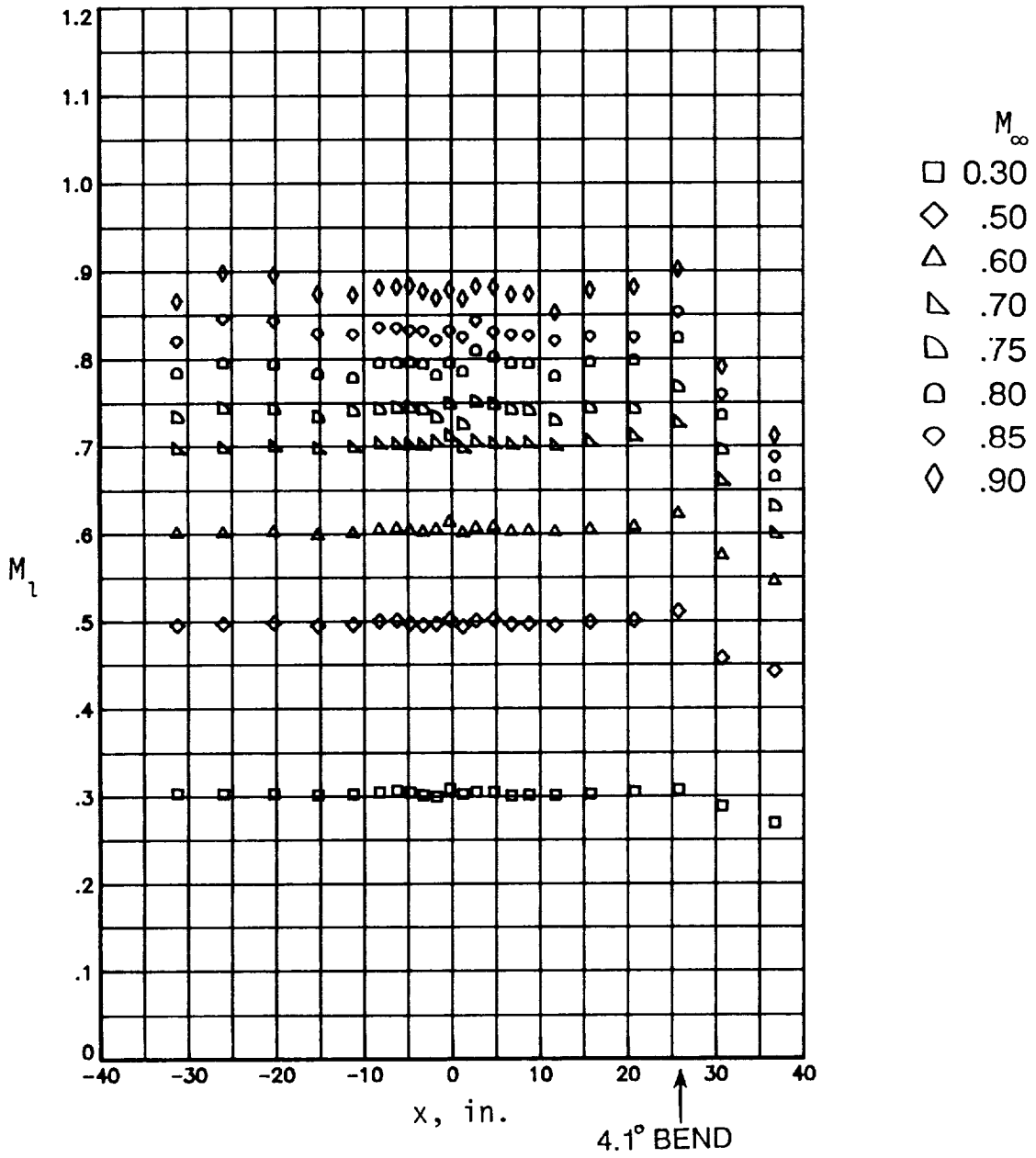

(c) $R = 40 \times 10^6$ per foot.

Figure 17. Continued.

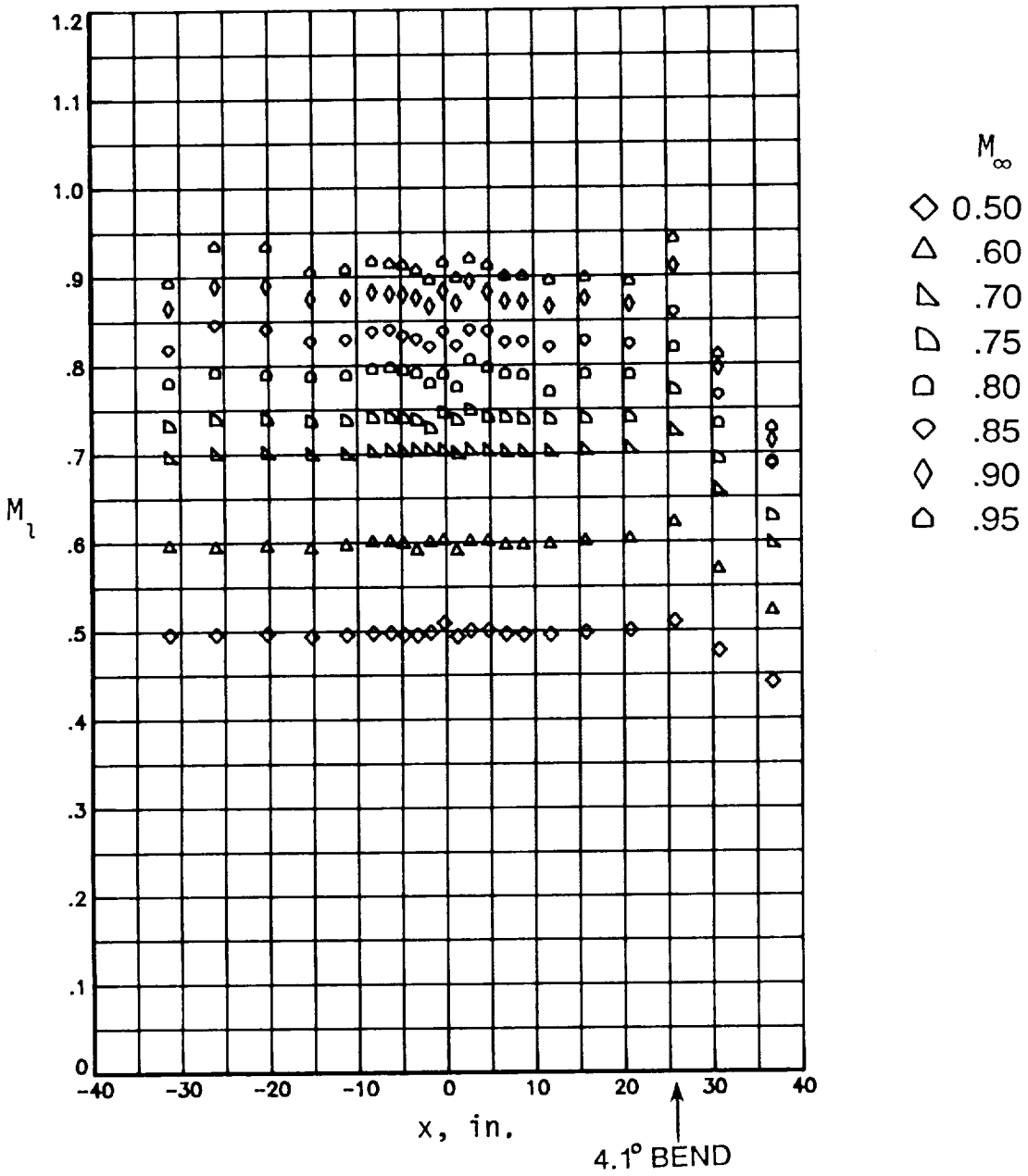

(d) $R = 60 \times 10^6$ per foot.

Figure 17. Continued.

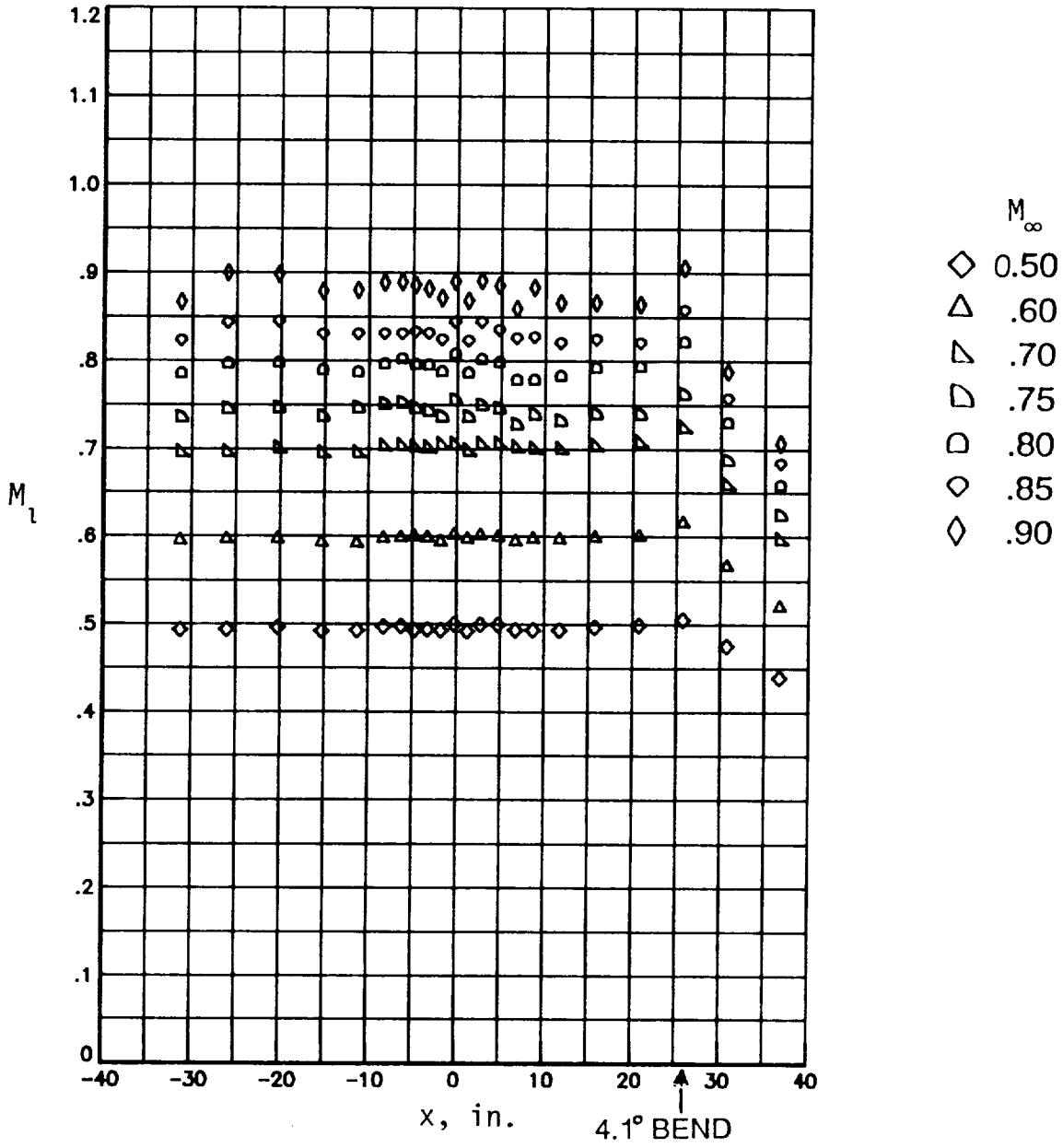

(e) $R = 80 \times 10^6$ per foot.

Figure 17. Continued.

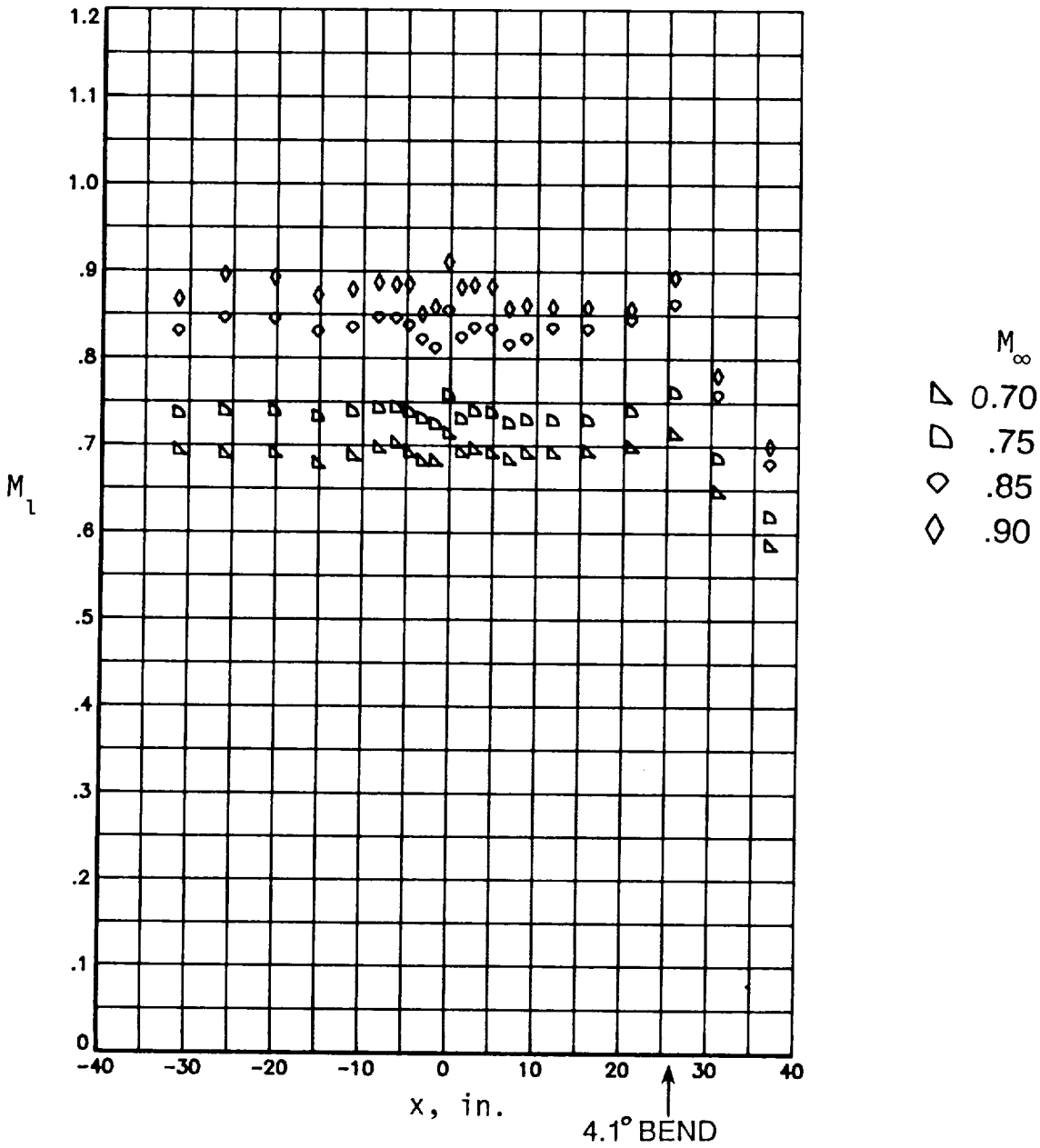

(f) $R = 100 \times 10^6$ per foot.

Figure 17. Concluded.

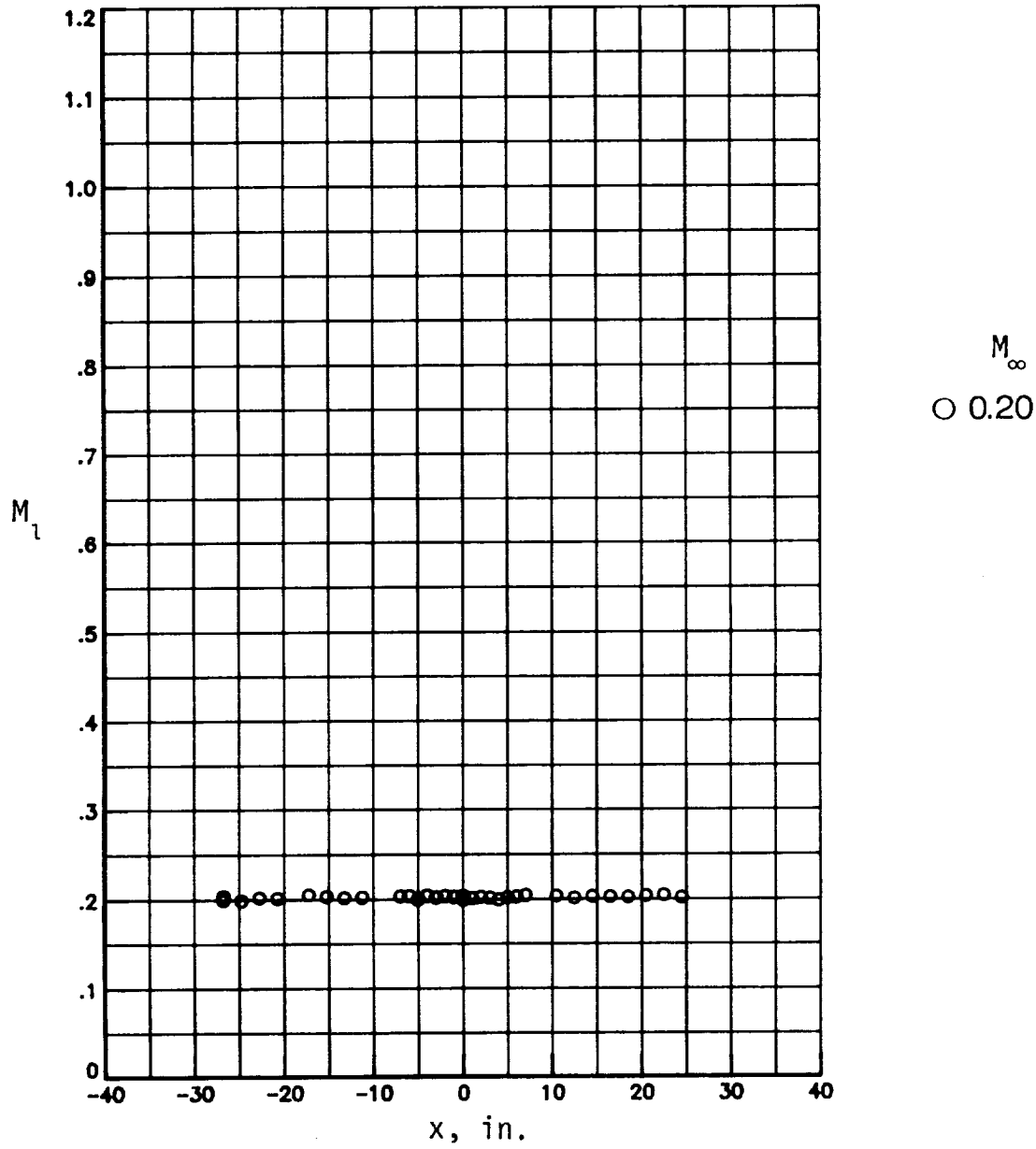

(a) $R = 10 \times 10^6$ per foot.

Figure 18. Local Mach number distributions on right sidewall and turntable with linear divergence.

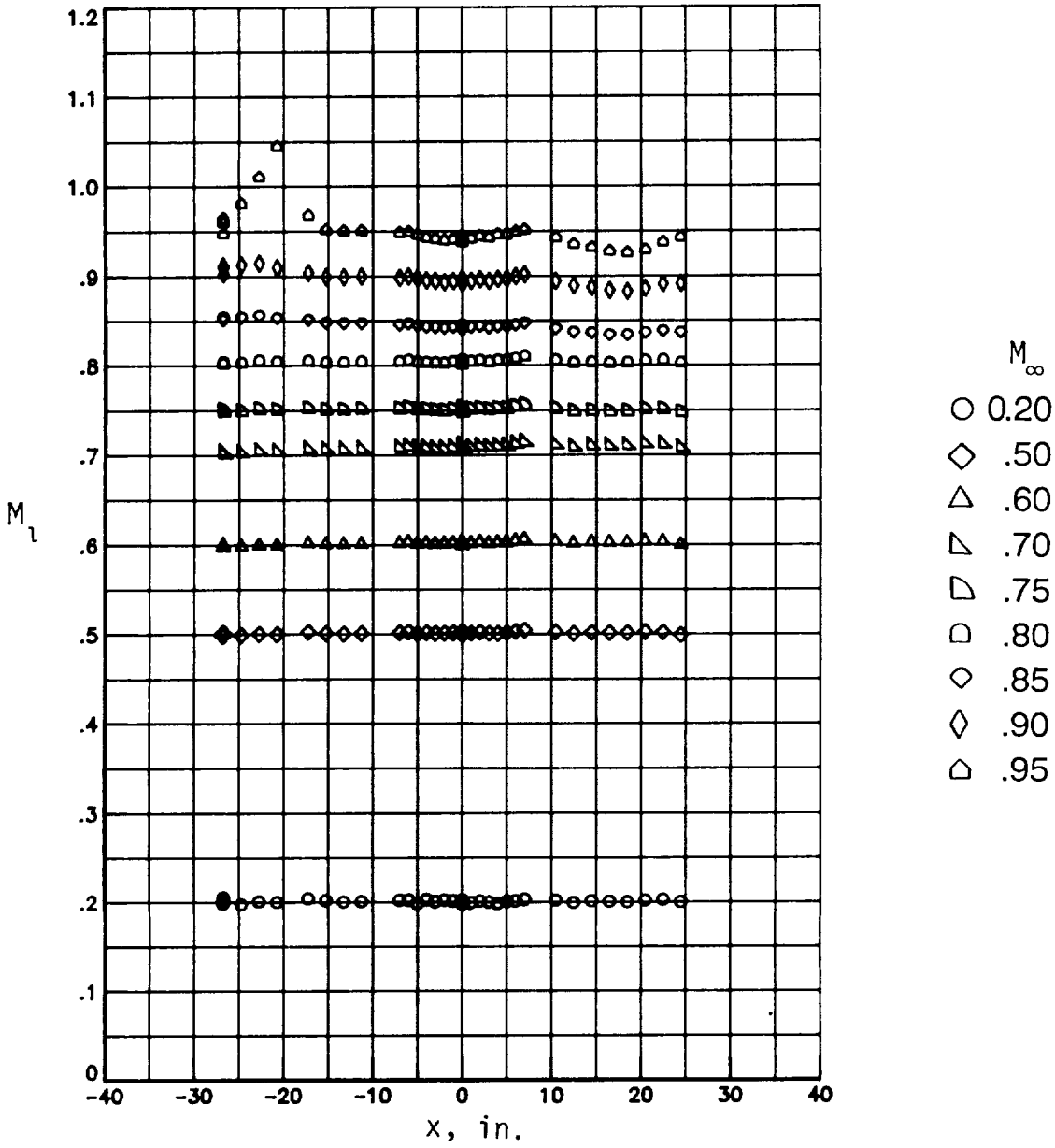

(b) $R = 20 \times 10^6$ per foot.

Figure 18. Continued.

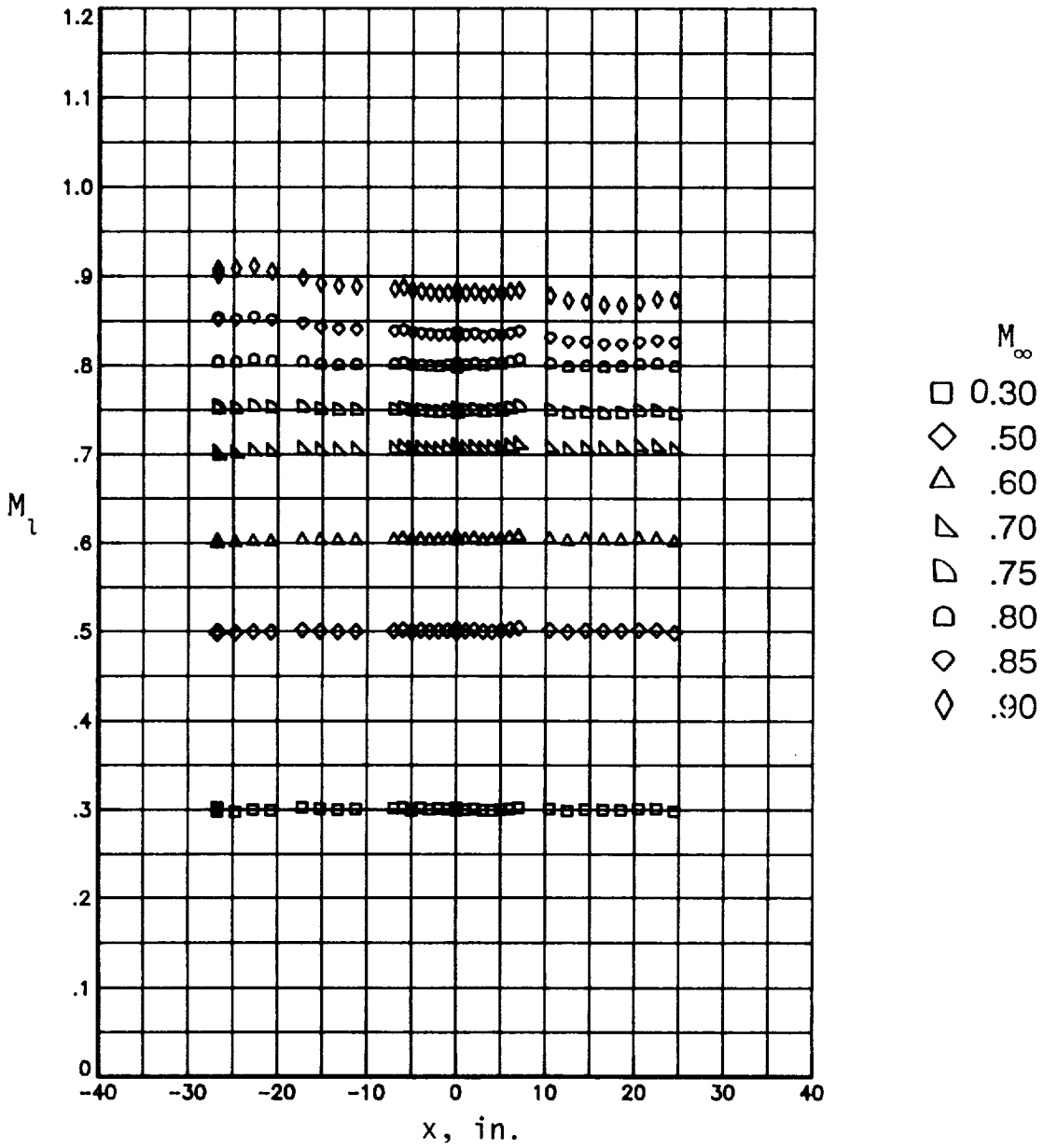

(c) $R = 40 \times 10^6$ per foot.

Figure 18. Continued.

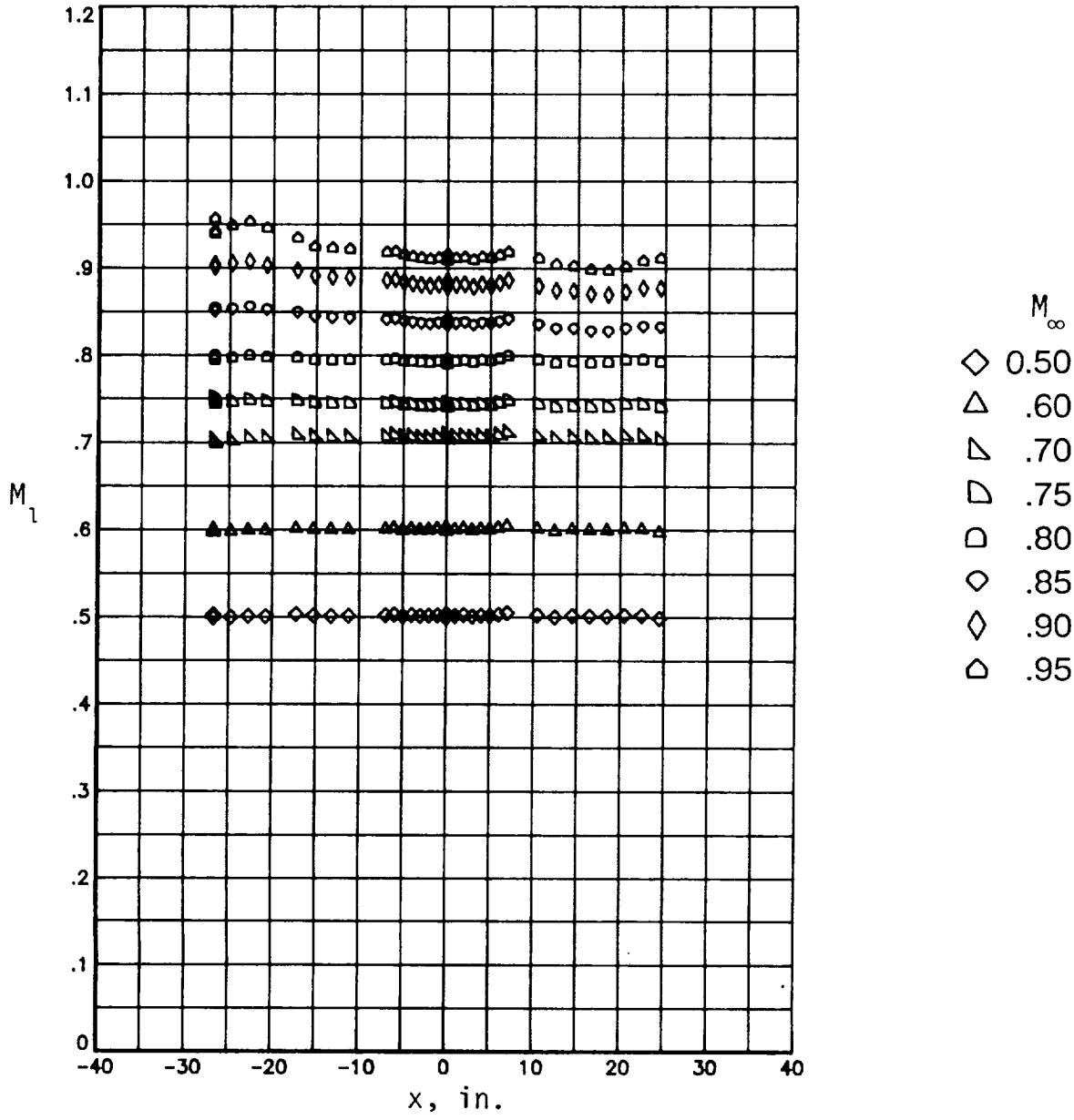

(d) $R = 60 \times 10^6$ per foot.

Figure 18. Continued.

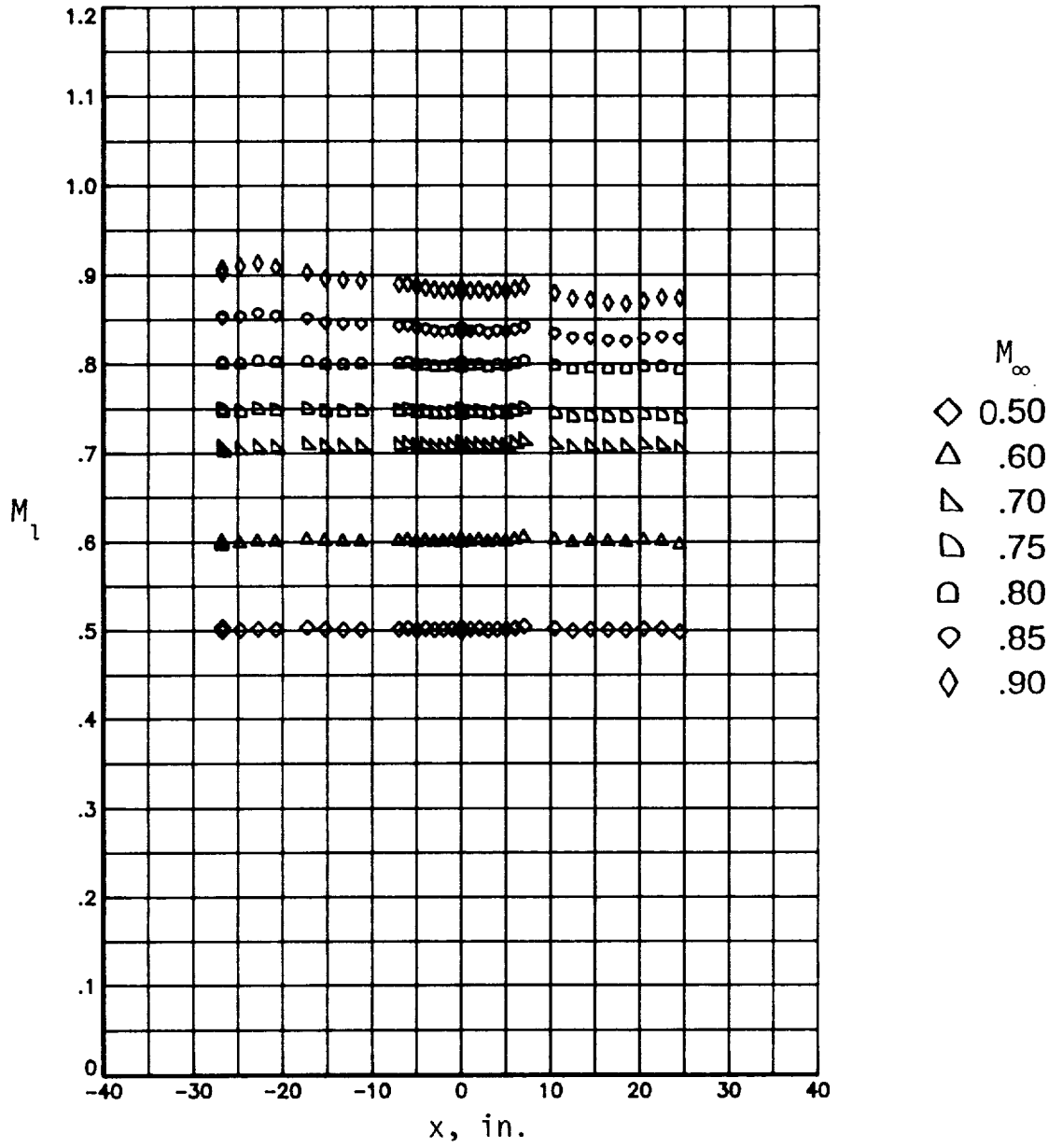

(e) $R = 80 \times 10^6$ per foot.

Figure 18. Continued.

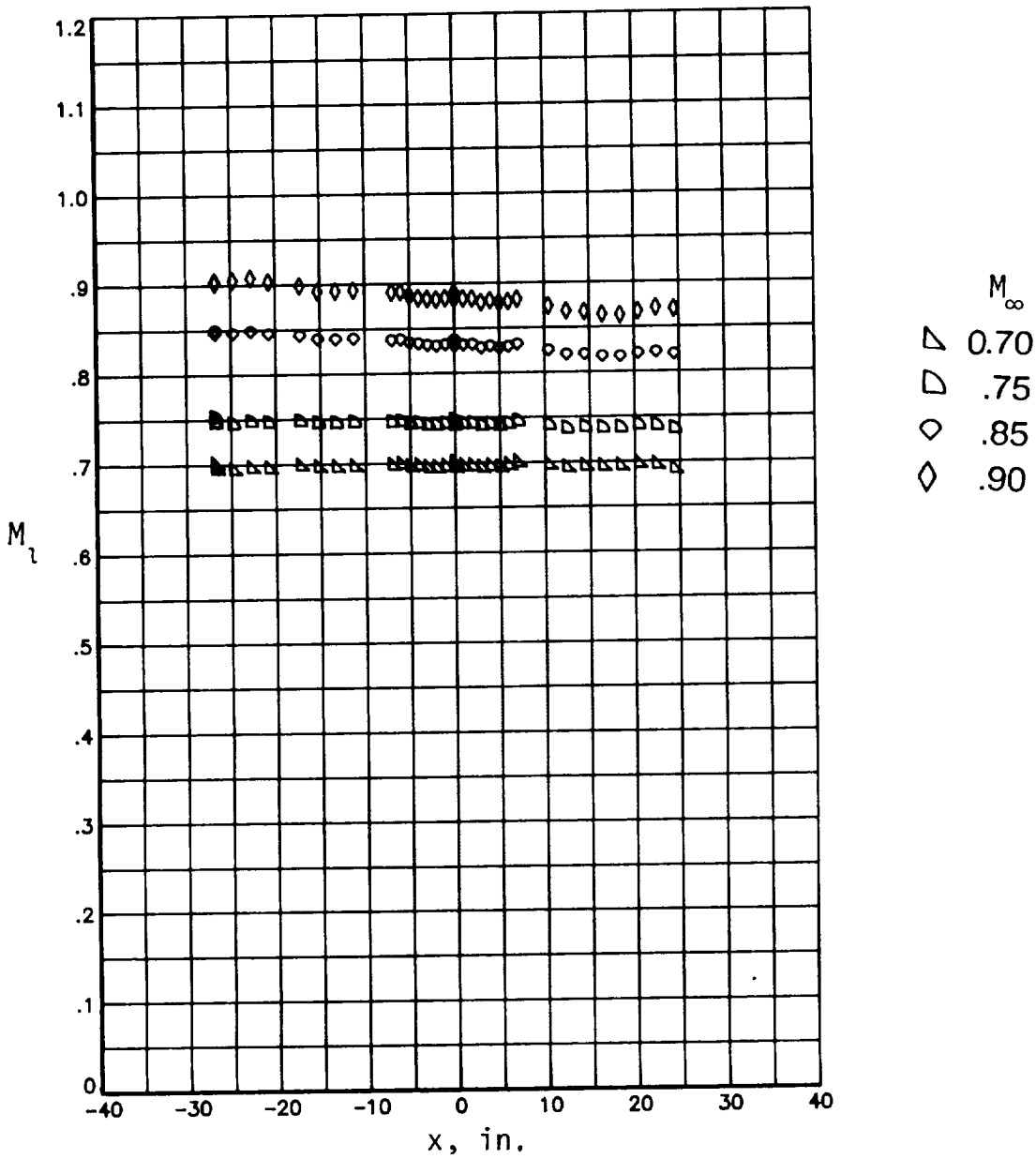

(f) $R = 100 \times 10^6$ per foot.

Figure 18. Concluded.

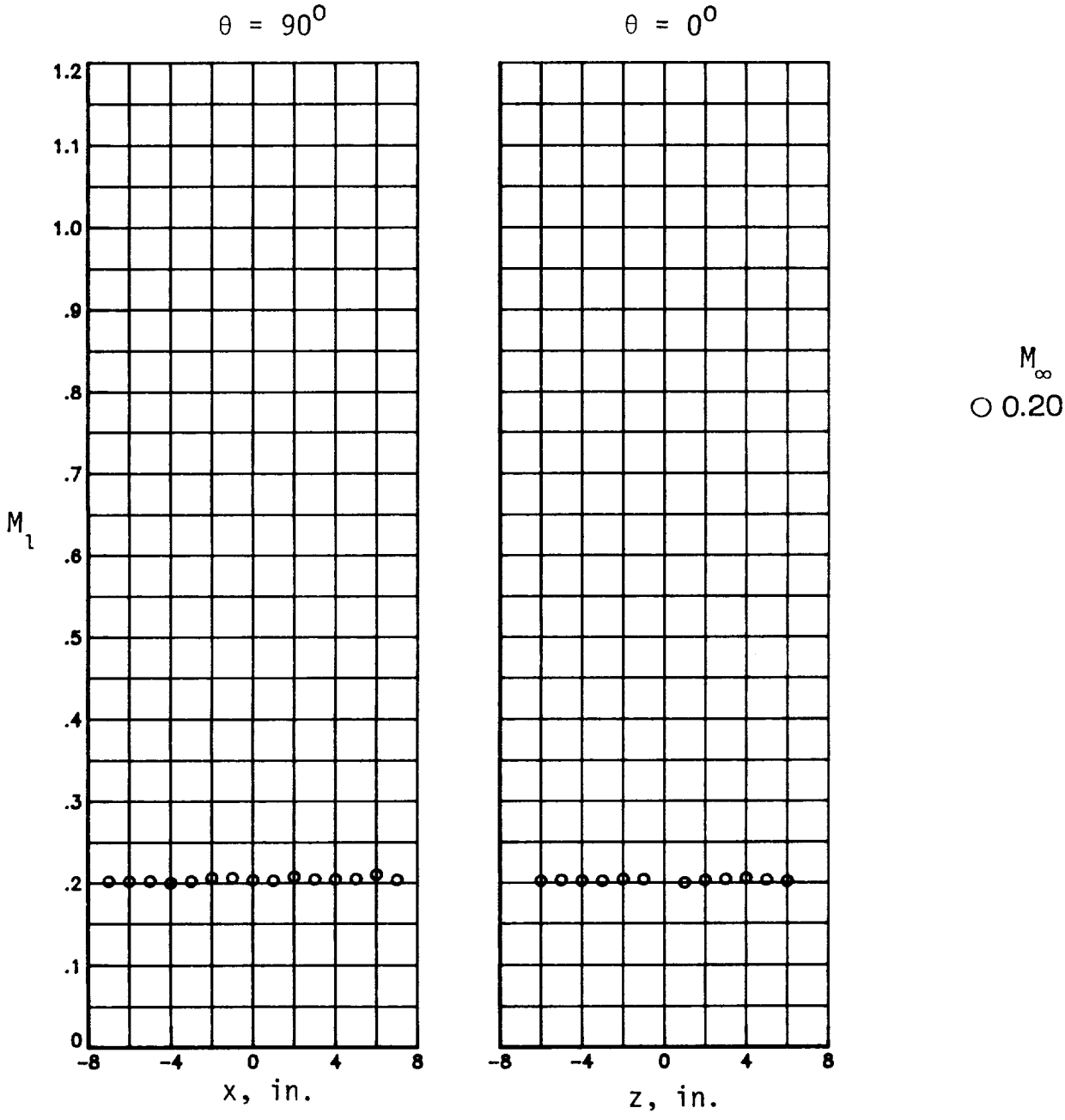

(a) $R = 10 \times 10^6$ per foot.

Figure 19. Local Mach number distributions on left turntable with linear divergence.

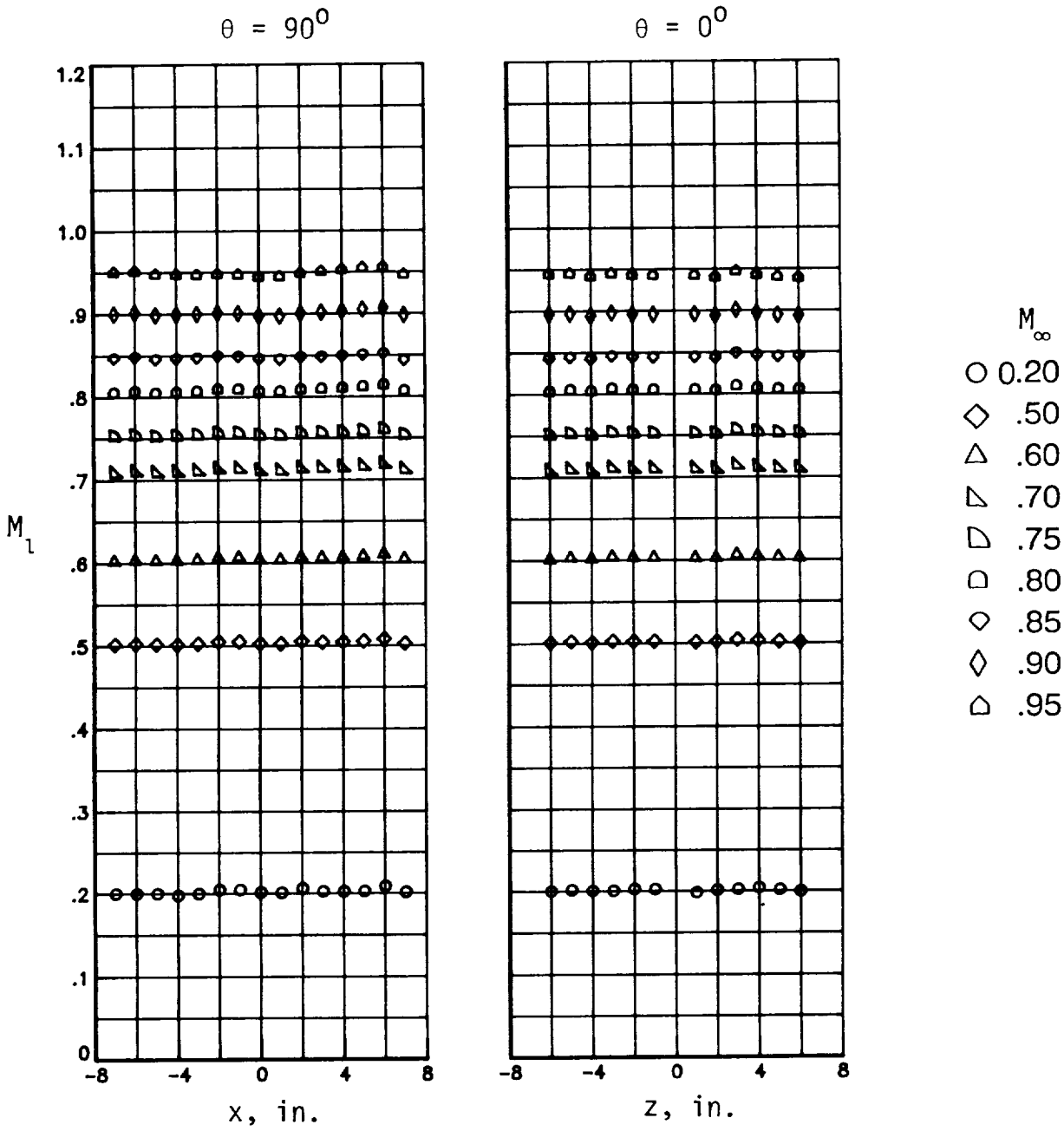

(b) $R = 20 \times 10^6$ per foot.

Figure 19. Continued.

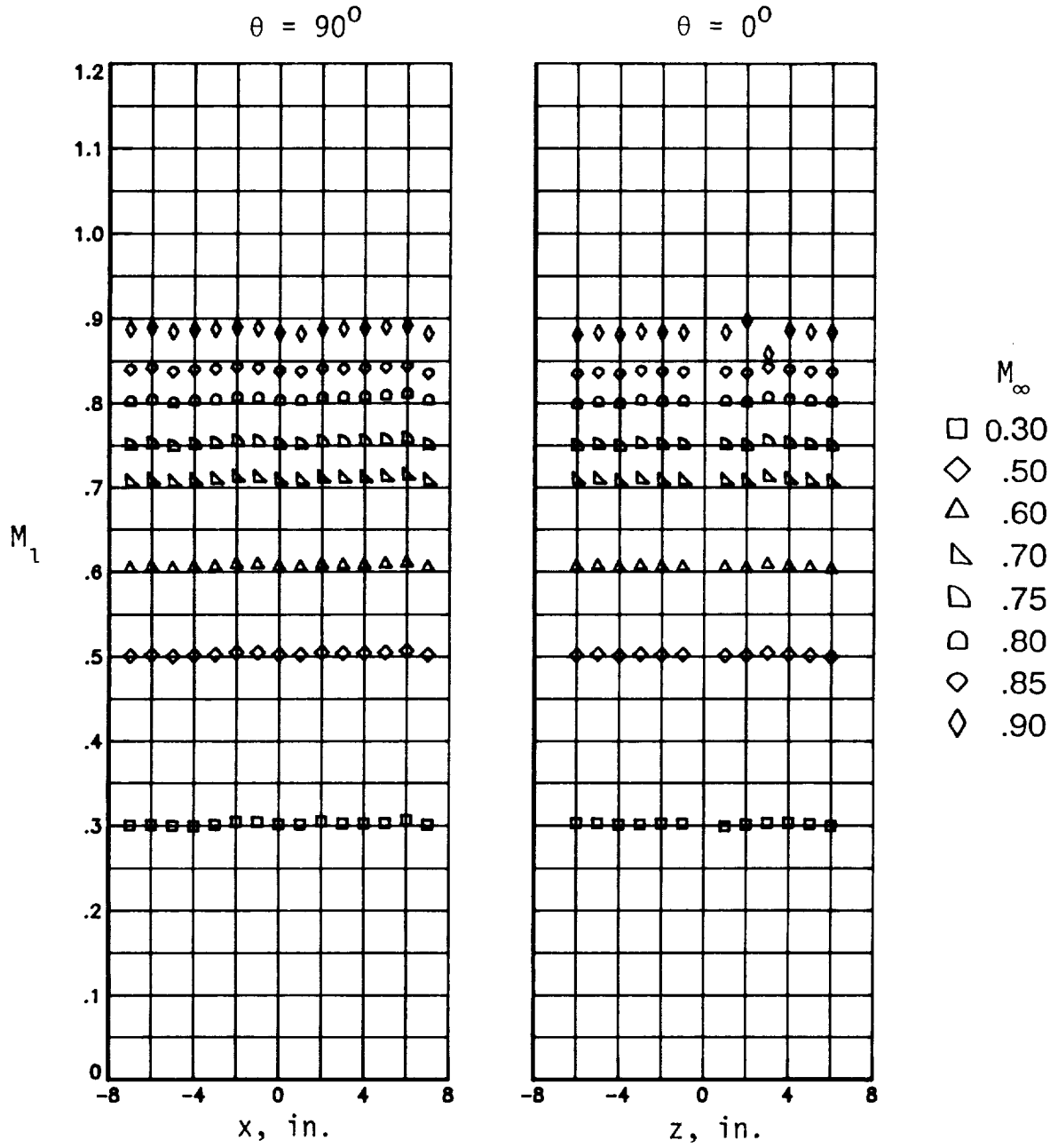

(c) $R = 40 \times 10^6$ per foot.

Figure 19. Continued.

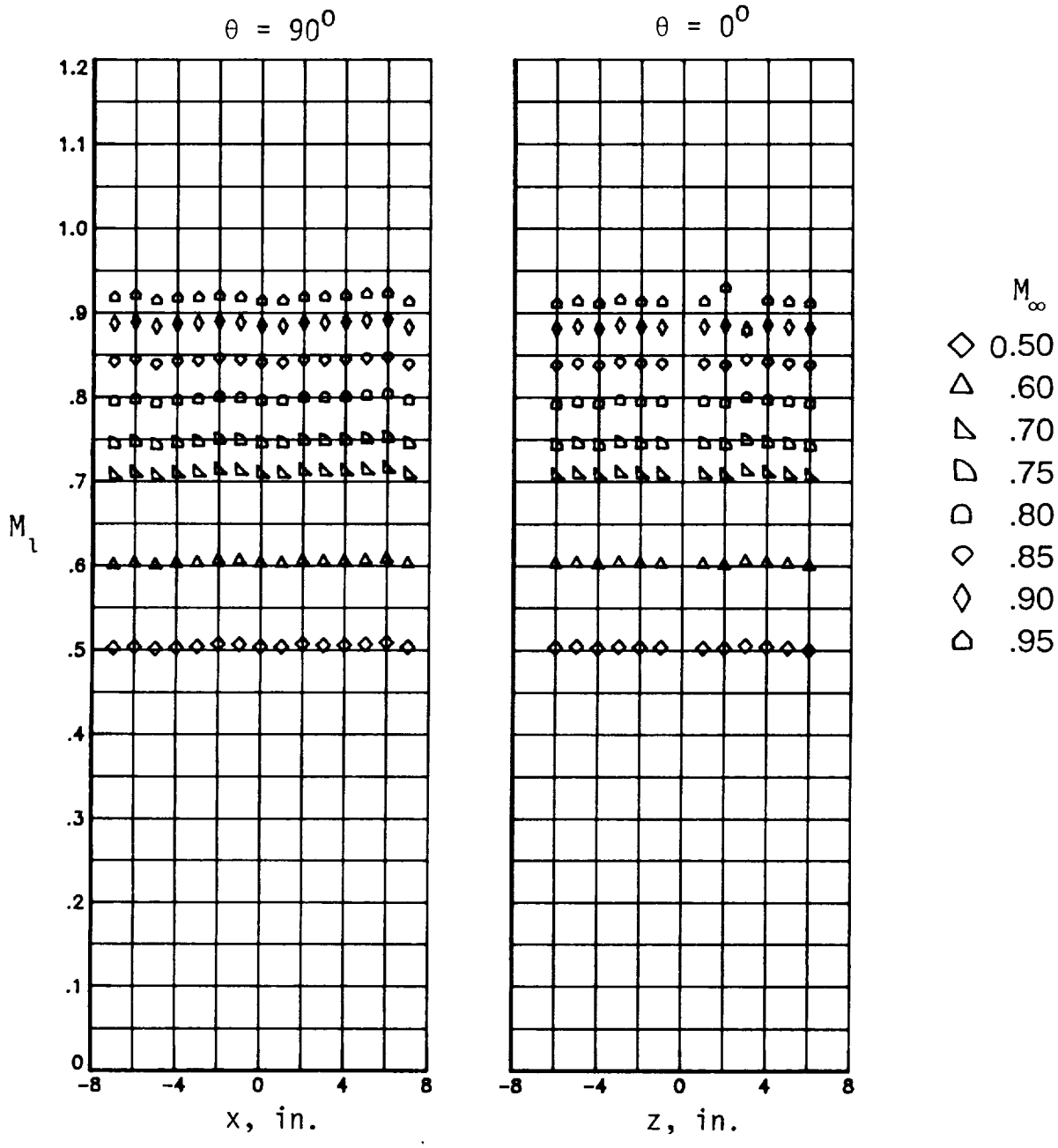

(d) $R = 60 \times 10^6$ per foot.

Figure 19. Continued.

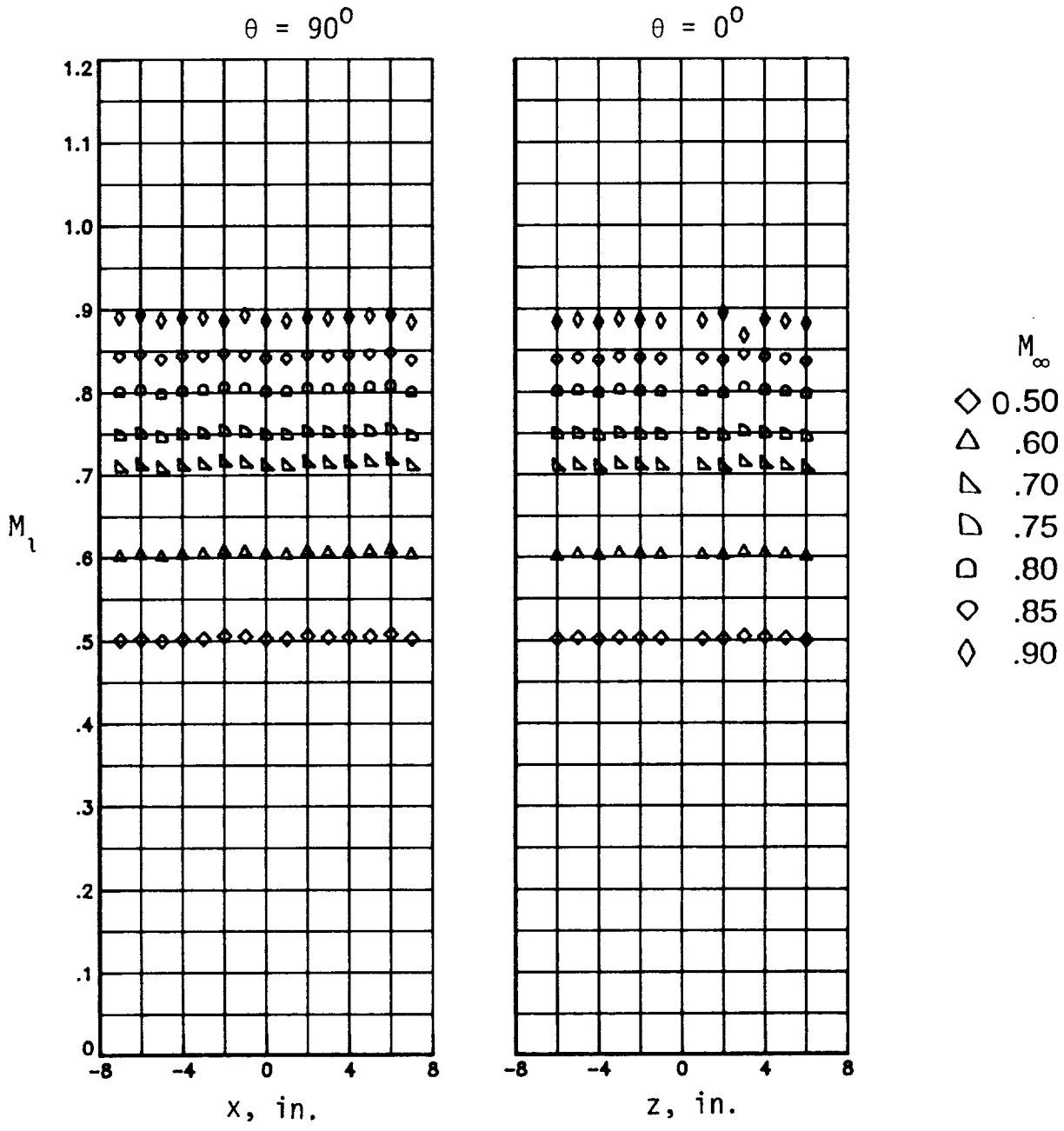

(e) $R = 80 \times 10^6$ per foot.

Figure 19. Continued.

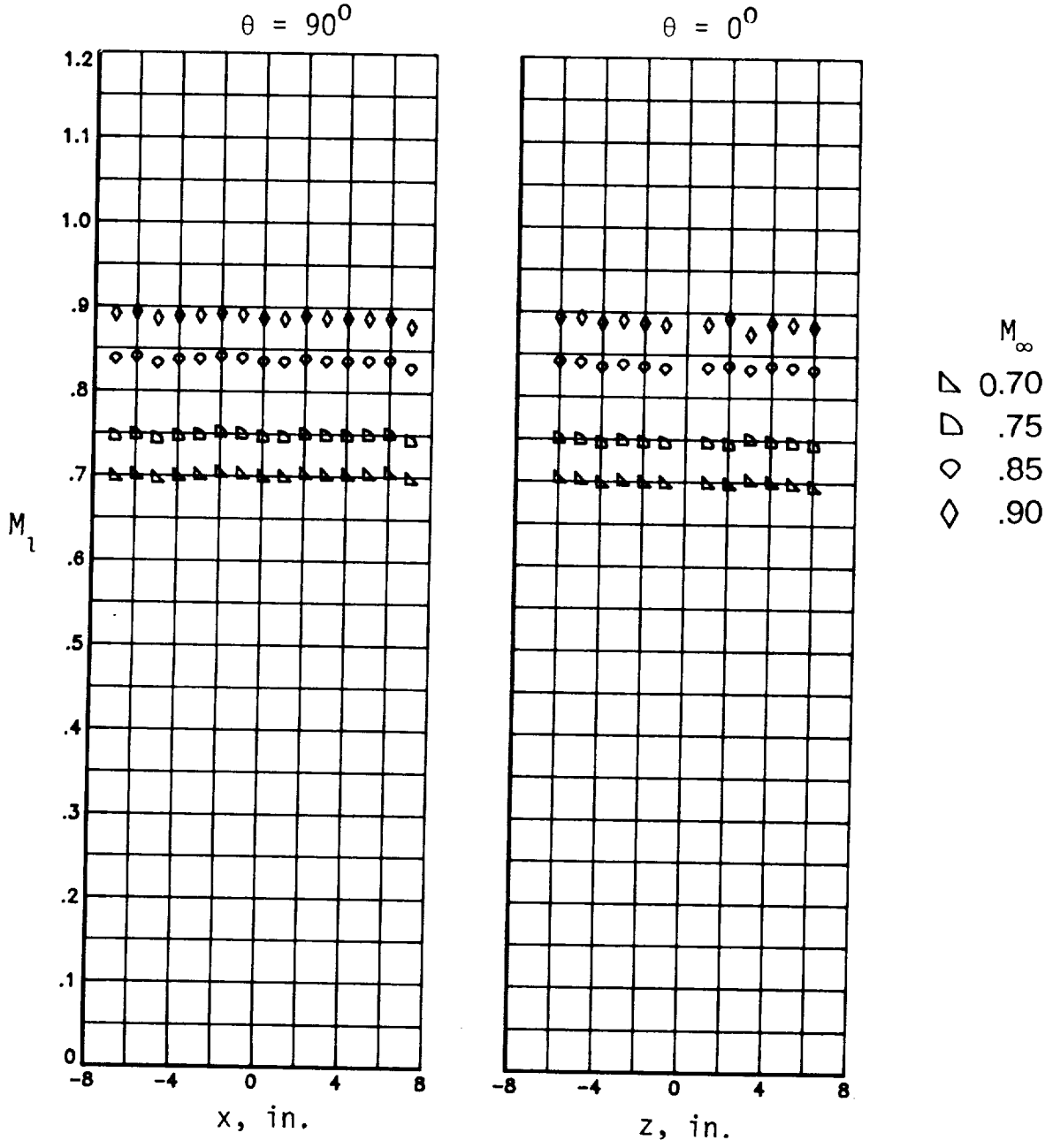

(f) $R = 100 \times 10^6$ per foot.

Figure 19. Concluded.

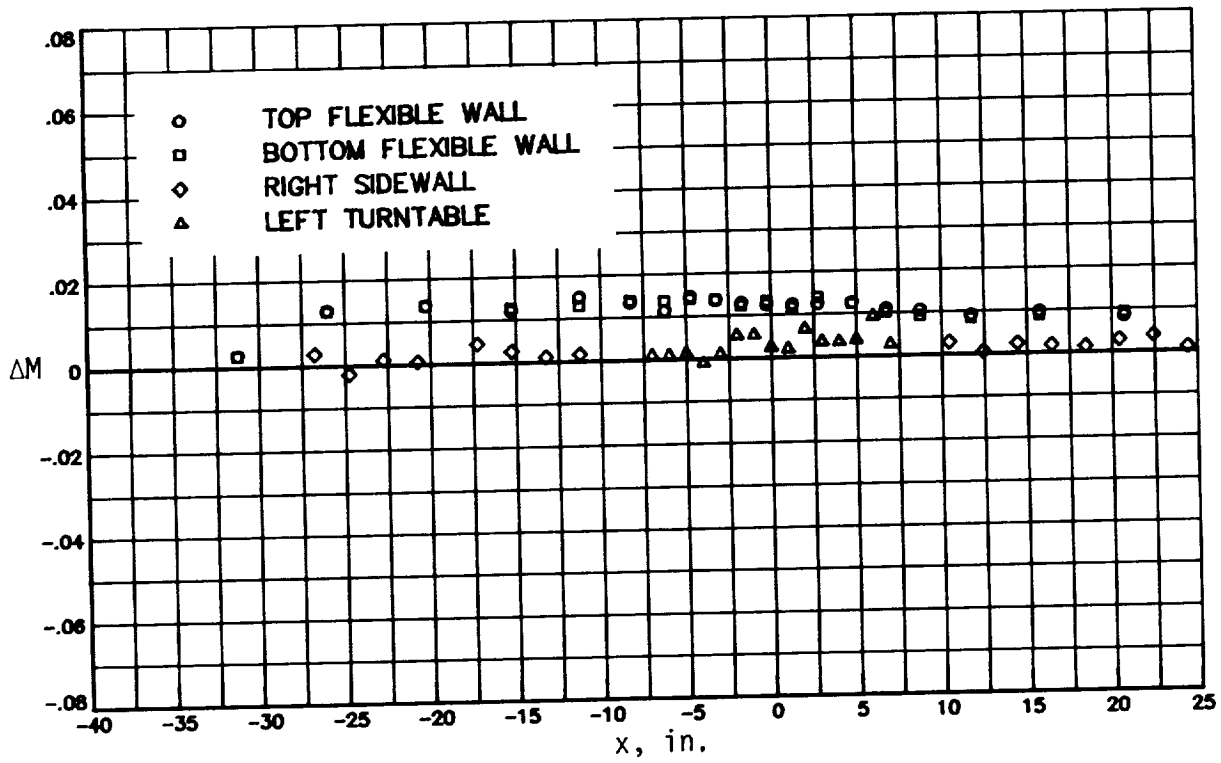

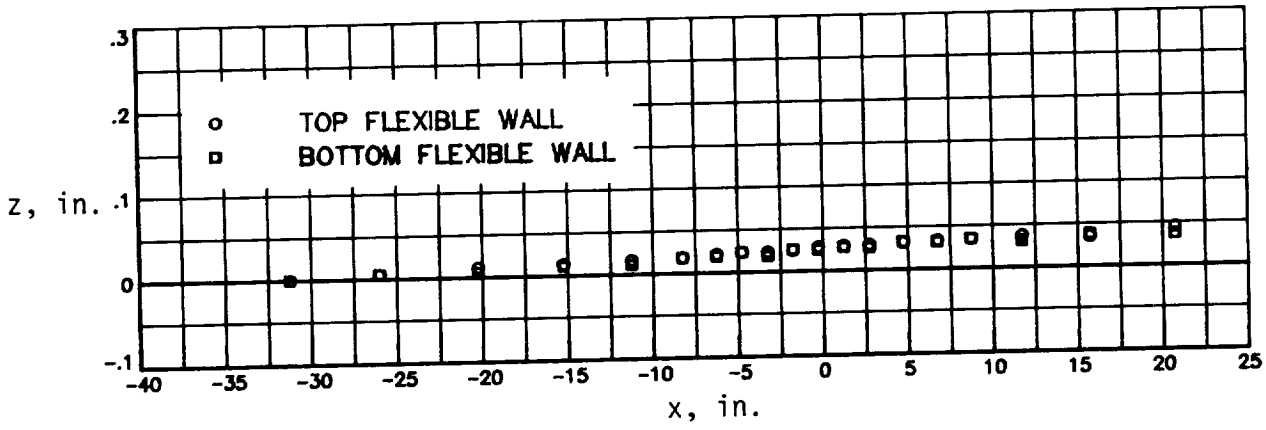

Figure 20. Test section flexible wall shape and wall Mach number distribution for $R = 10 \times 10^6$ per foot and $M_\infty = 0.20$.

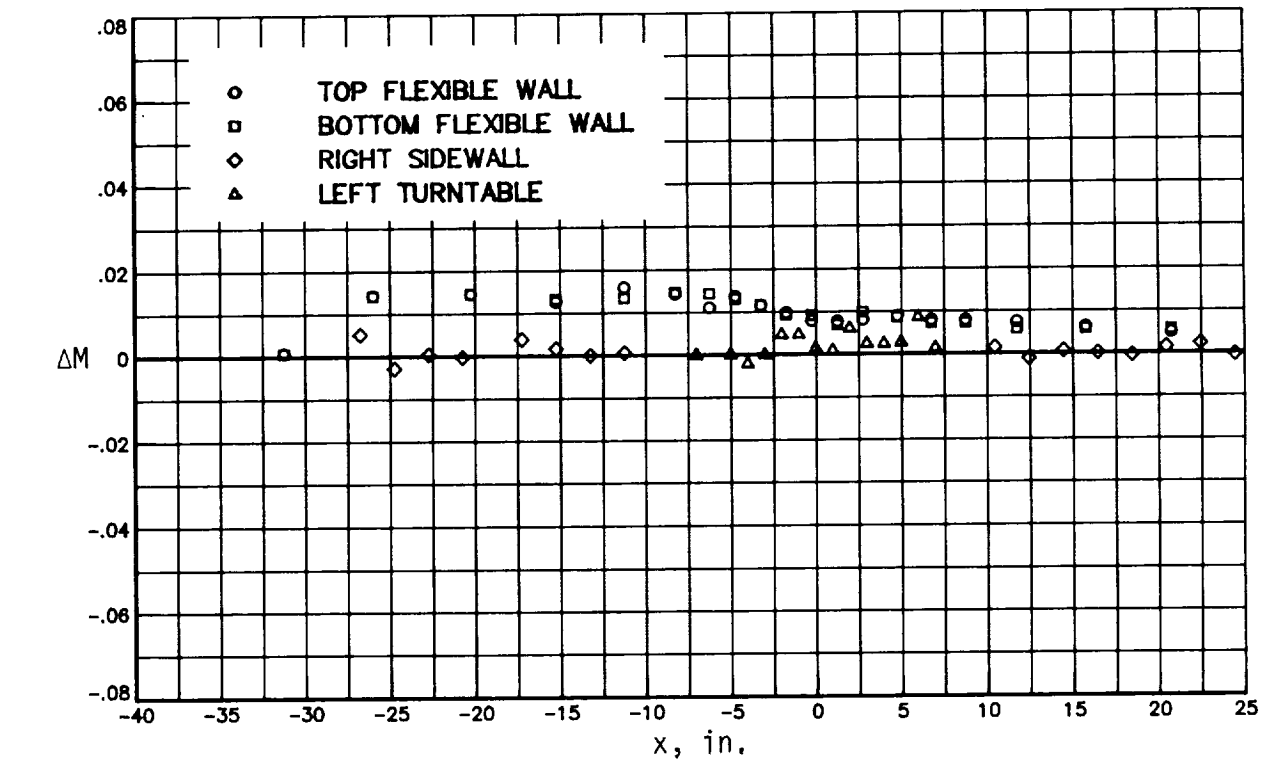

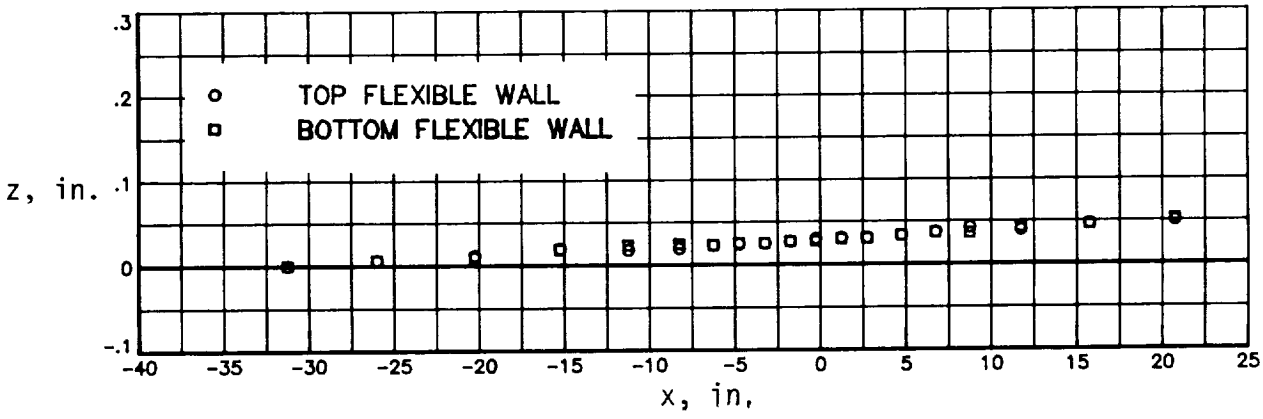

(a) $M_\infty = 0.20$.

Figure 21. Test section flexible wall shape and wall Mach number distribution for $R = 20 \times 10^6$ per foot.

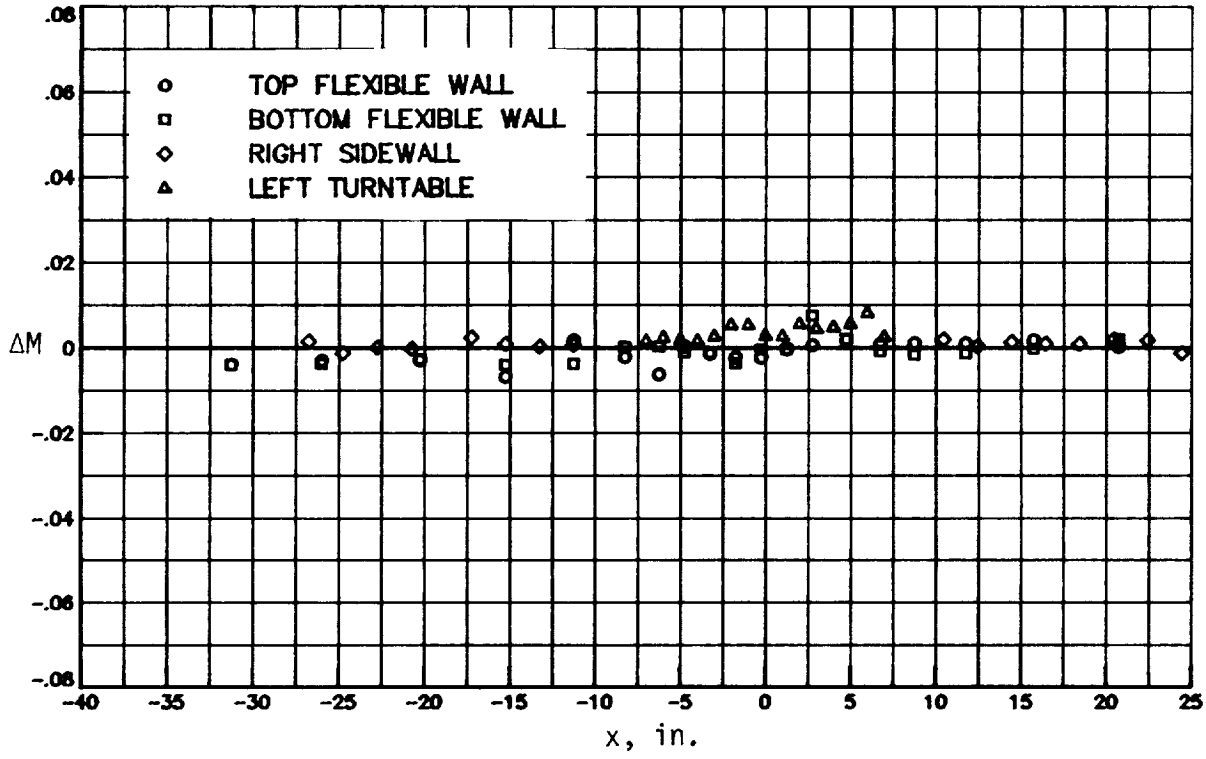

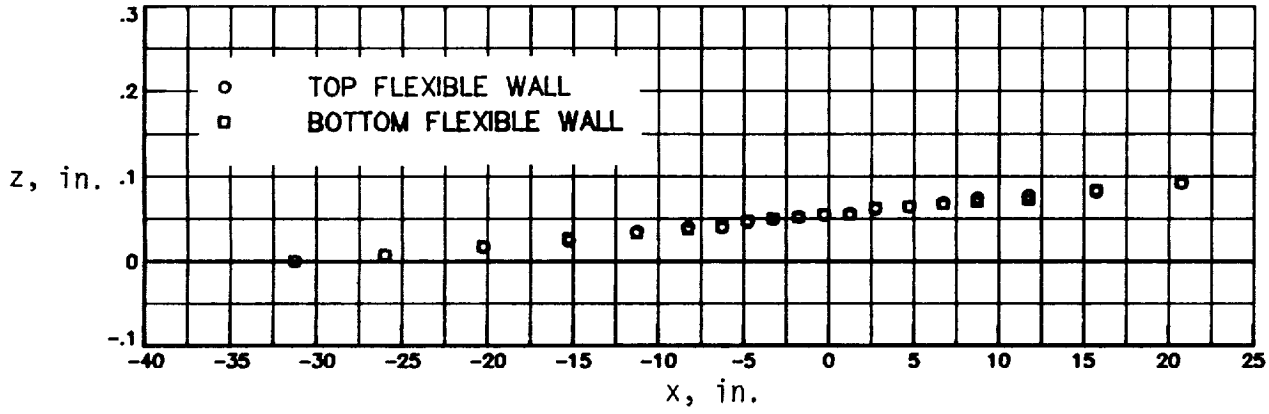

(b) $M_\infty = 0.50$.

Figure 21. Continued.

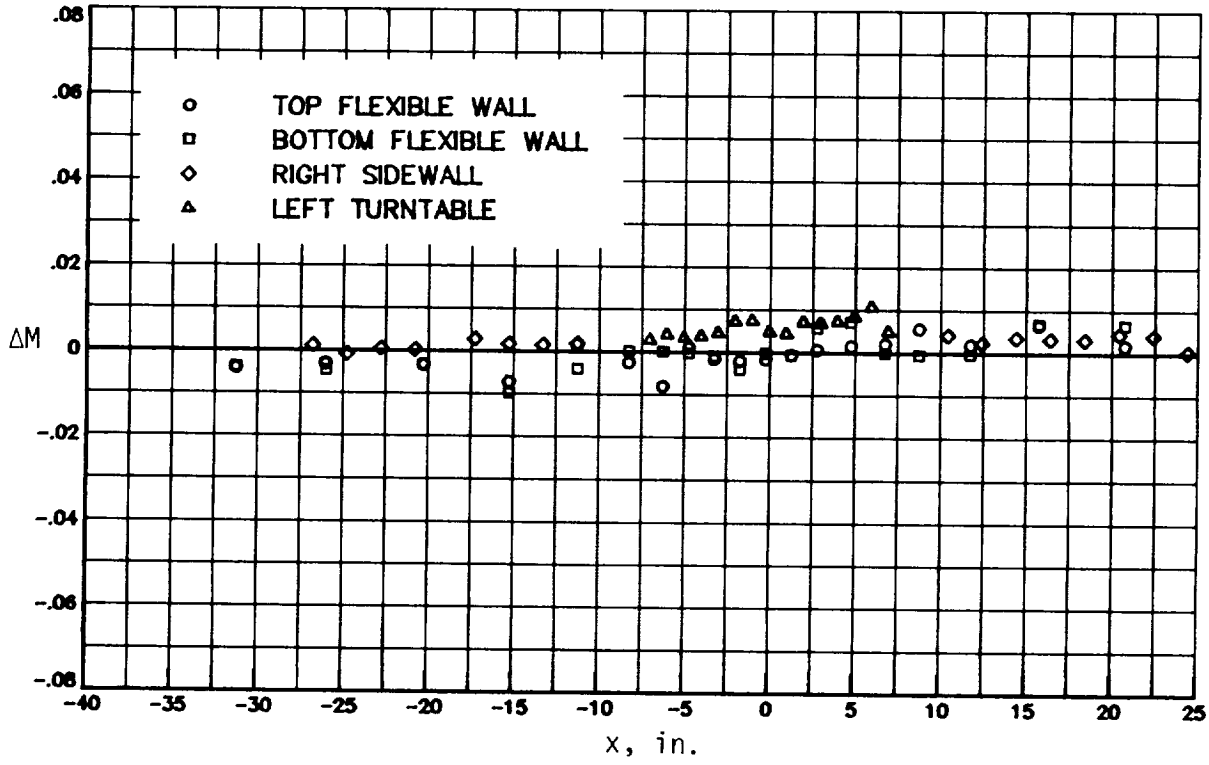

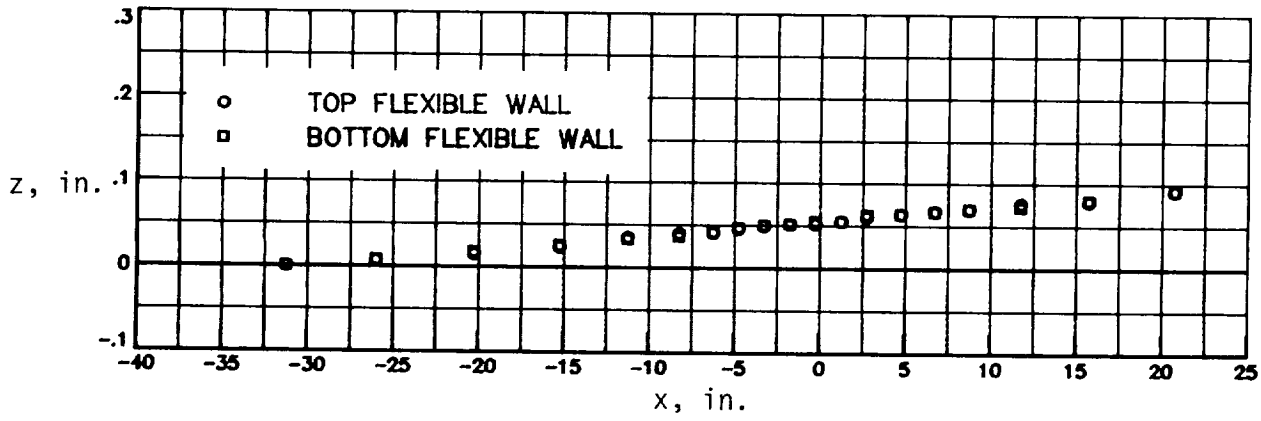

(c) $M_\infty = 0.60$.

Figure 21. Continued.

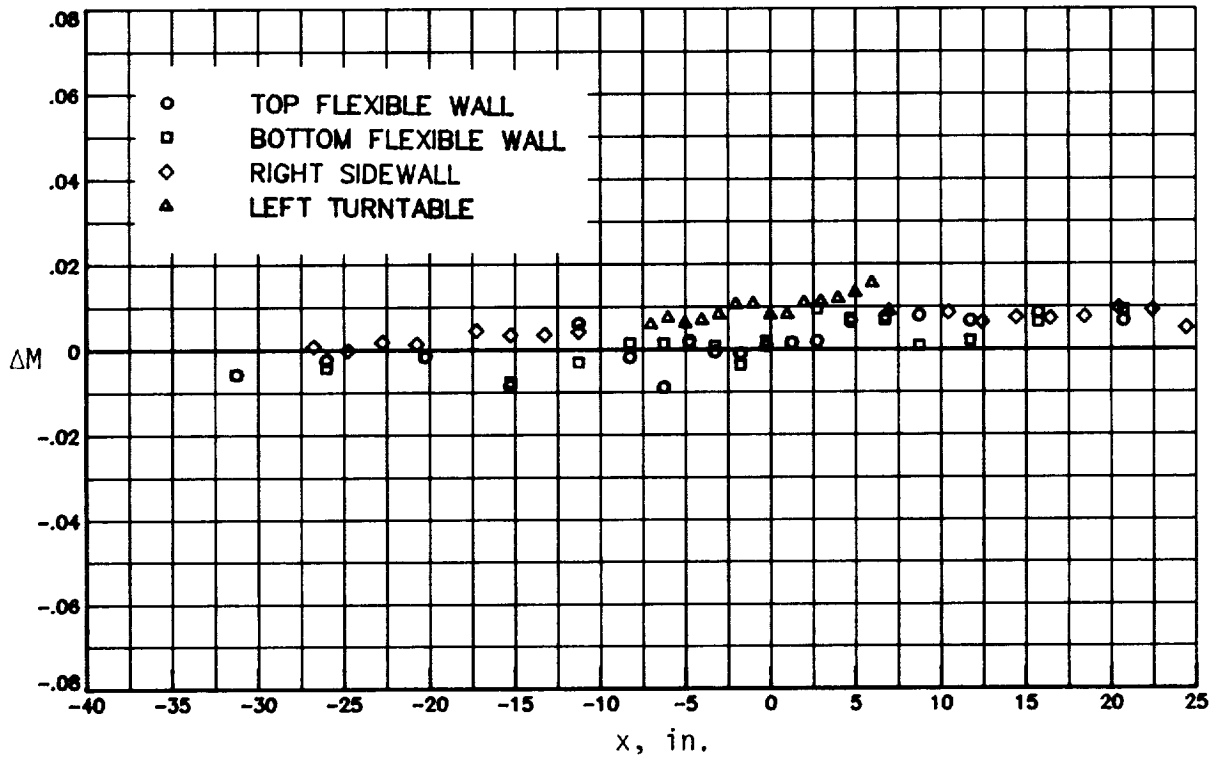

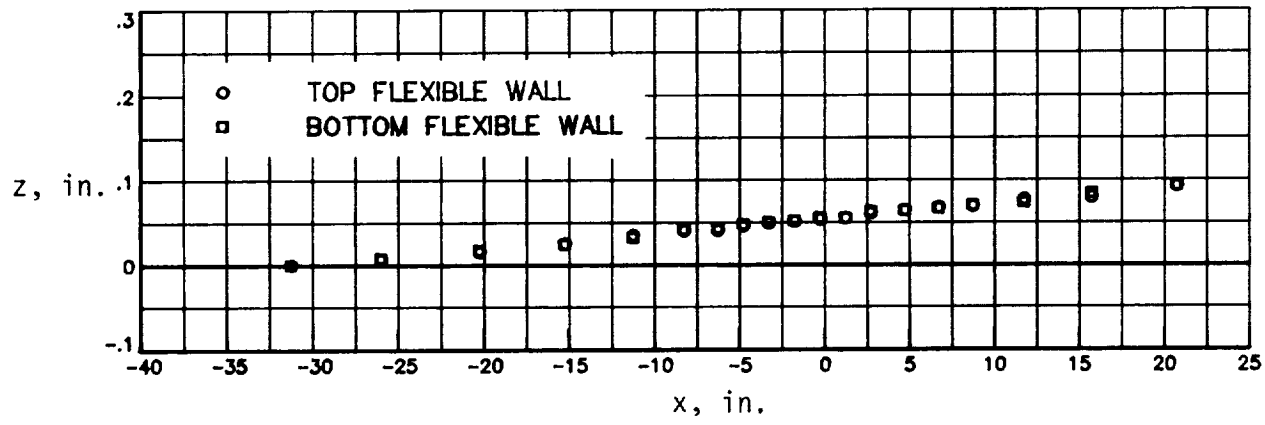

(d) $M_\infty = 0.70$.

Figure 21. Continued.

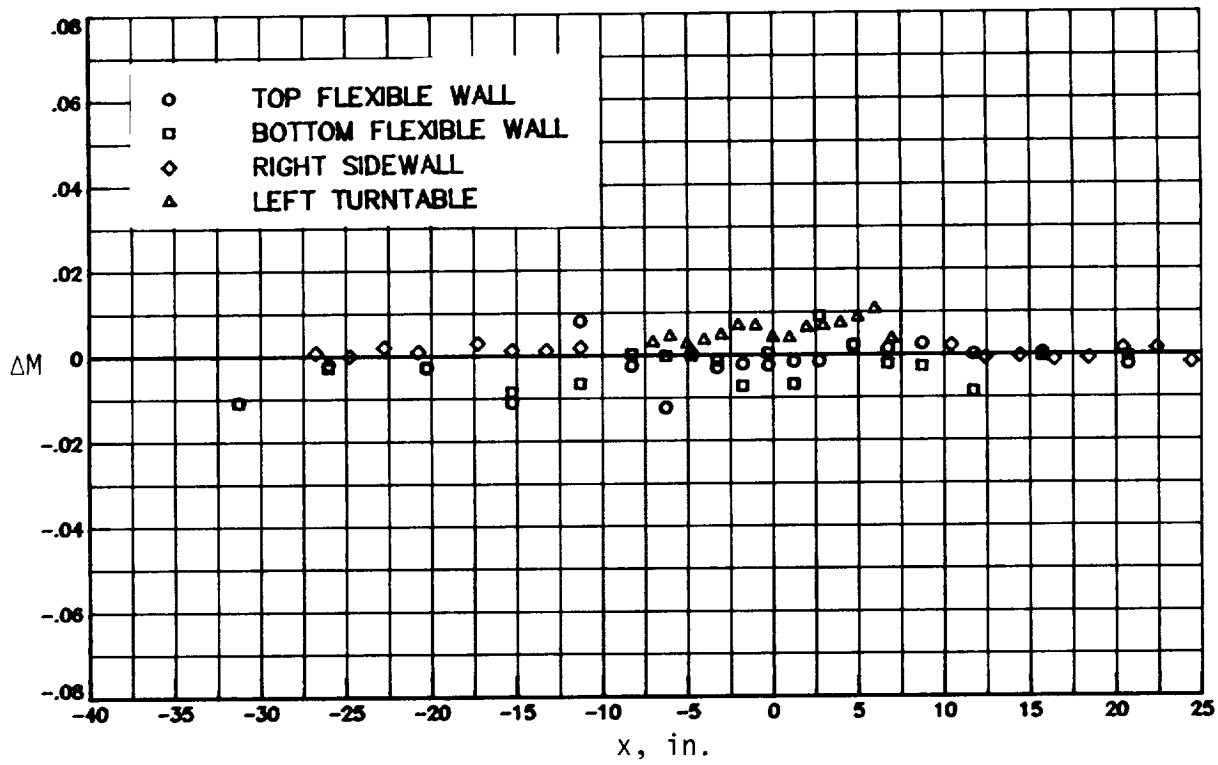

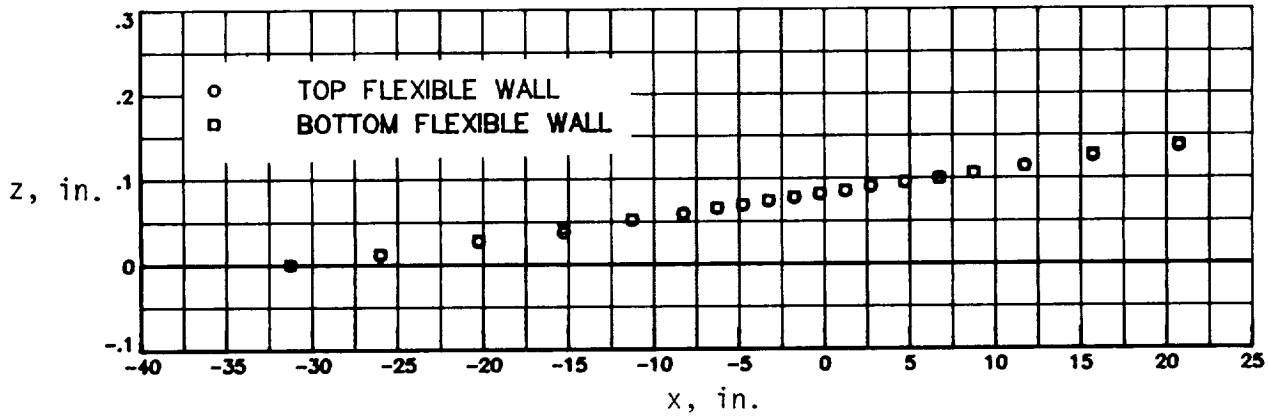

(e) $M_\infty = 0.75$.

Figure 21. Continued.

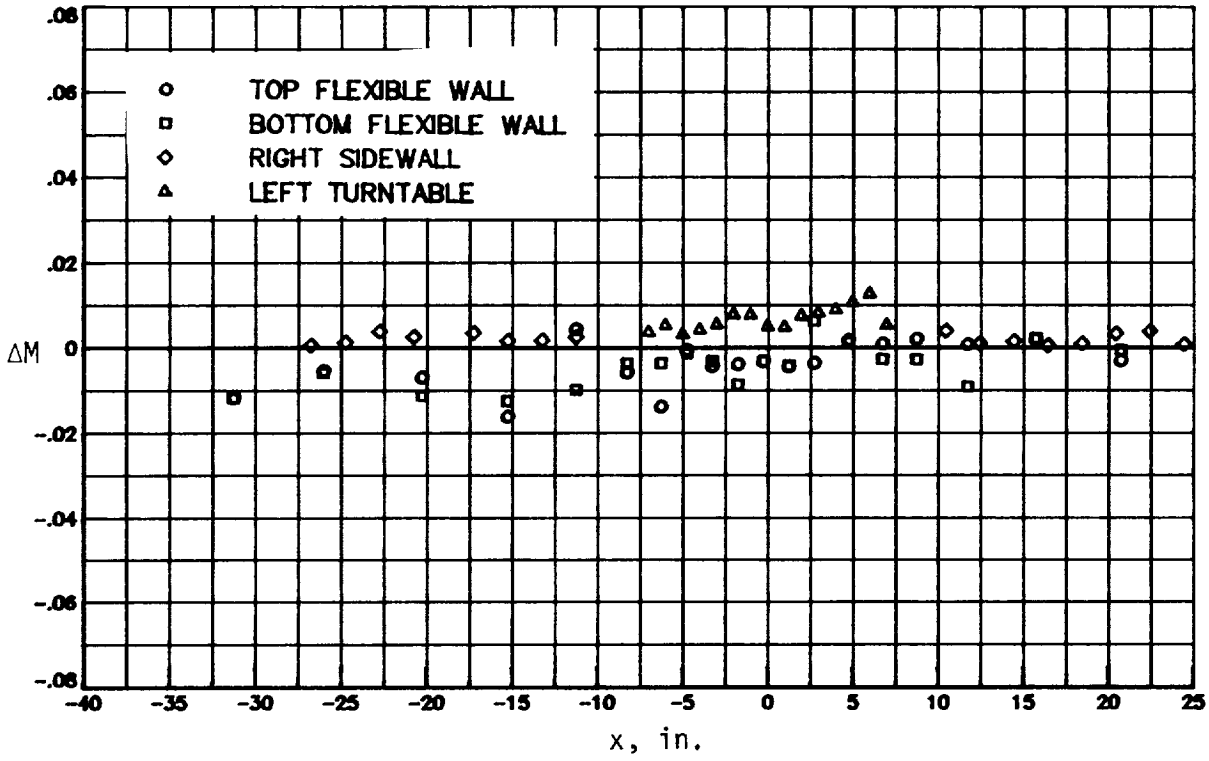

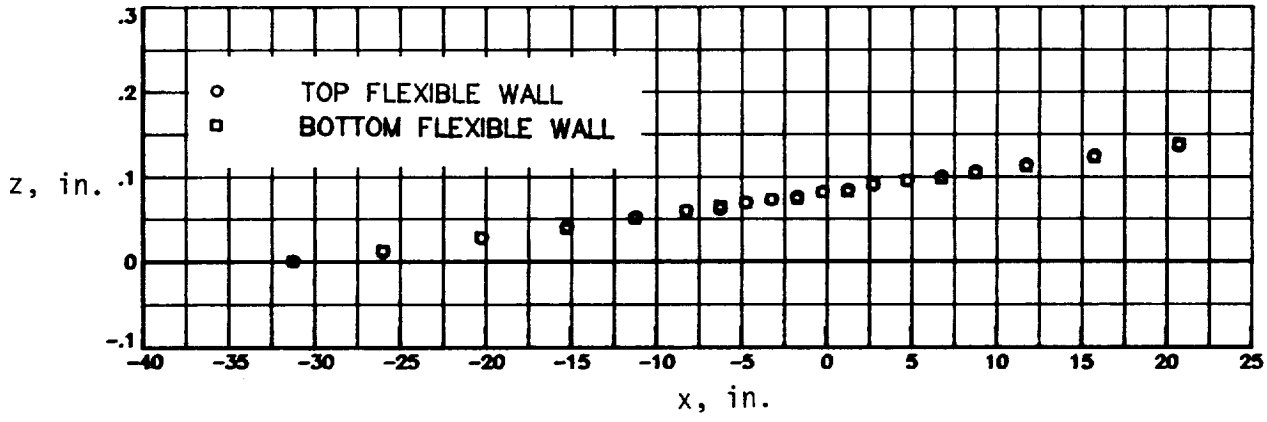

(f) $M_\infty = 0.80$.

Figure 21. Continued.

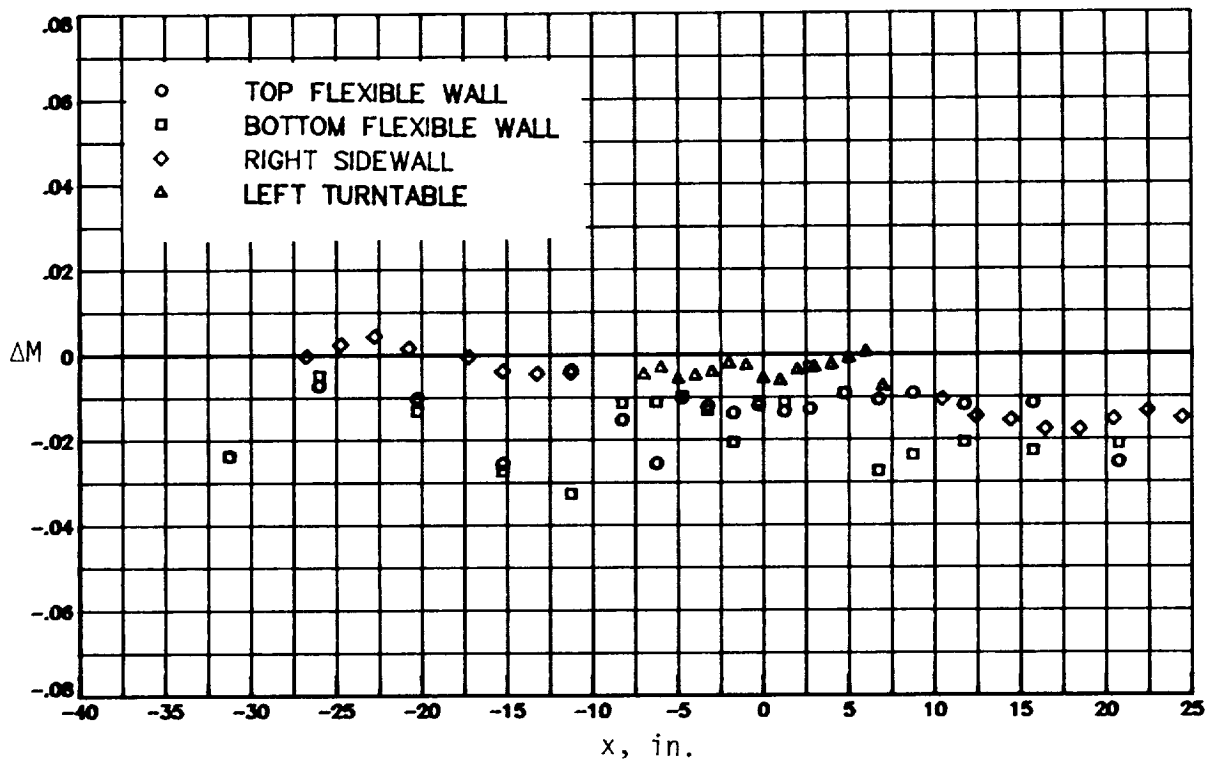

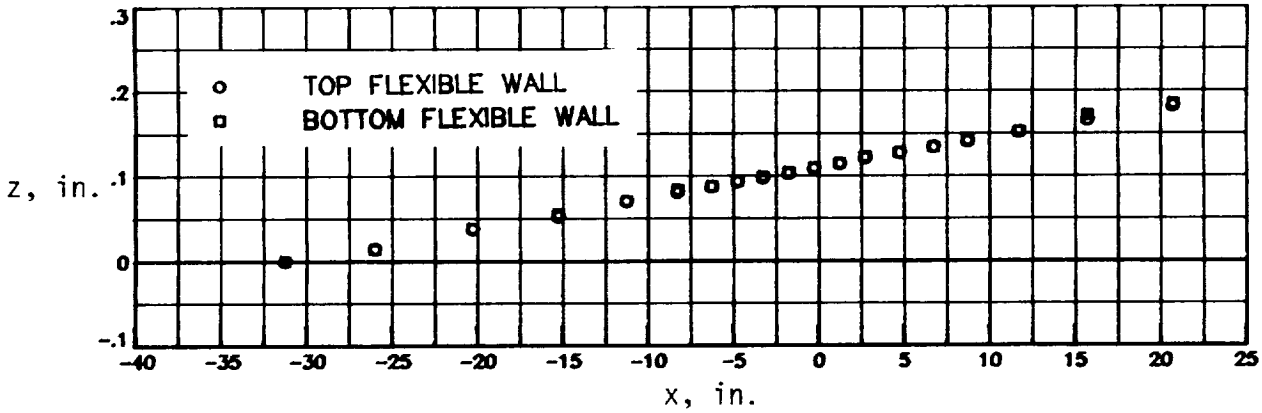

(g) $M_\infty = 0.85$.

Figure 21. Continued.

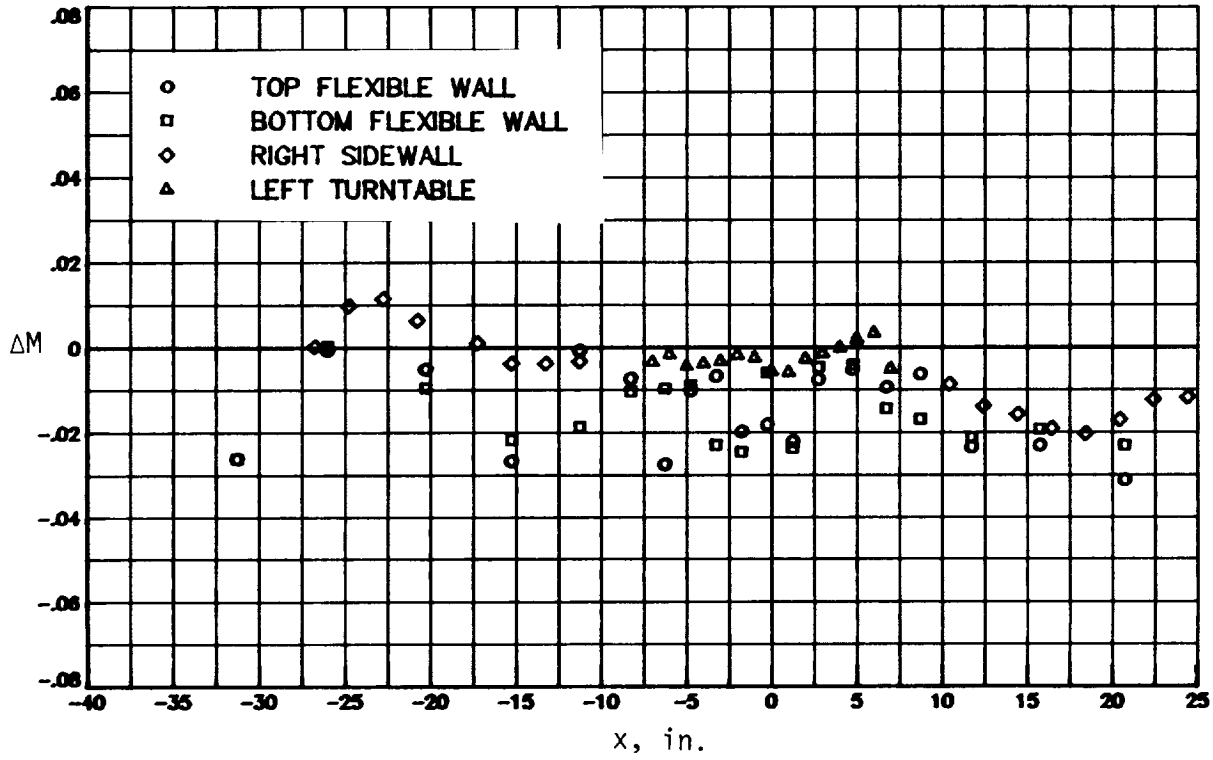

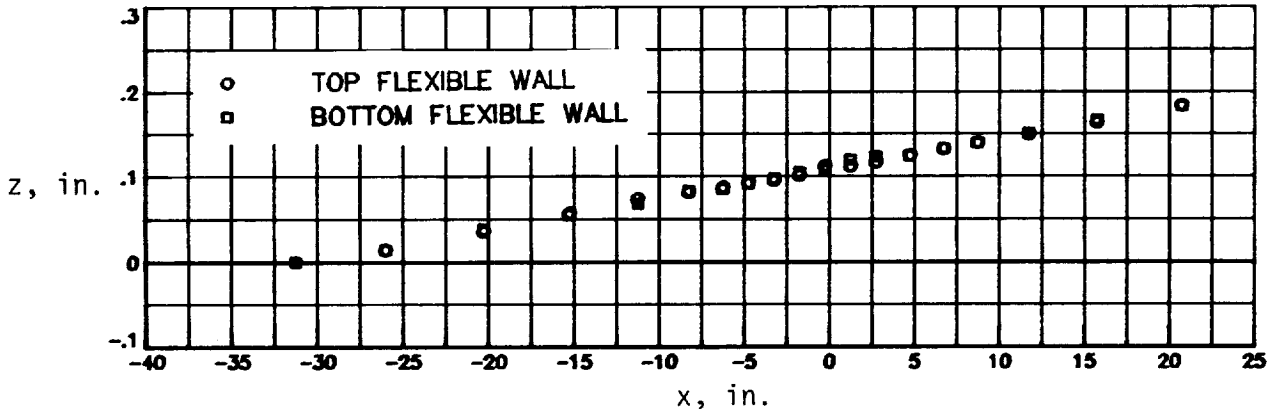

(h) $M_\infty = 0.90$.

Figure 21. Continued.

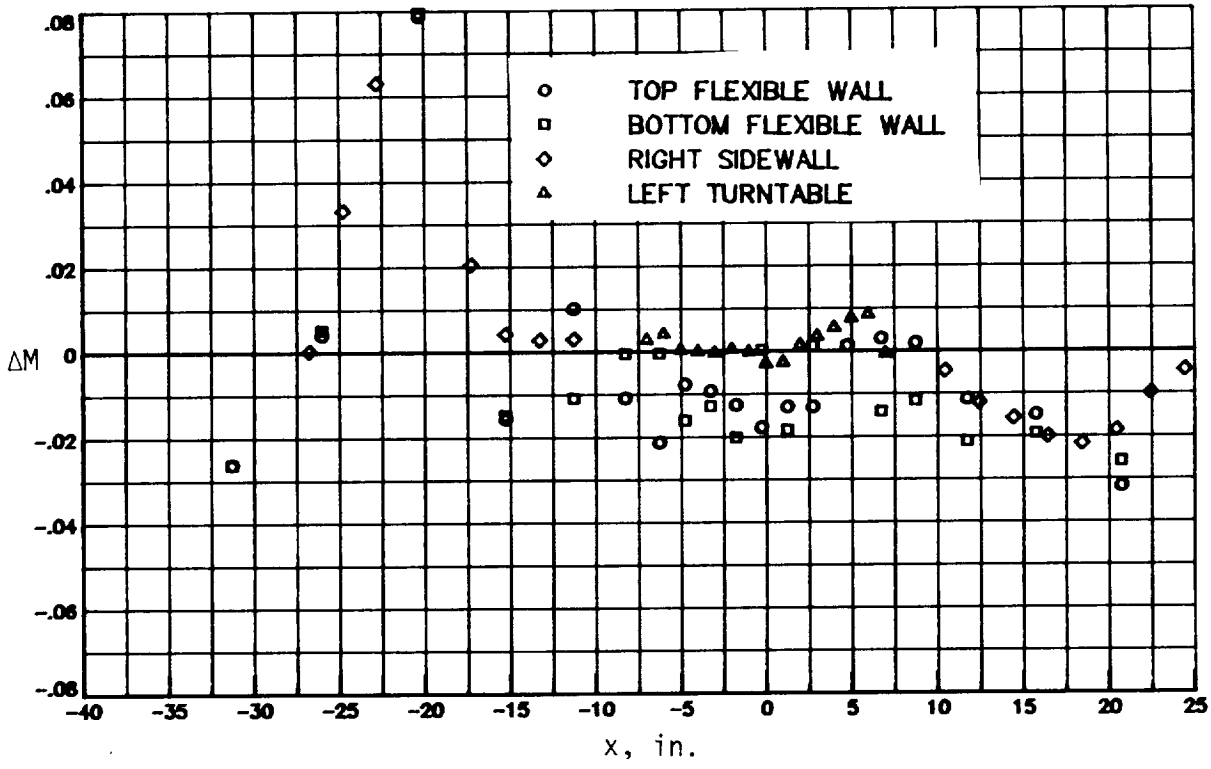

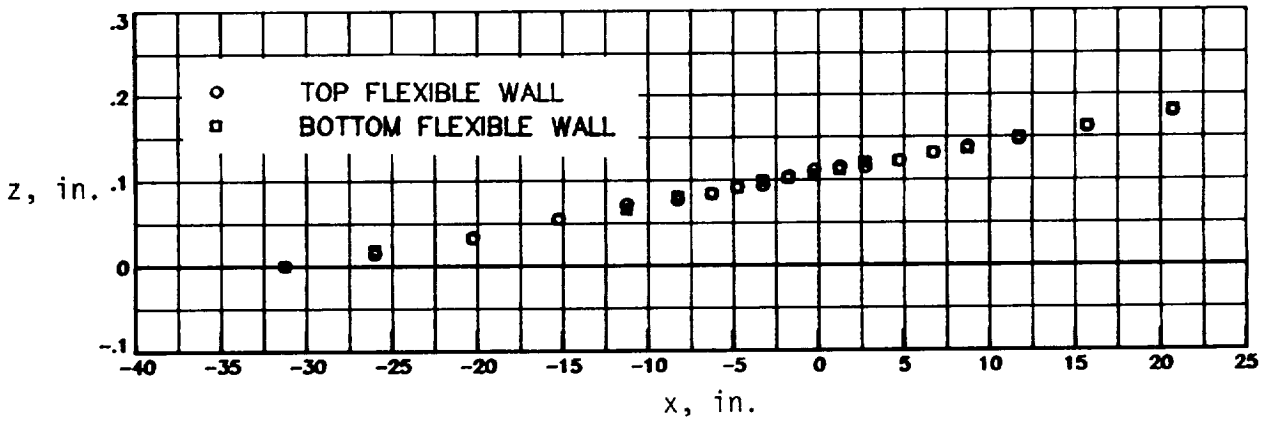

(i) $M_\infty = 0.95$.

Figure 21. Concluded.

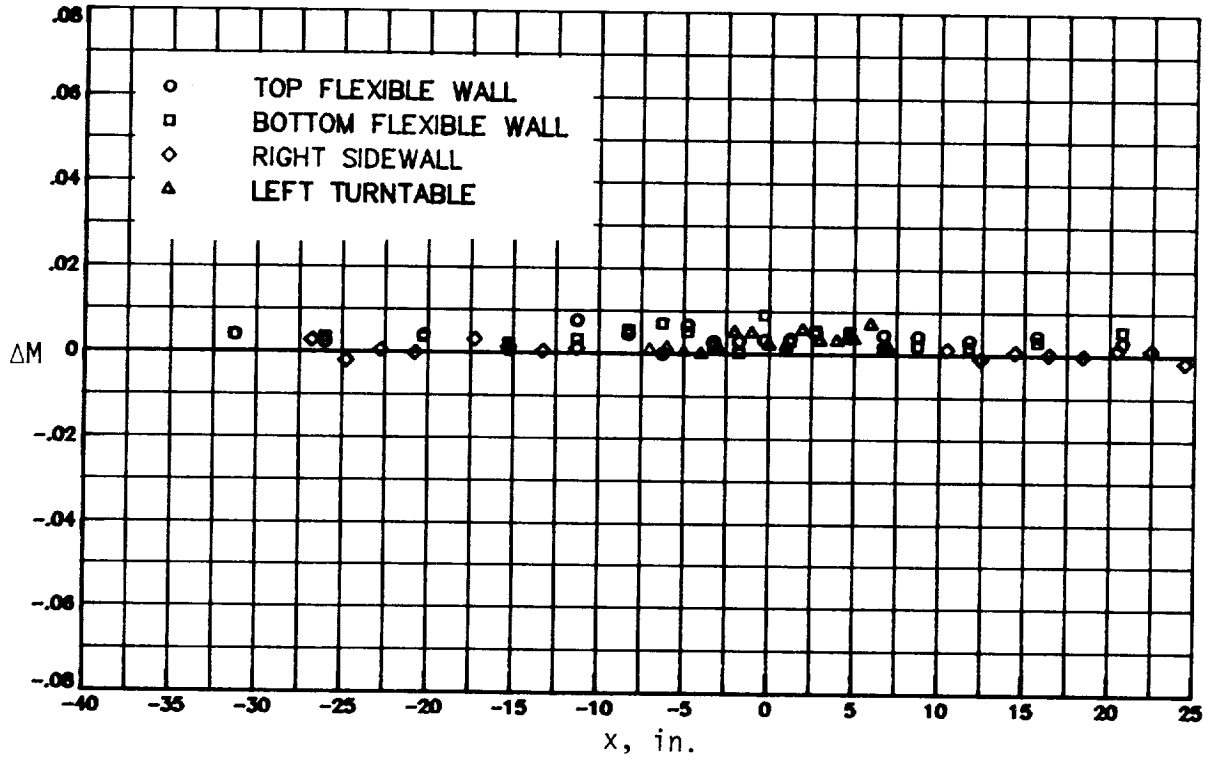

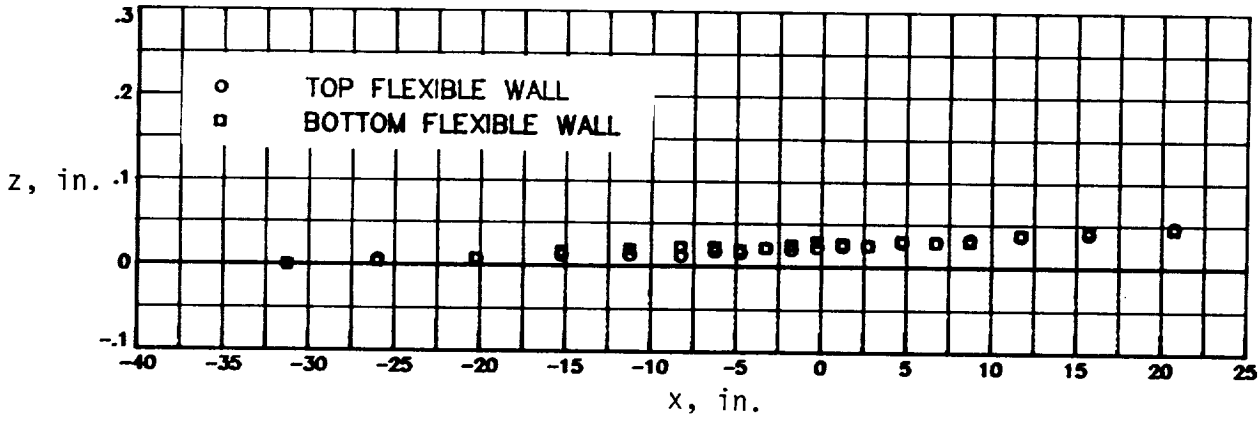

(a) $M_\infty = 0.30$.

Figure 22. Test section flexible wall shape and wall Mach number distribution for $R = 40 \times 10^6$ per foot.

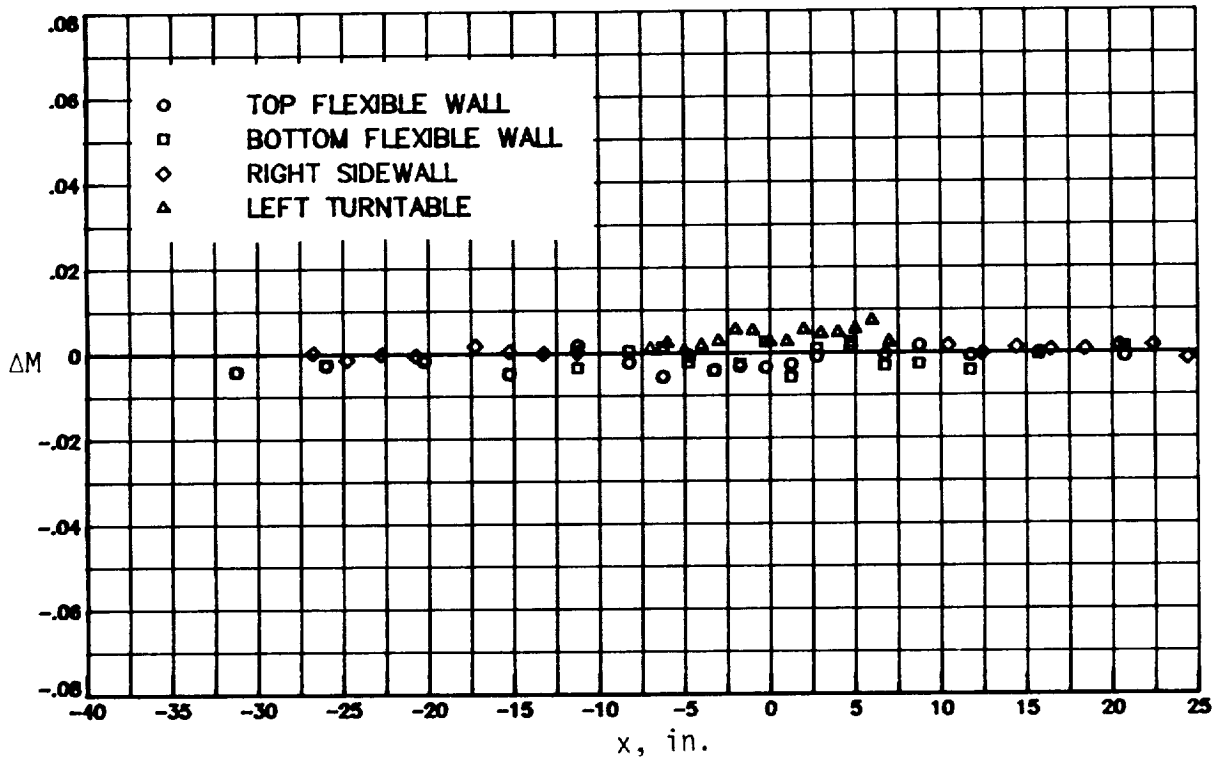

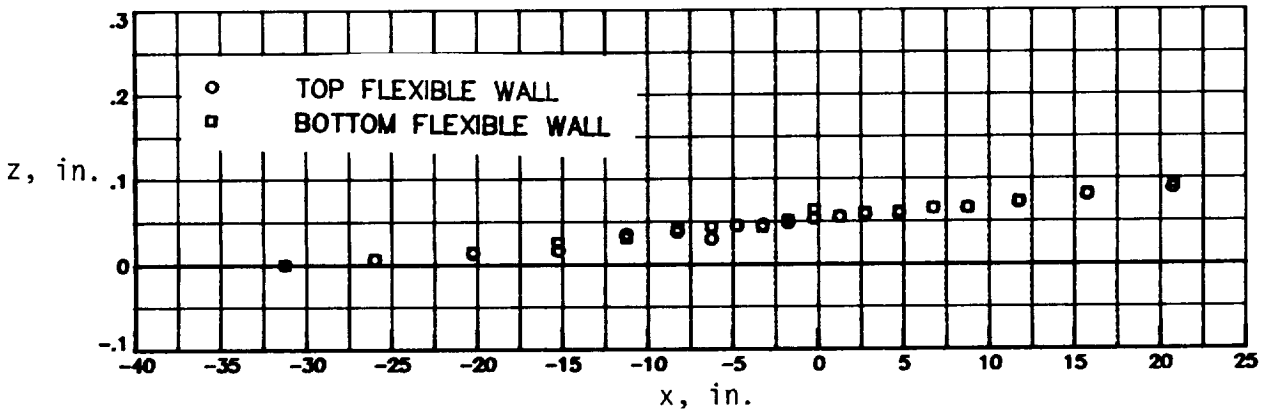

(b) $M_\infty = 0.50$.

Figure 22. Continued.

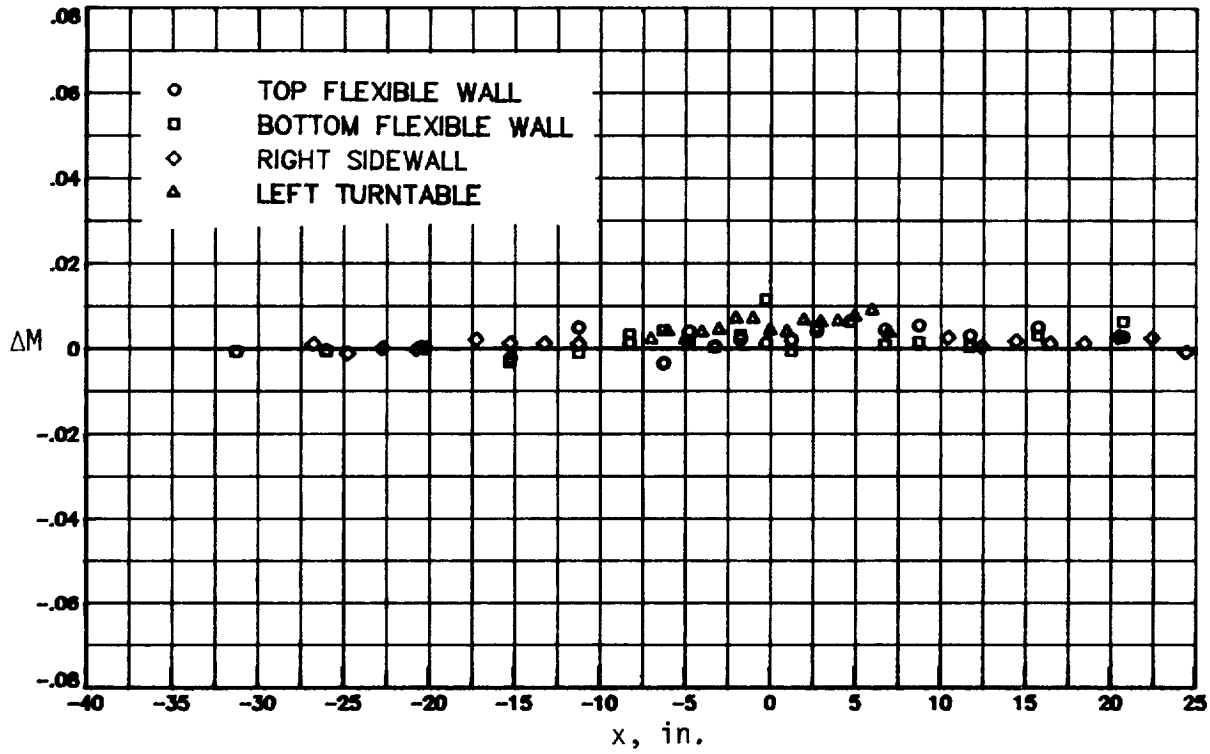

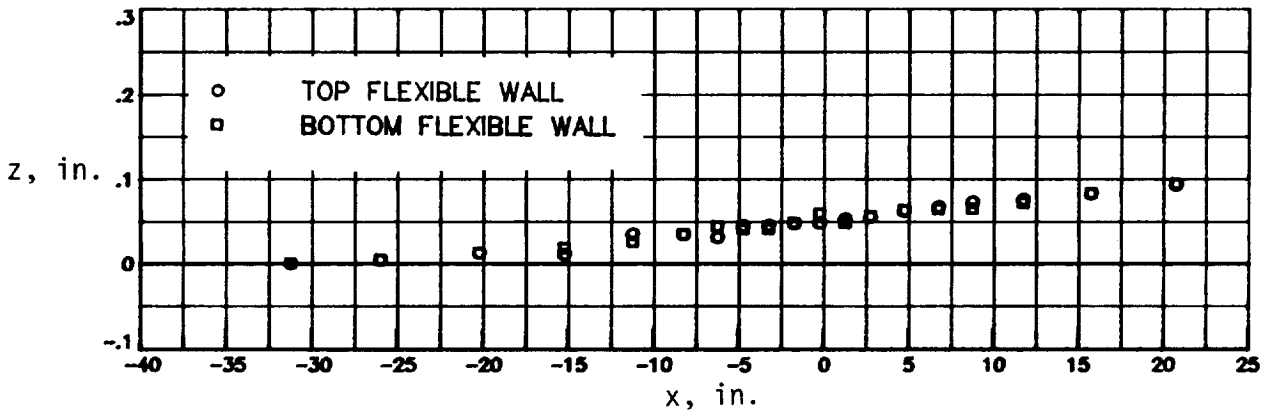

(c) $M_\infty = 0.60$.

Figure 22. Continued.

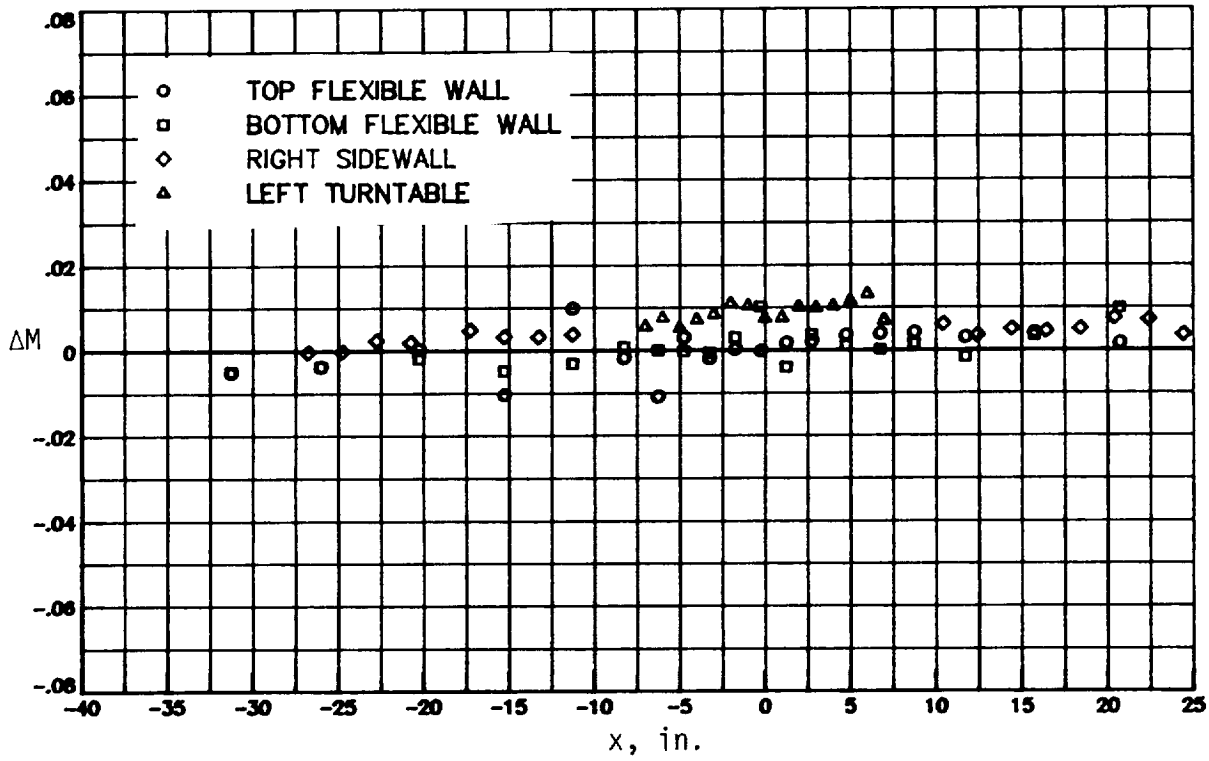

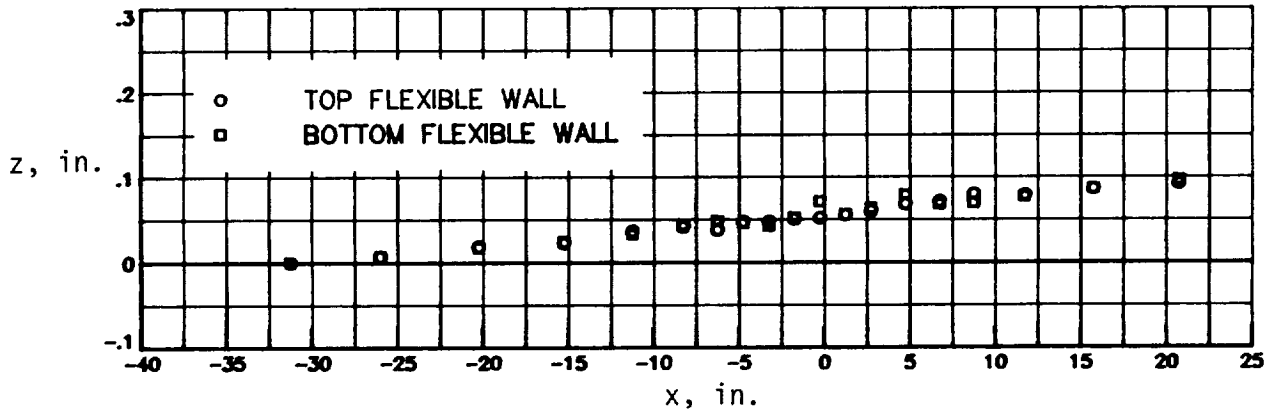

(d) $M_\infty = 0.70$.

Figure 22. Continued.

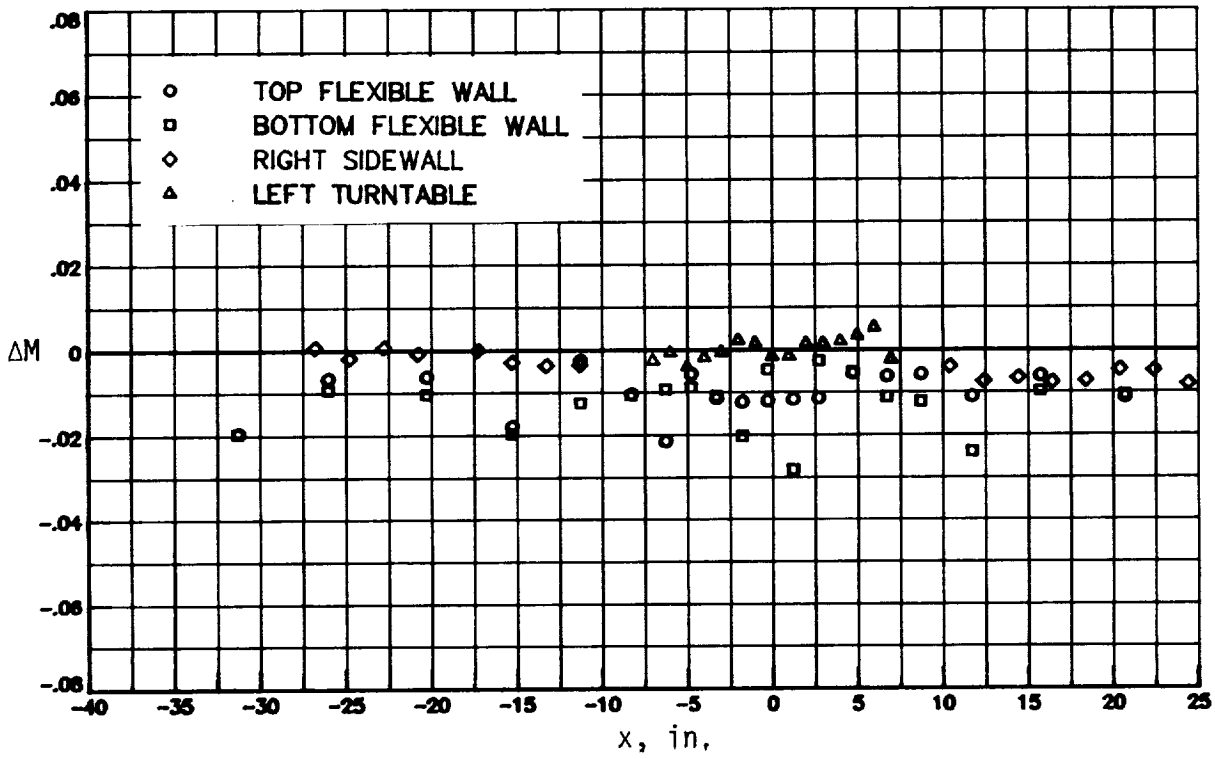

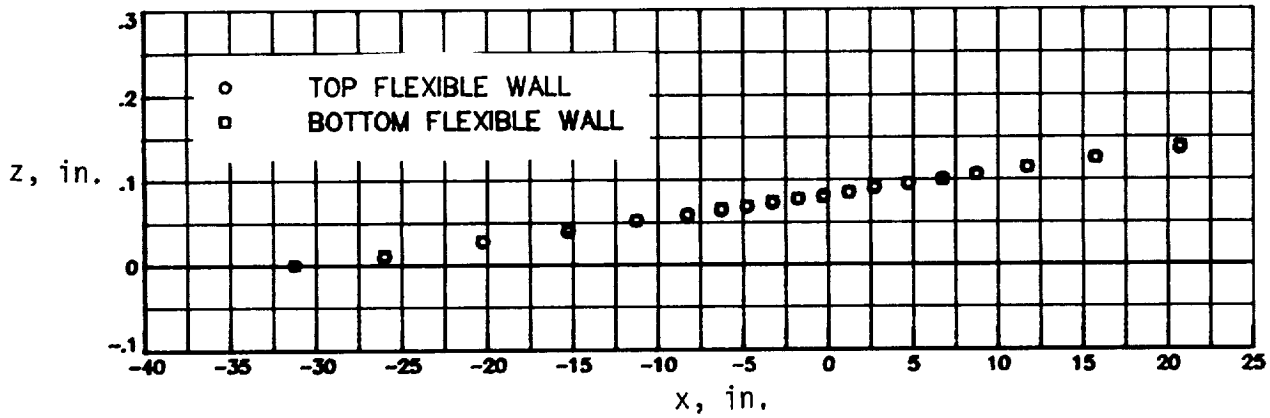

(e) $M_\infty = 0.75$.

Figure 22. Continued.

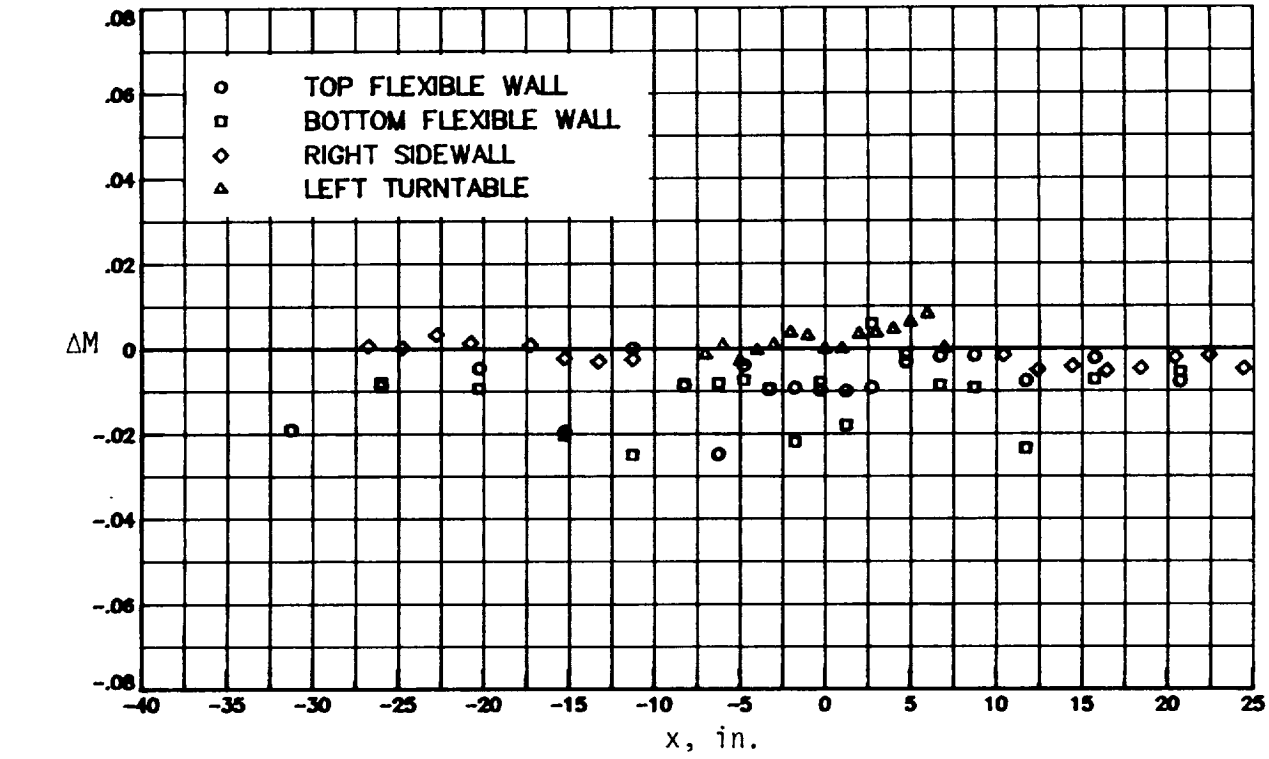

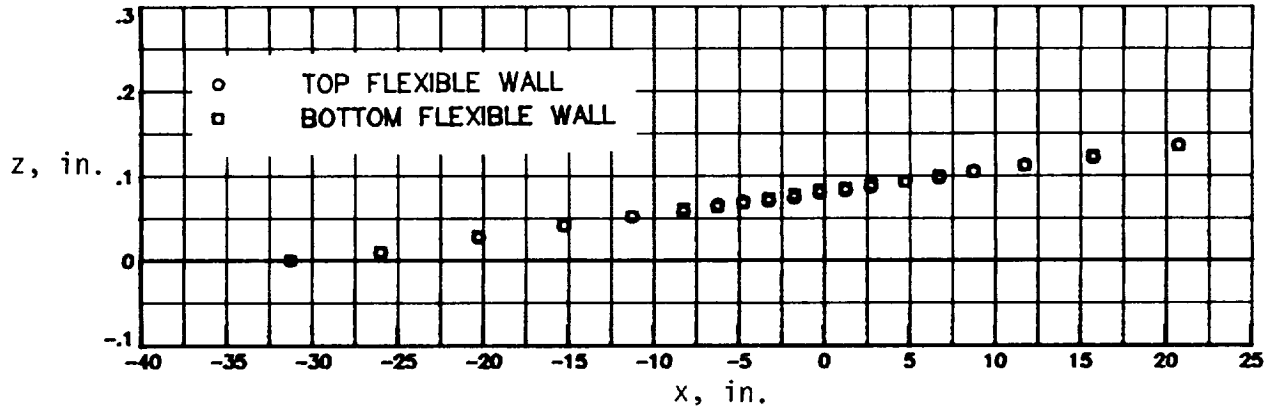

(f) $M_\infty = 0.80$.

Figure 22. Continued.

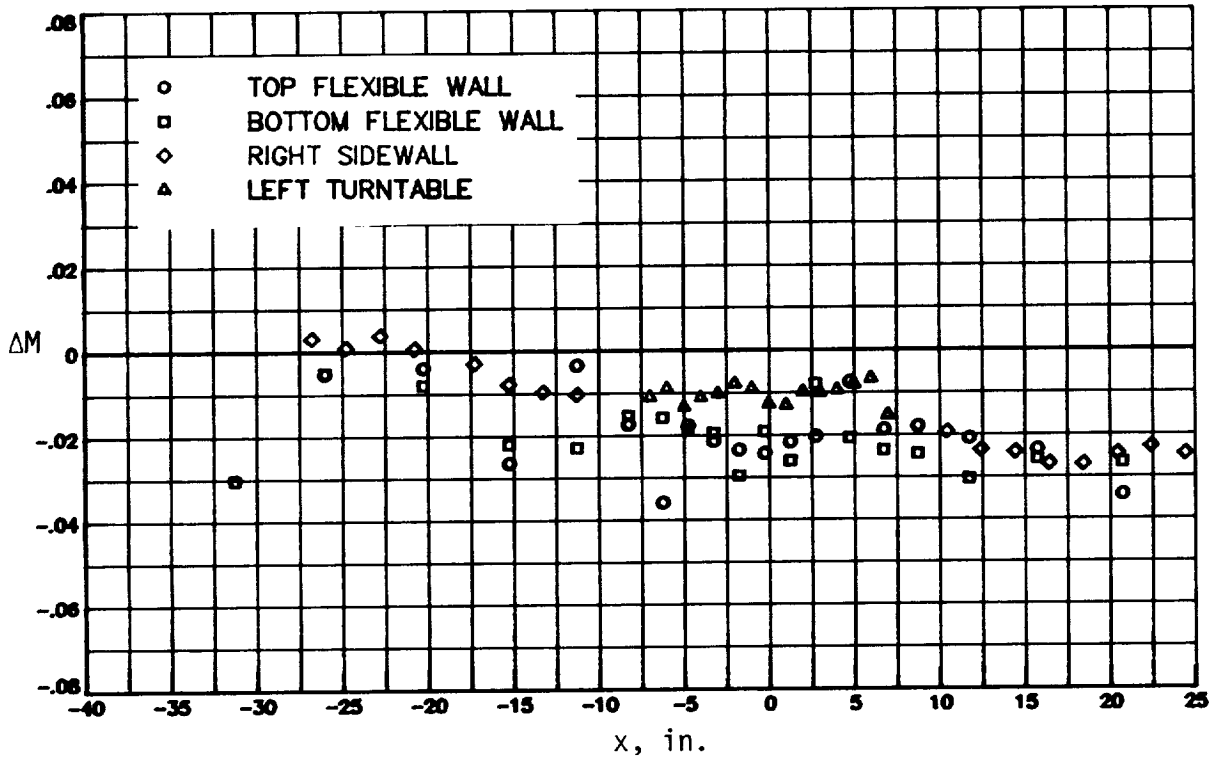

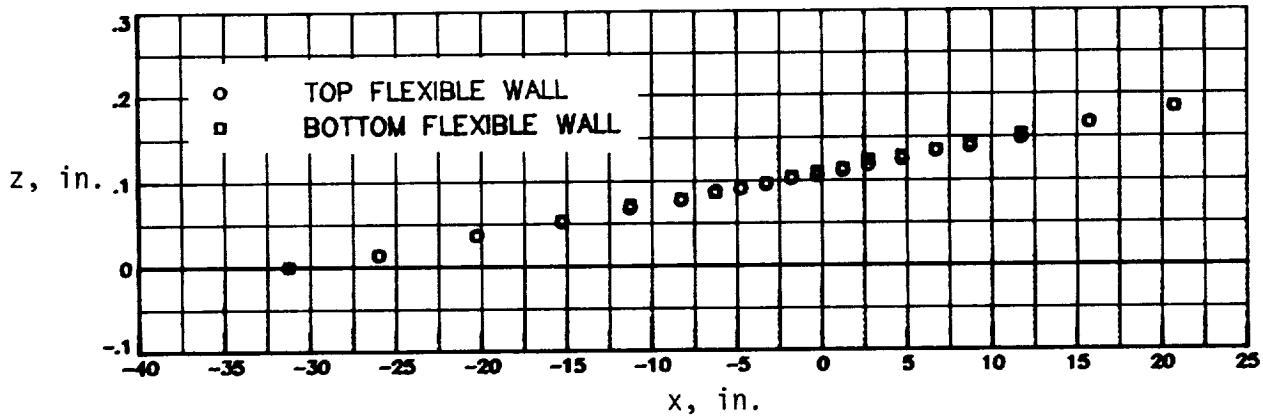

(g) $M_\infty = 0.85$.

Figure 22. Continued.

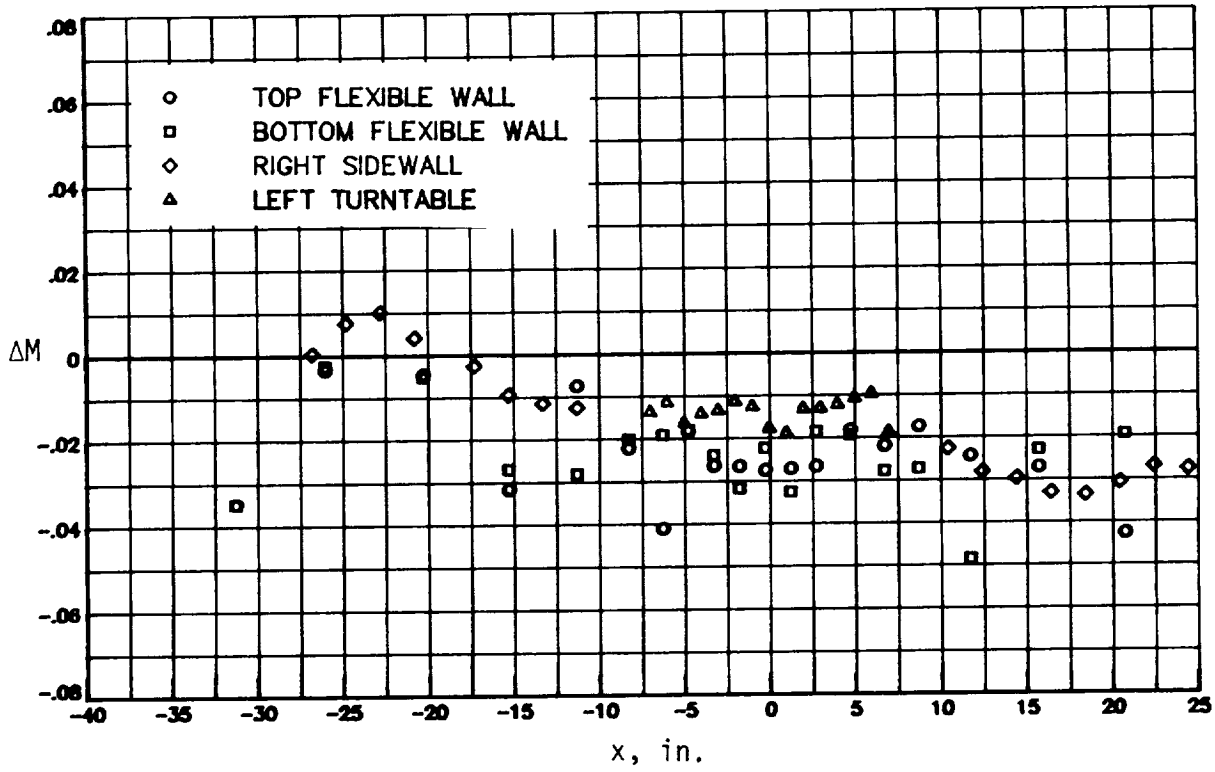

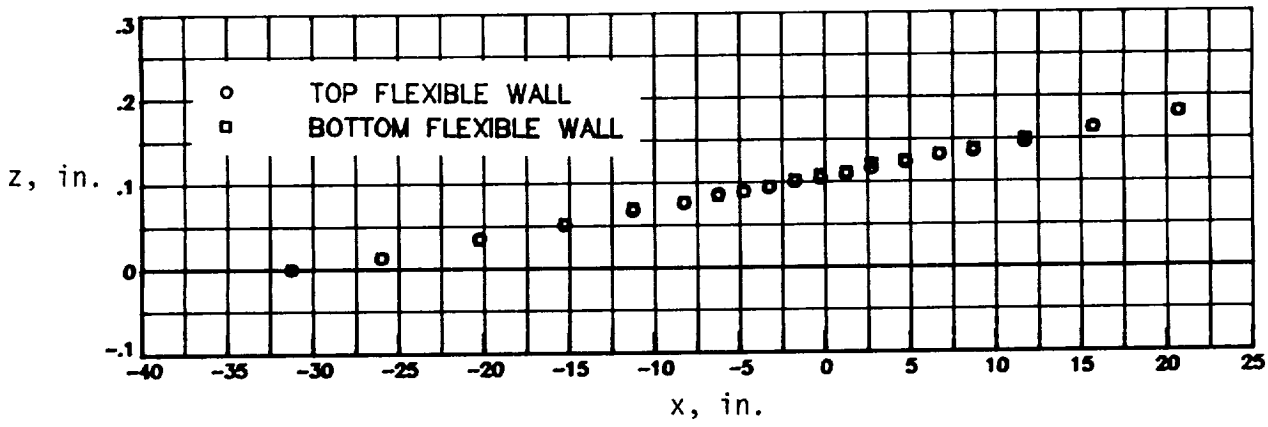

(h) $M_\infty = 0.90$.

Figure 22. Concluded.

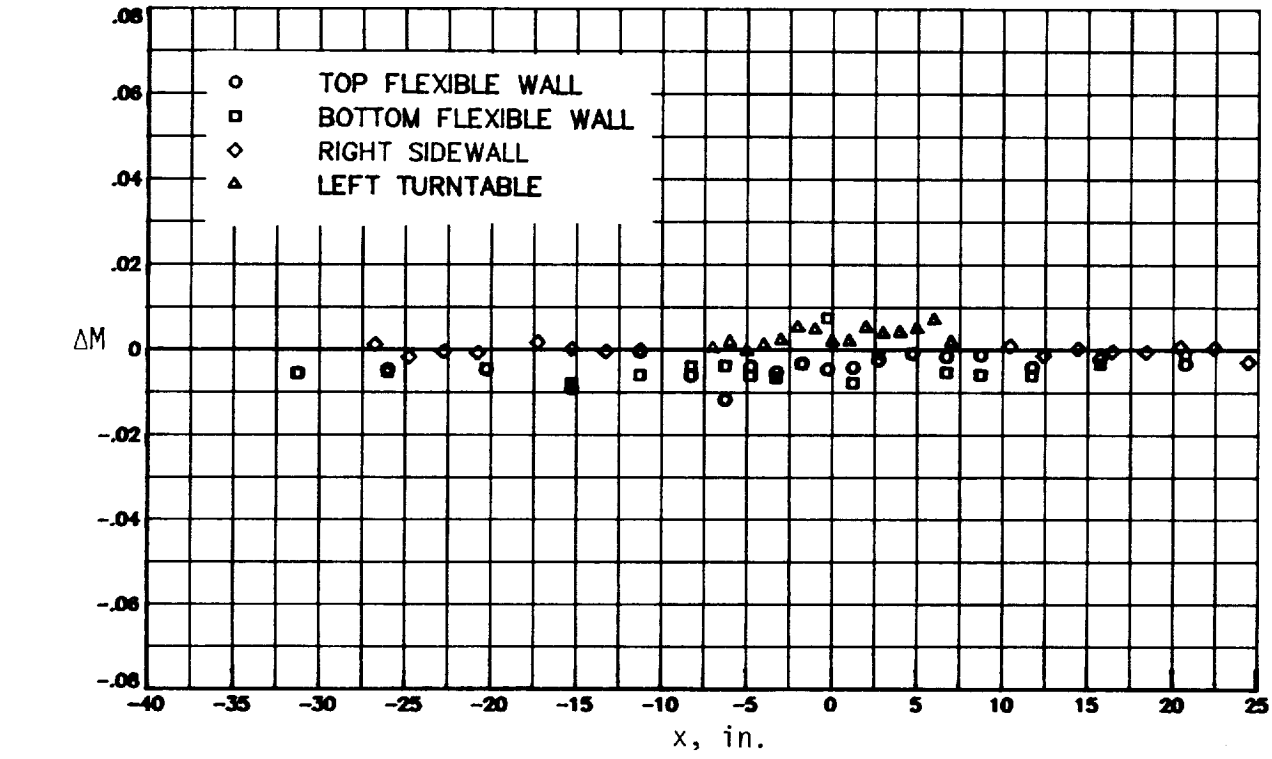

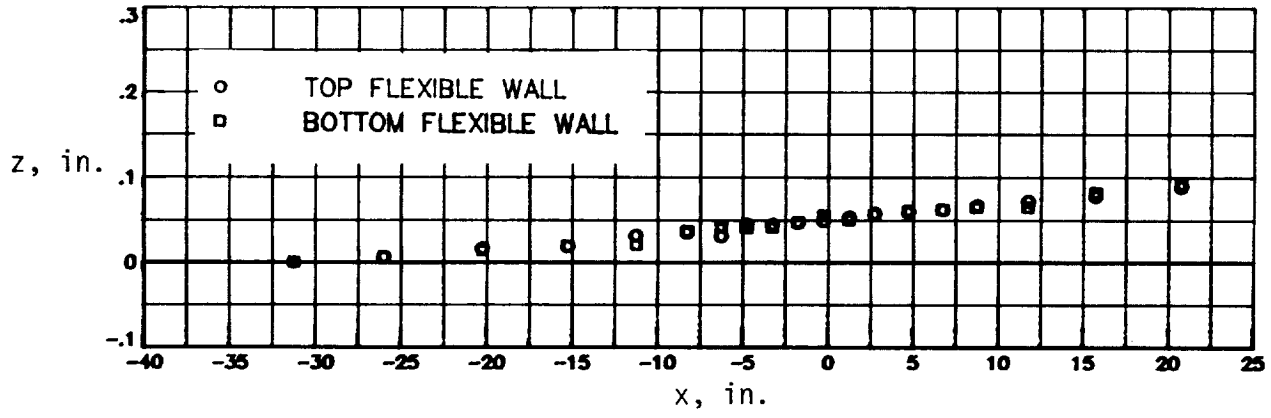

(a) $M_\infty = 0.50$.

Figure 23. Test section flexible wall shape and wall Mach number distribution for $R = 60 \times 10^6$ per foot.

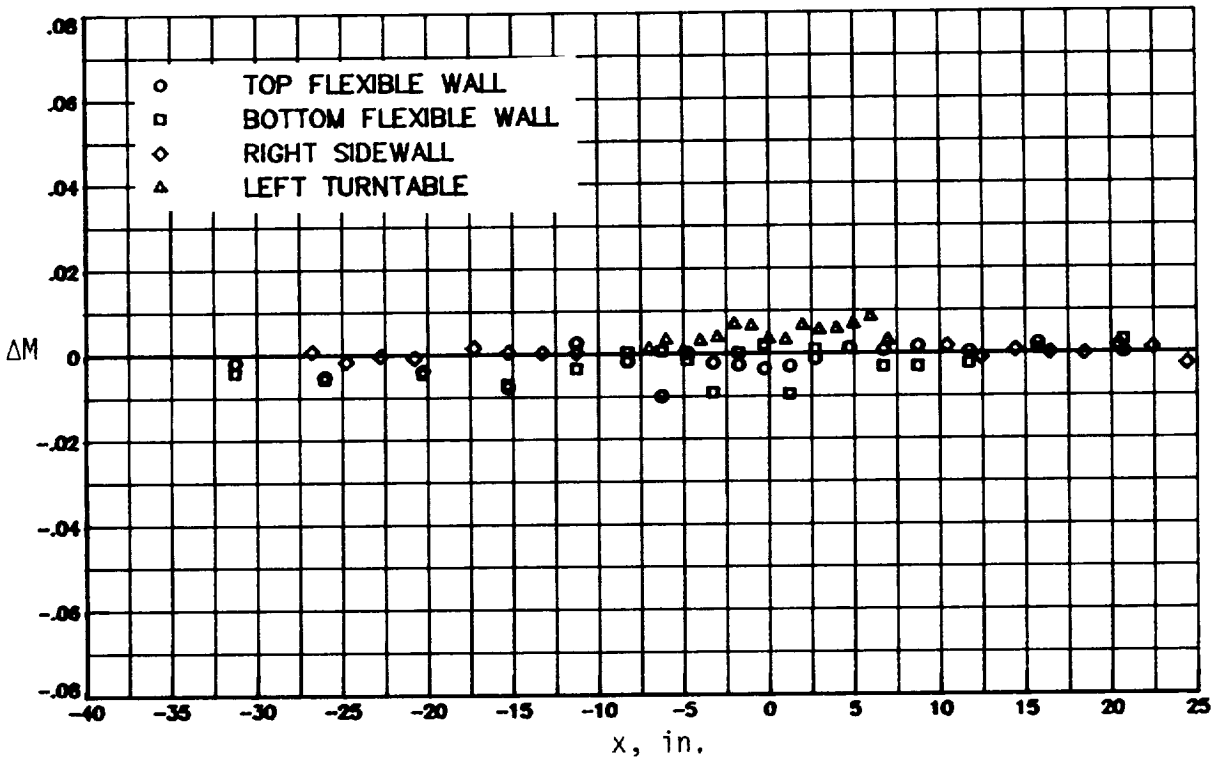

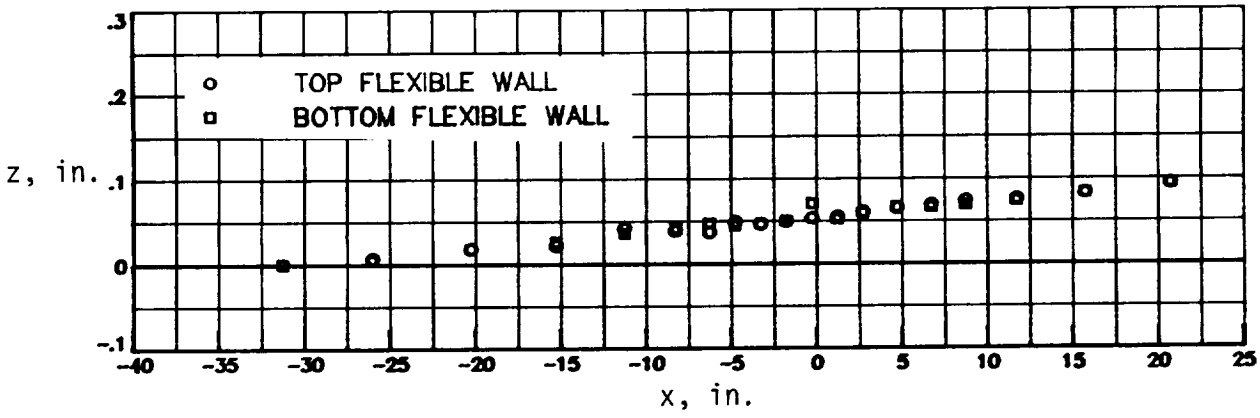

(b) $M_\infty = 0.60$.

Figure 23. Continued.

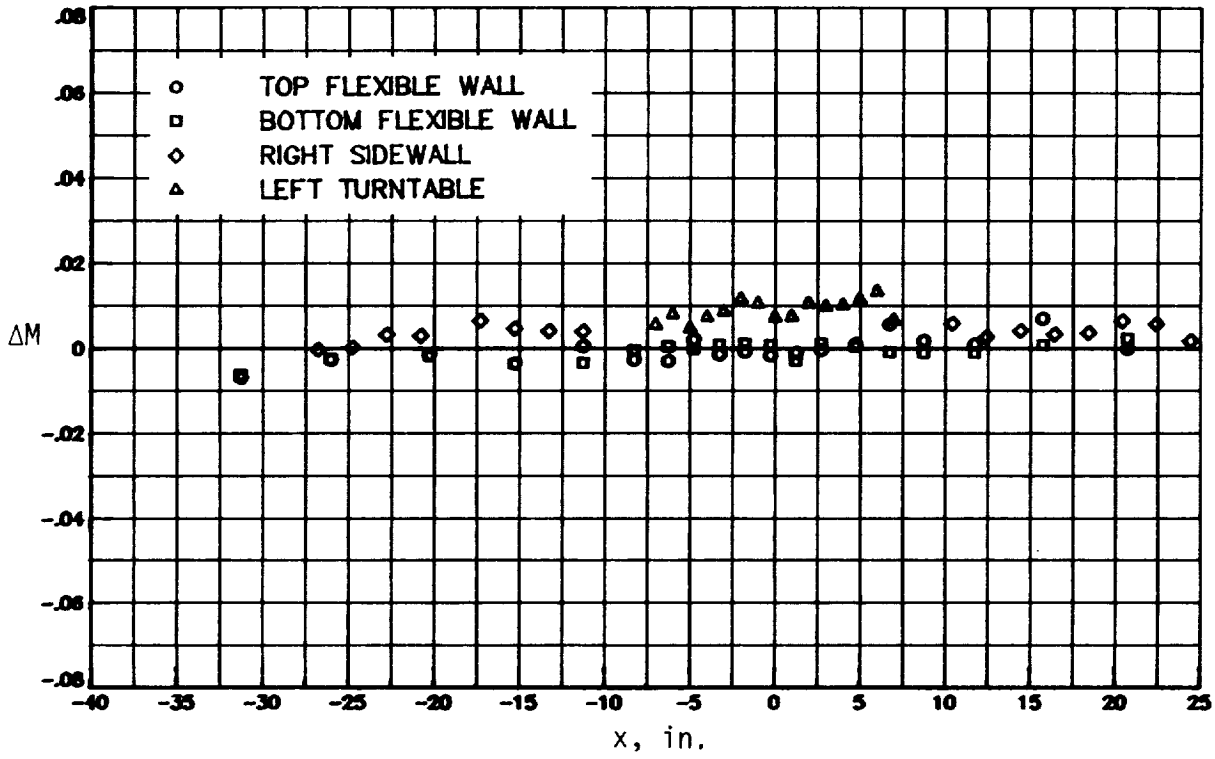

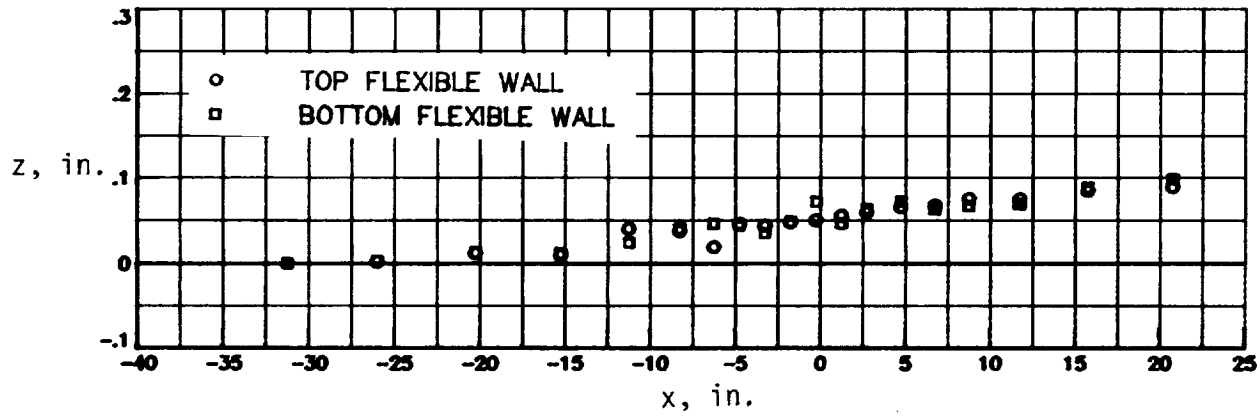

(c) $M_\infty = 0.70$.

Figure 23. Continued.

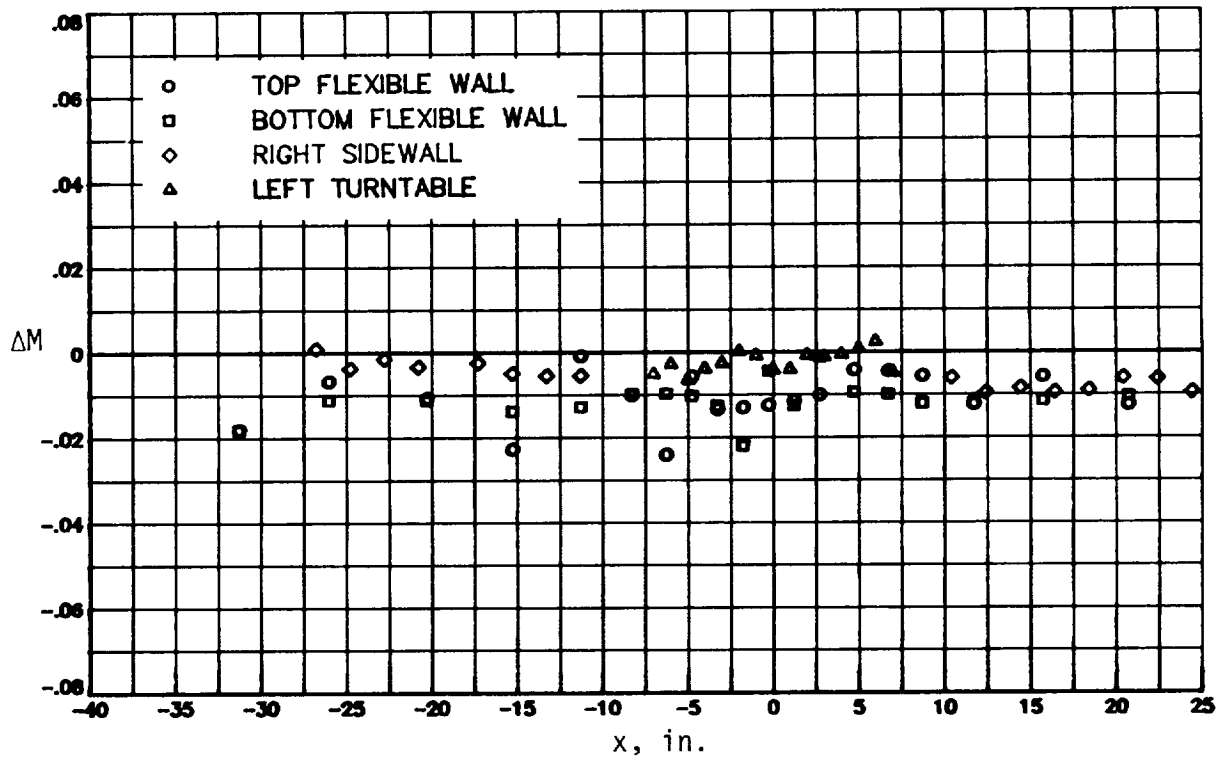

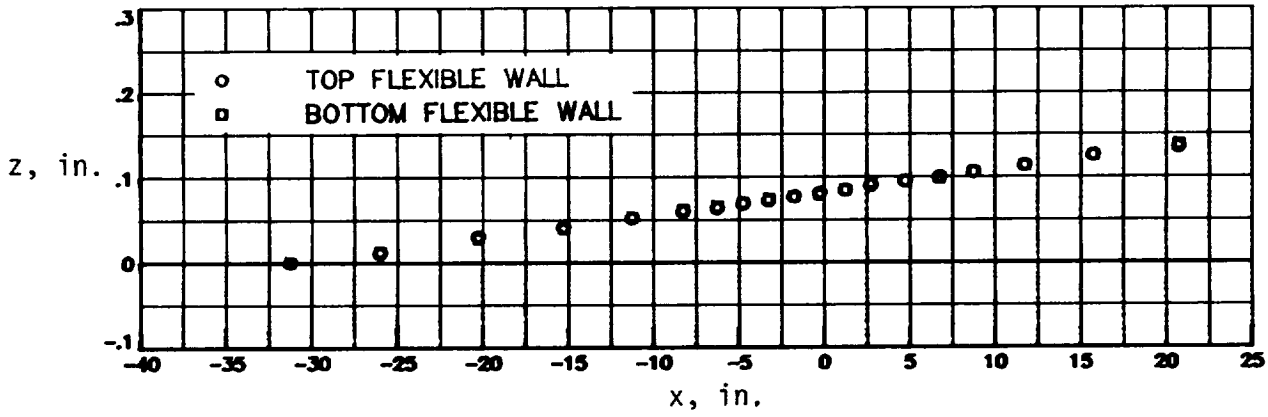

(d) $M_\infty = 0.75$.

Figure 23. Continued.

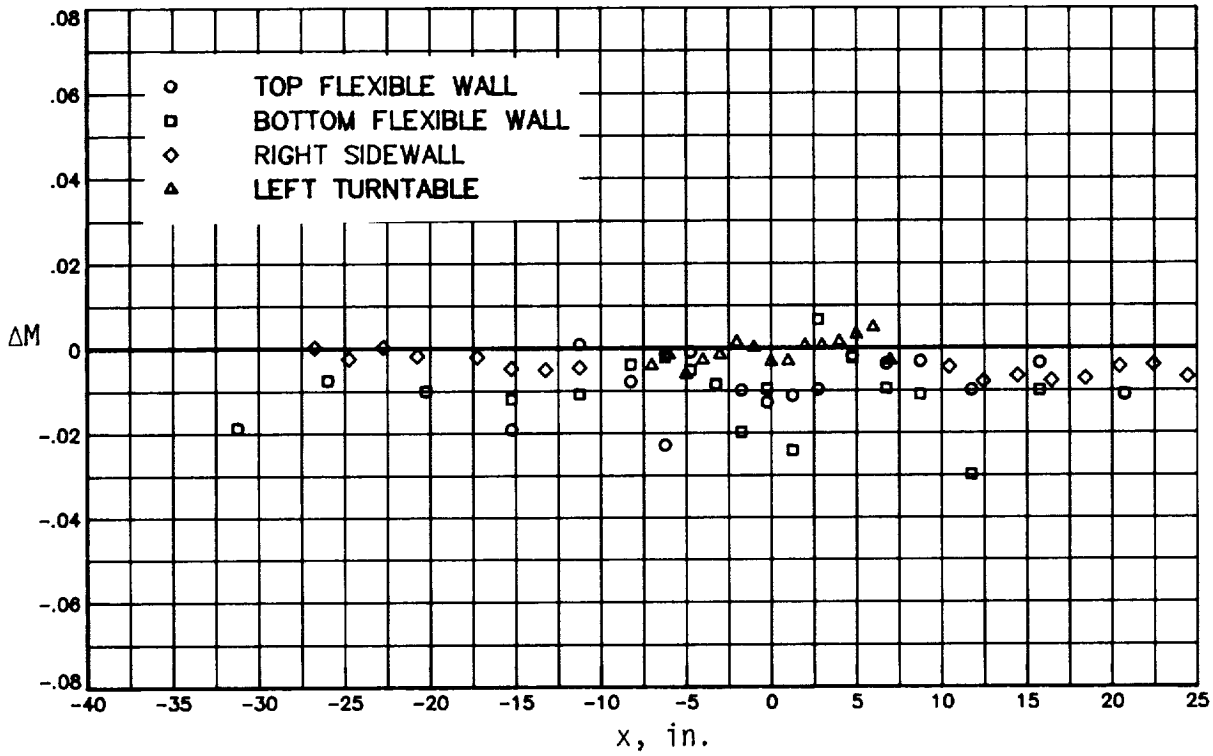

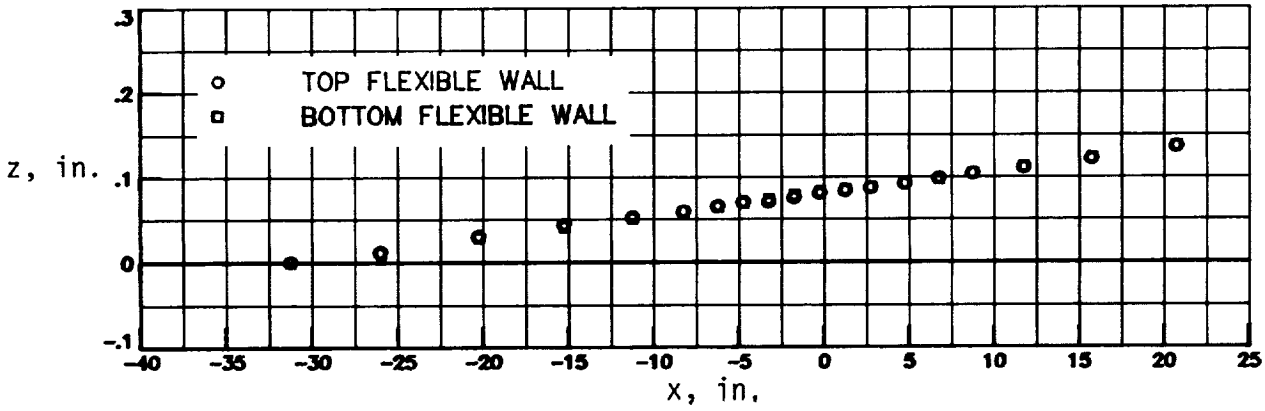

(e) $M_\infty = 0.80$.

Figure 23. Continued.

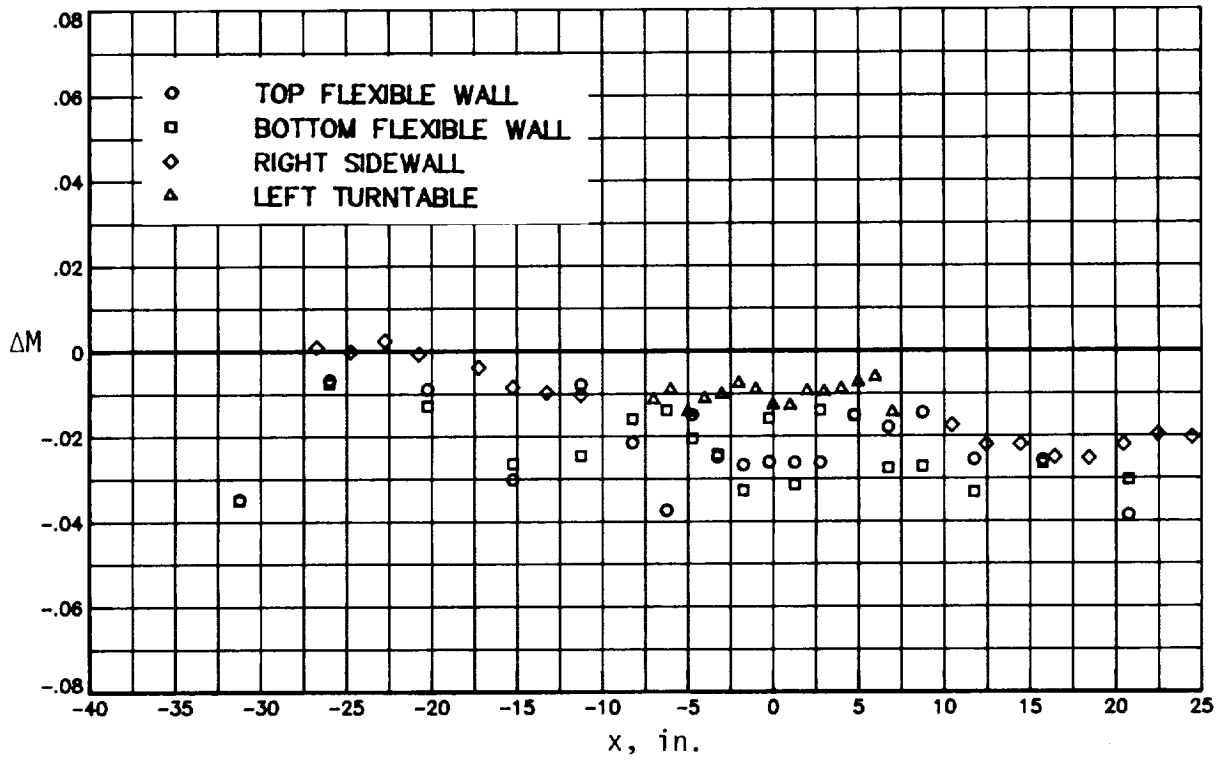

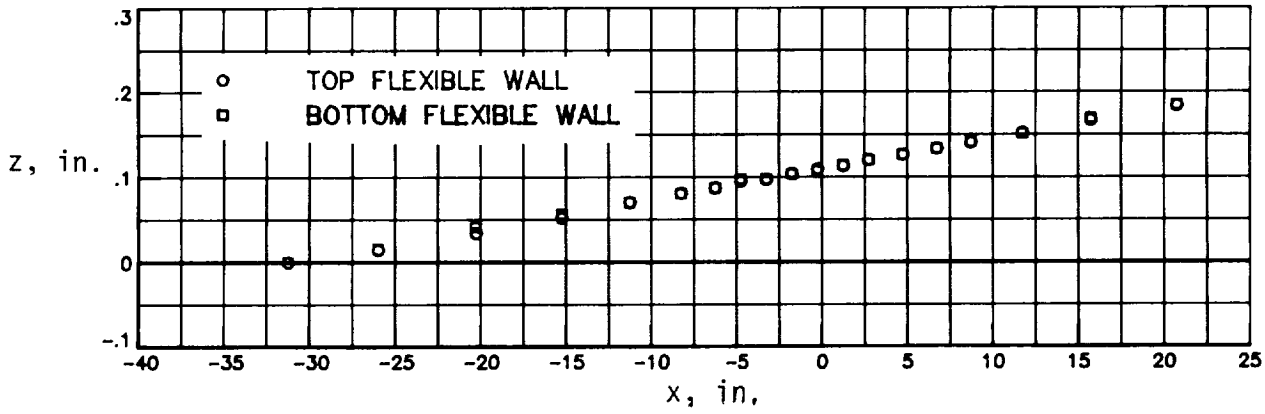

(f) $M_\infty = 0.85$.

Figure 23. Continued.

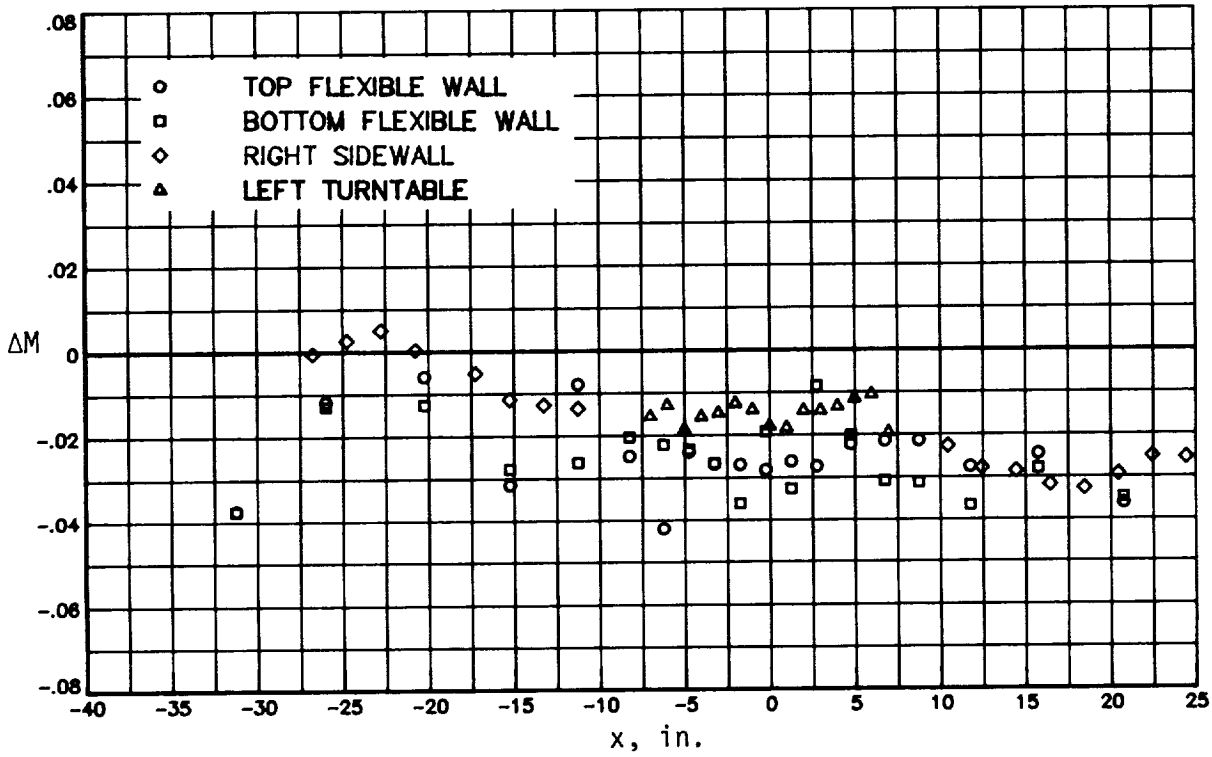

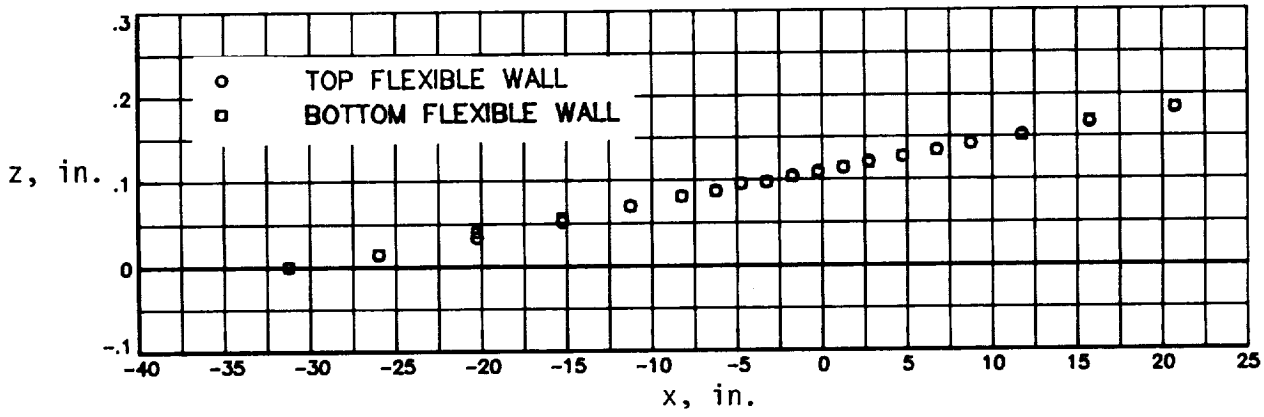

(g) $M_\infty = 0.90$.

Figure 23. Continued.

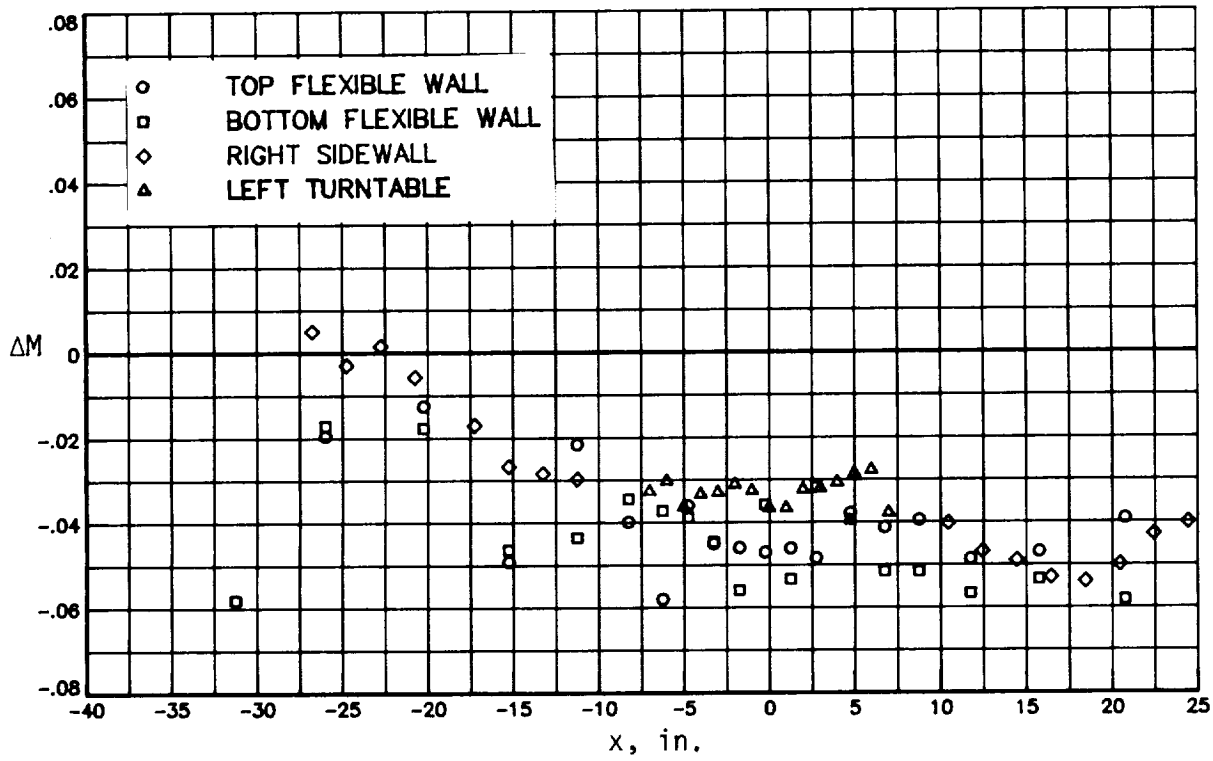

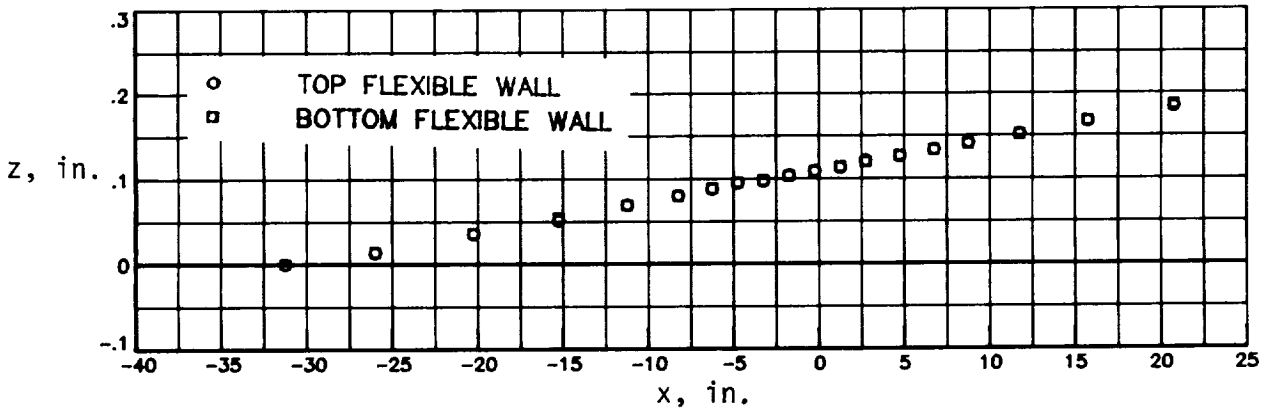

(h) $M_\infty = 0.95$.

Figure 23. Concluded.

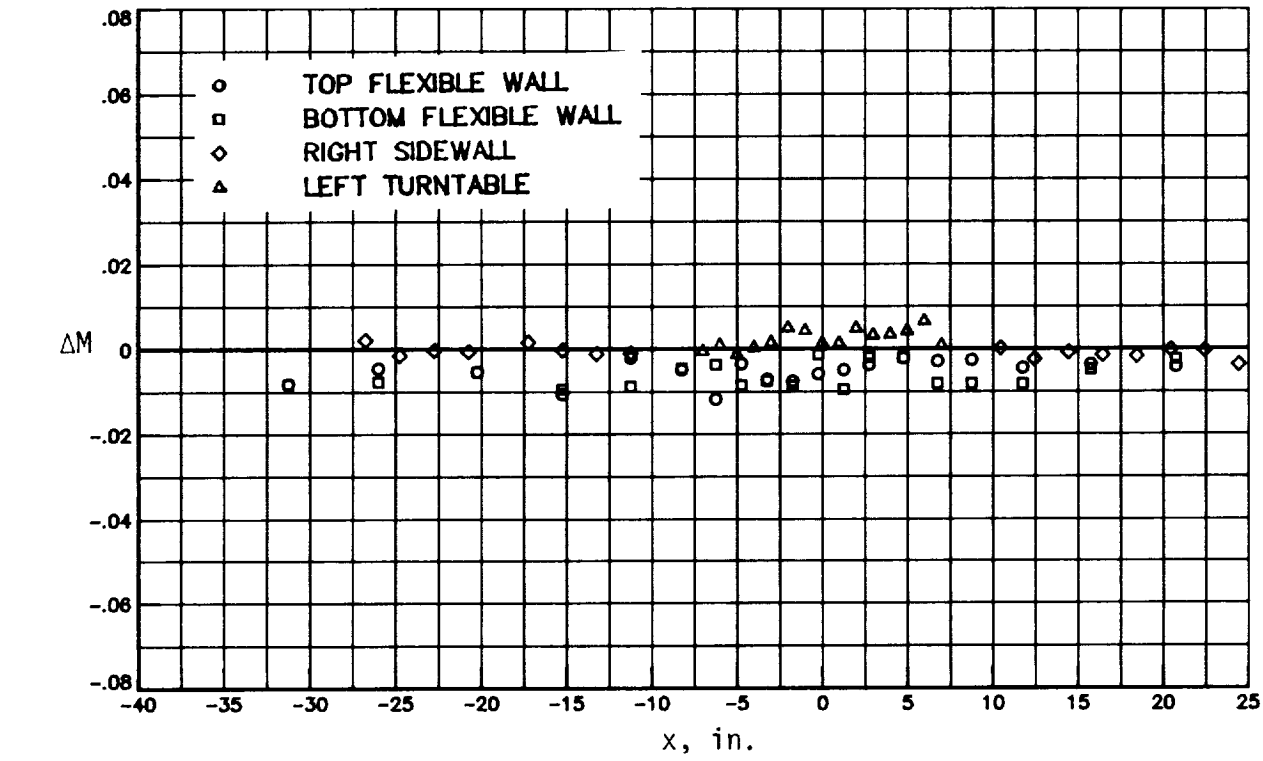

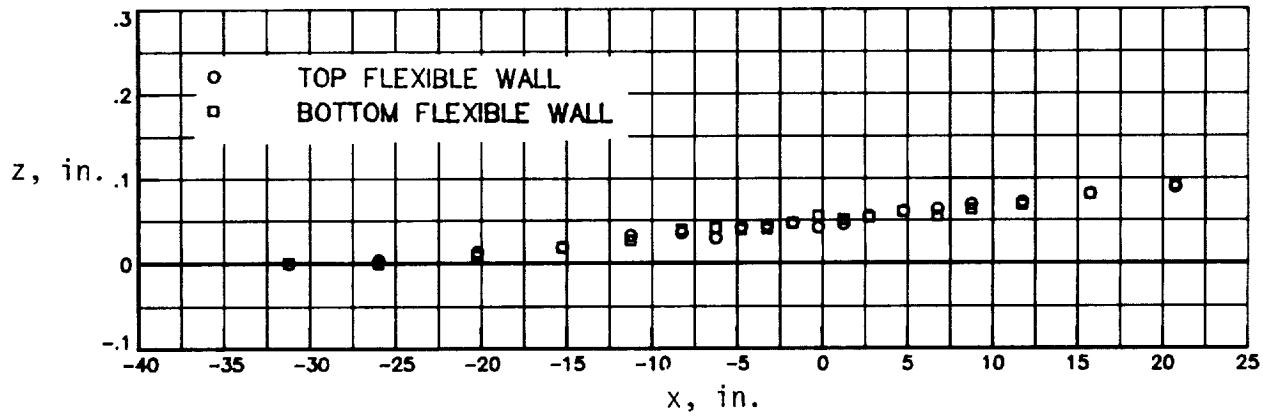

(a) $M_\infty = 0.50$.

Figure 24. Test section flexible wall shape and wall Mach number distribution for $R = 80 \times 10^6$ per foot.

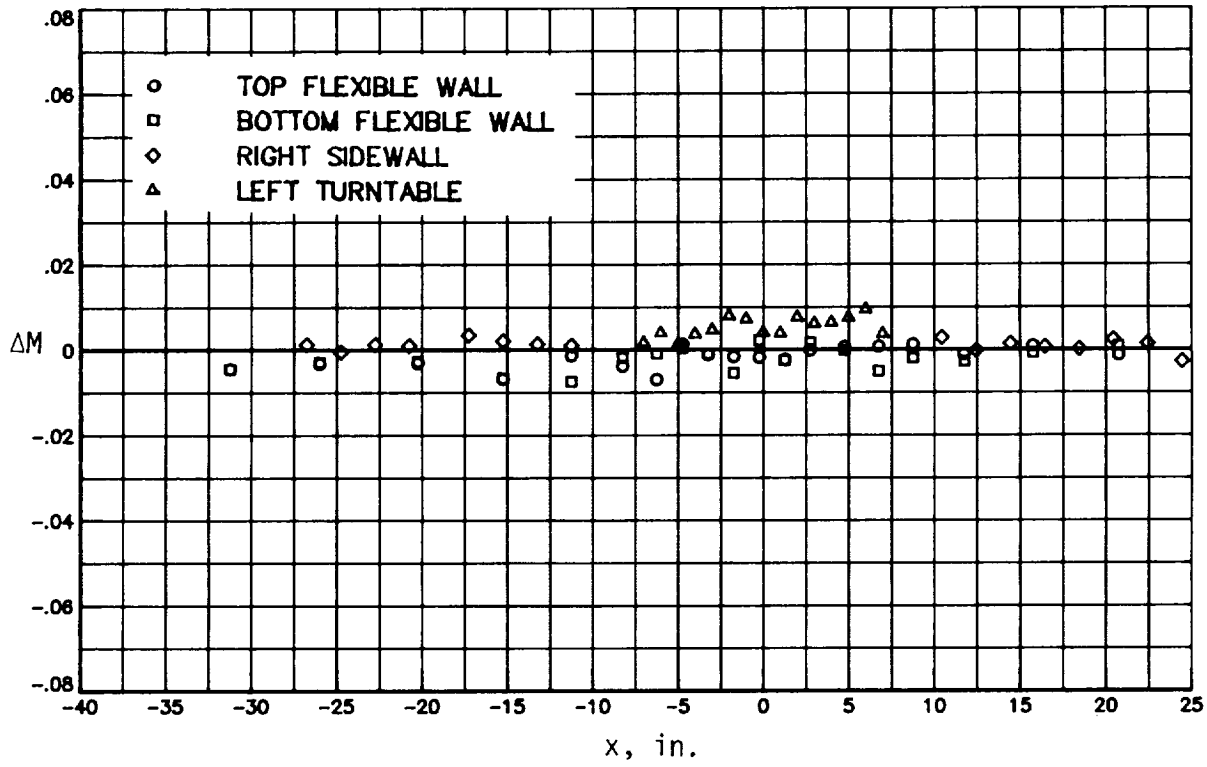

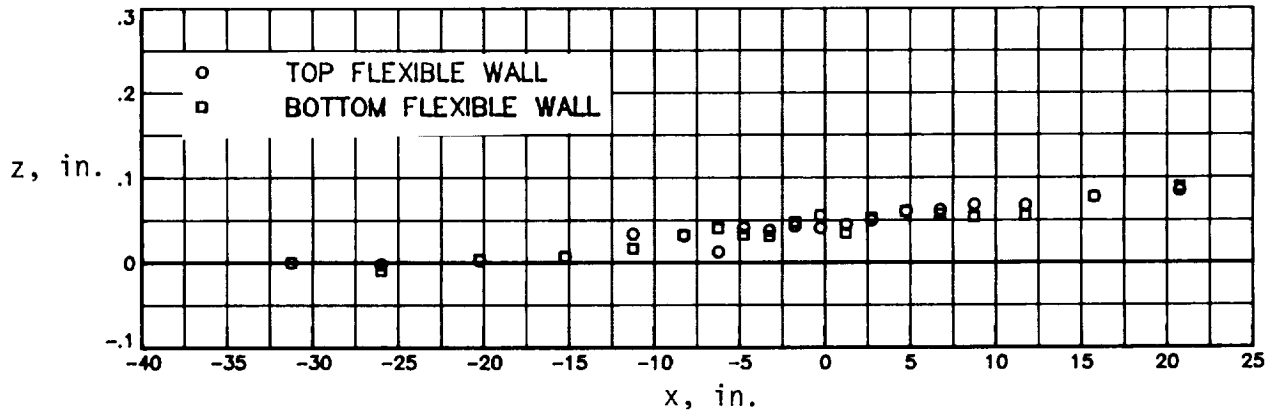

(b) $M_\infty = 0.60$.

Figure 24. Continued.

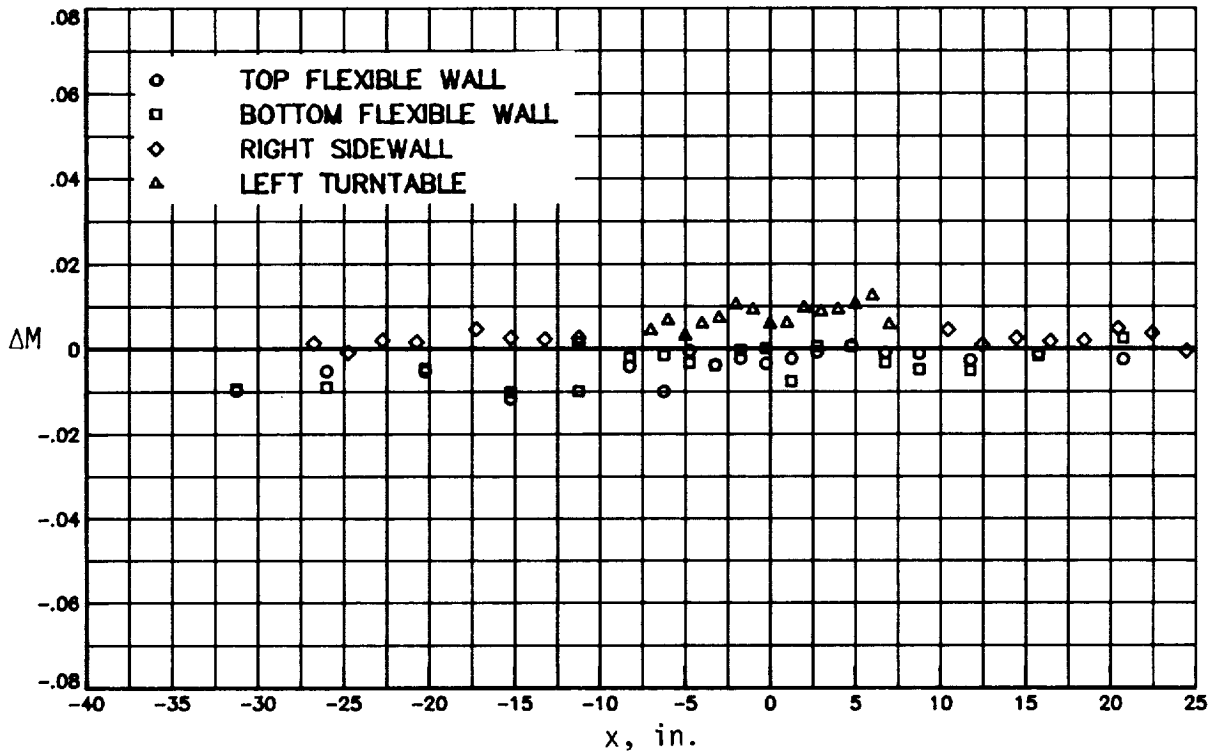

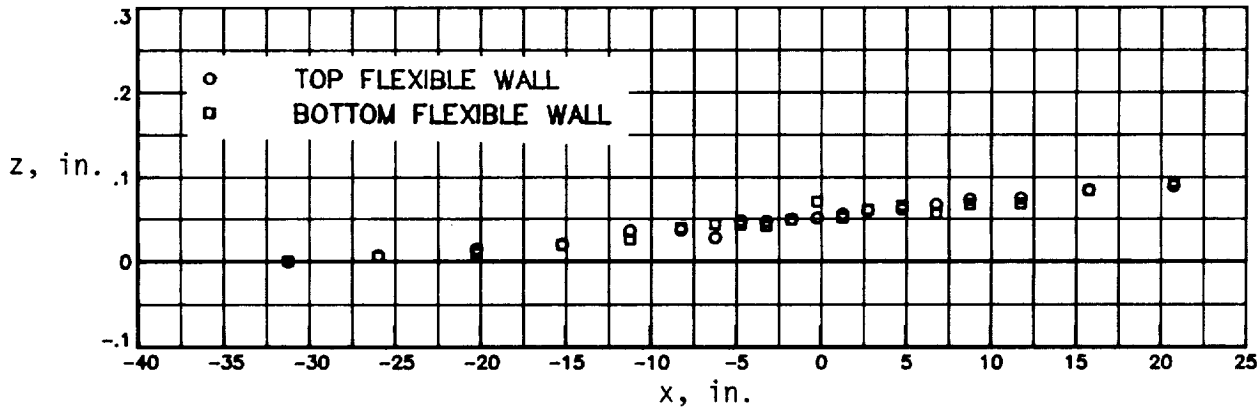

(c) $M_\infty = 0.70$.

Figure 24. Continued.

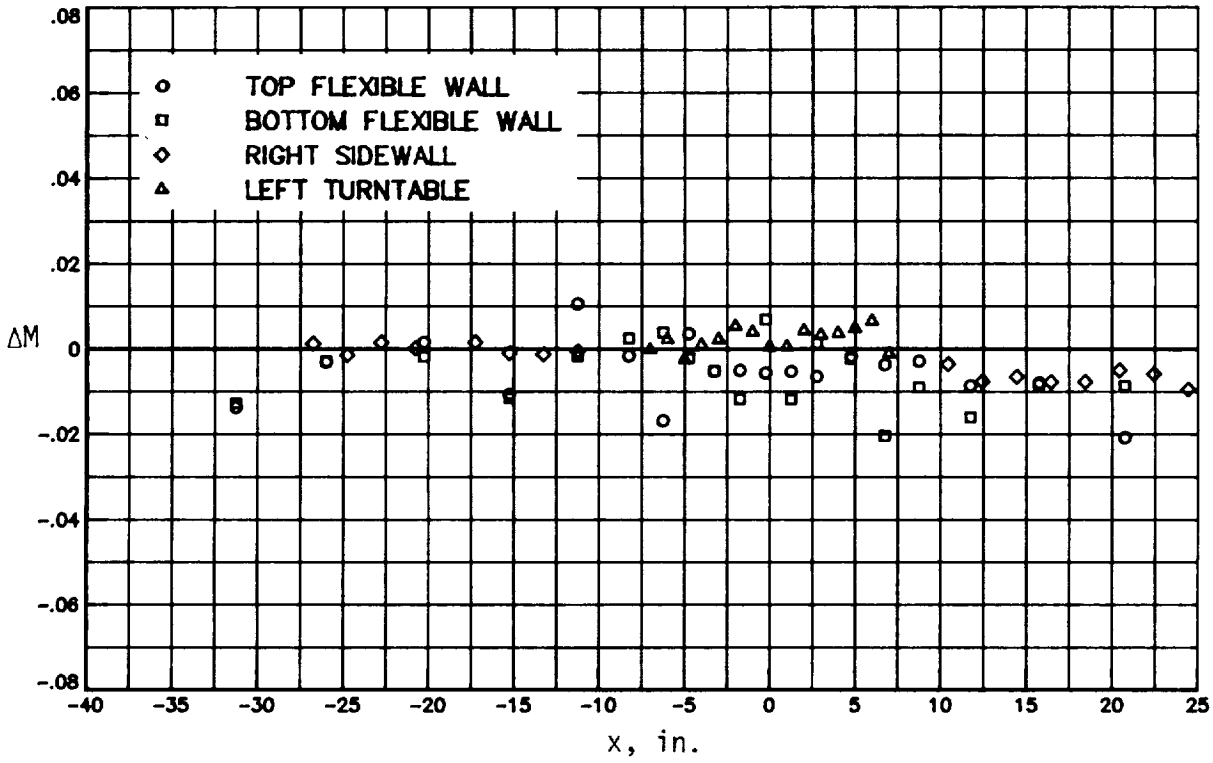

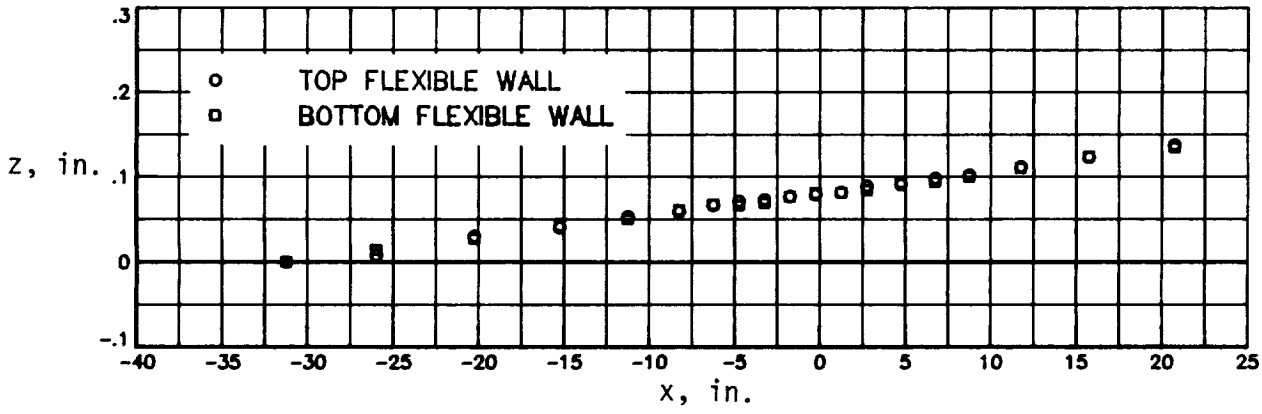

(d) $M_\infty = 0.75$.

Figure 24. Continued.

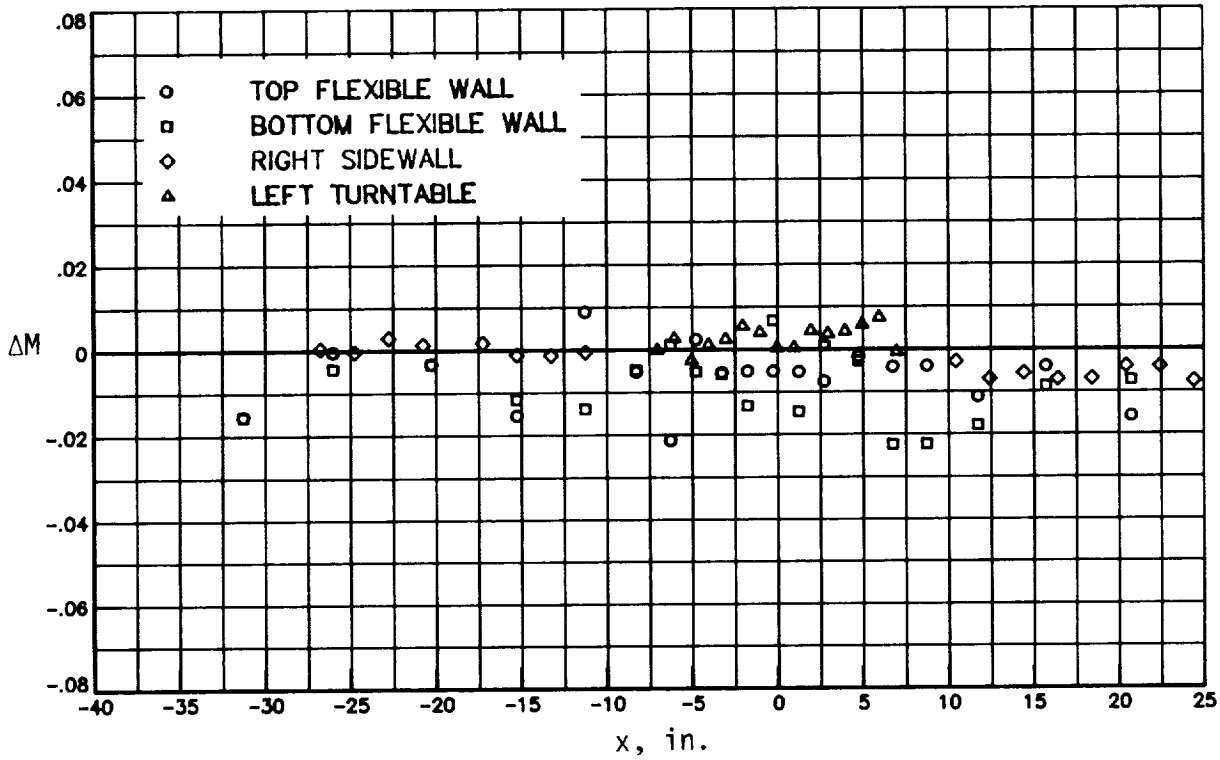

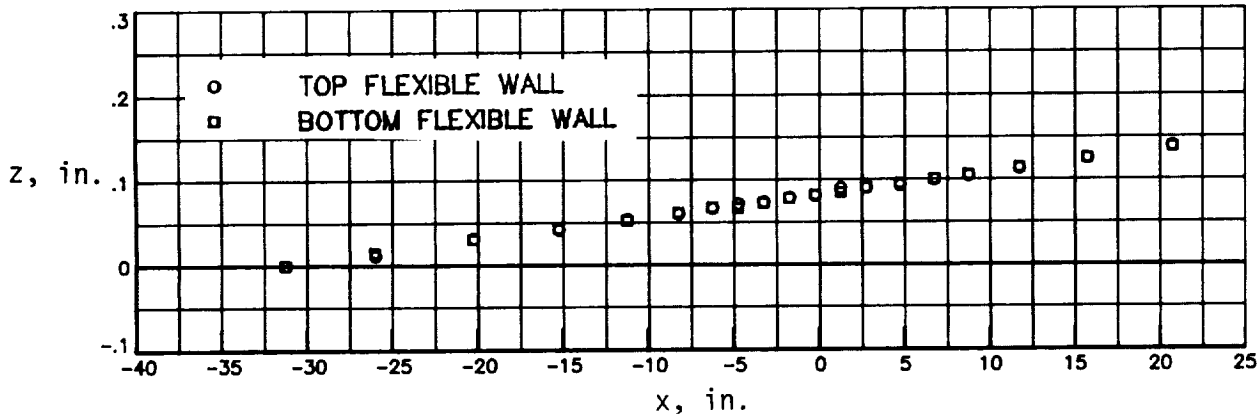

(e) $M_\infty = 0.80$.

Figure 24. Continued.

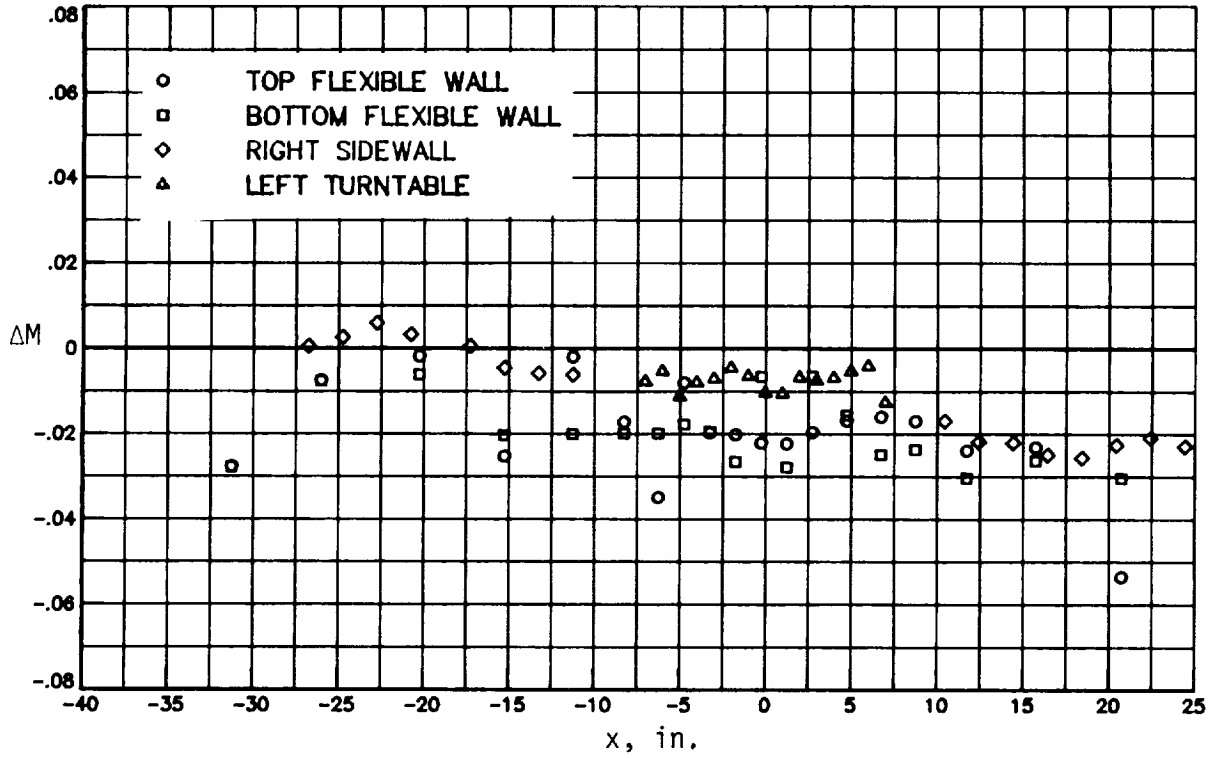

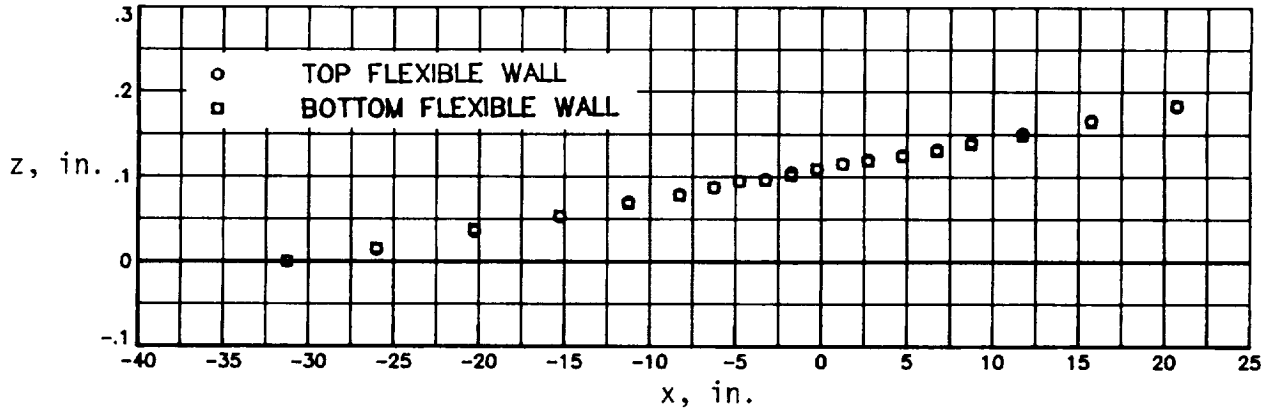

(f) $M_\infty = 0.85$.

Figure 24. Continued.

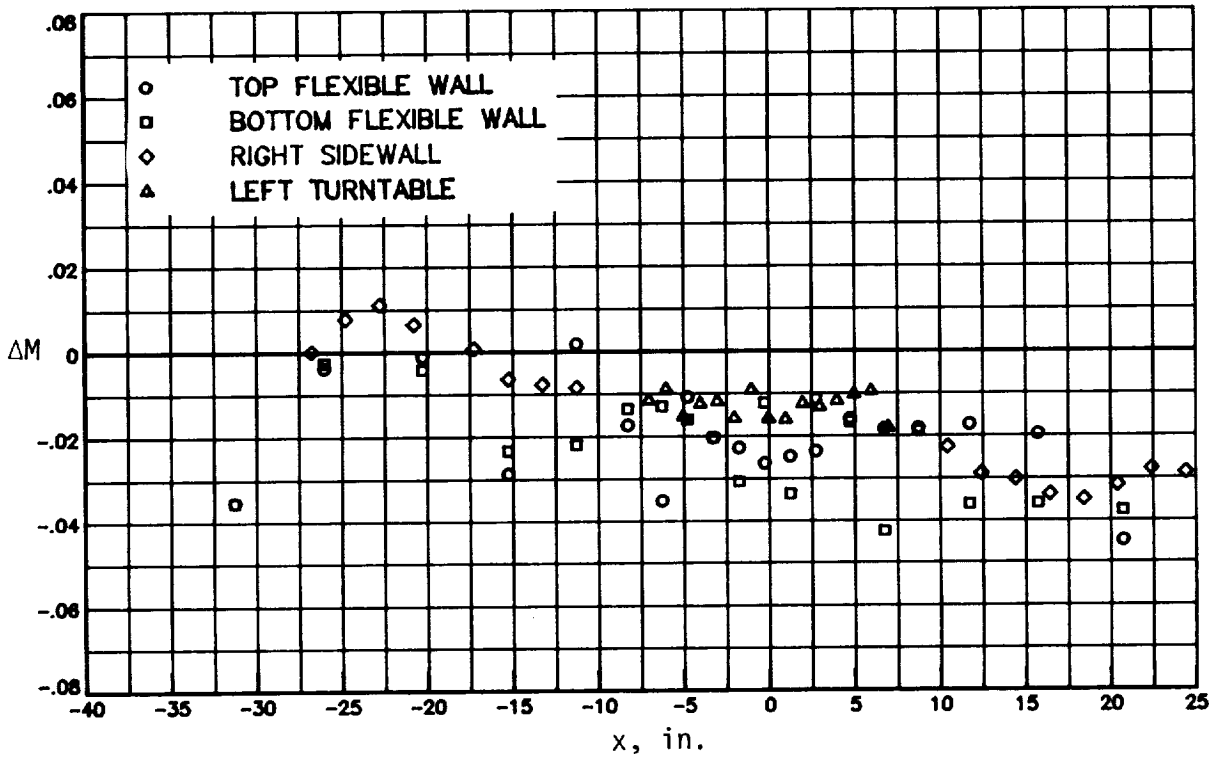

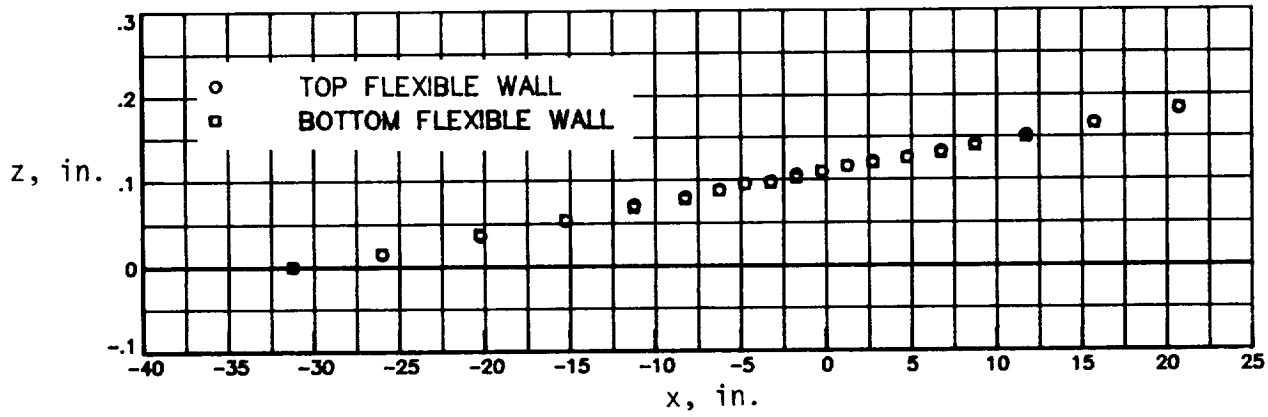

(g) $M_\infty = 0.90$.

Figure 24. Concluded.

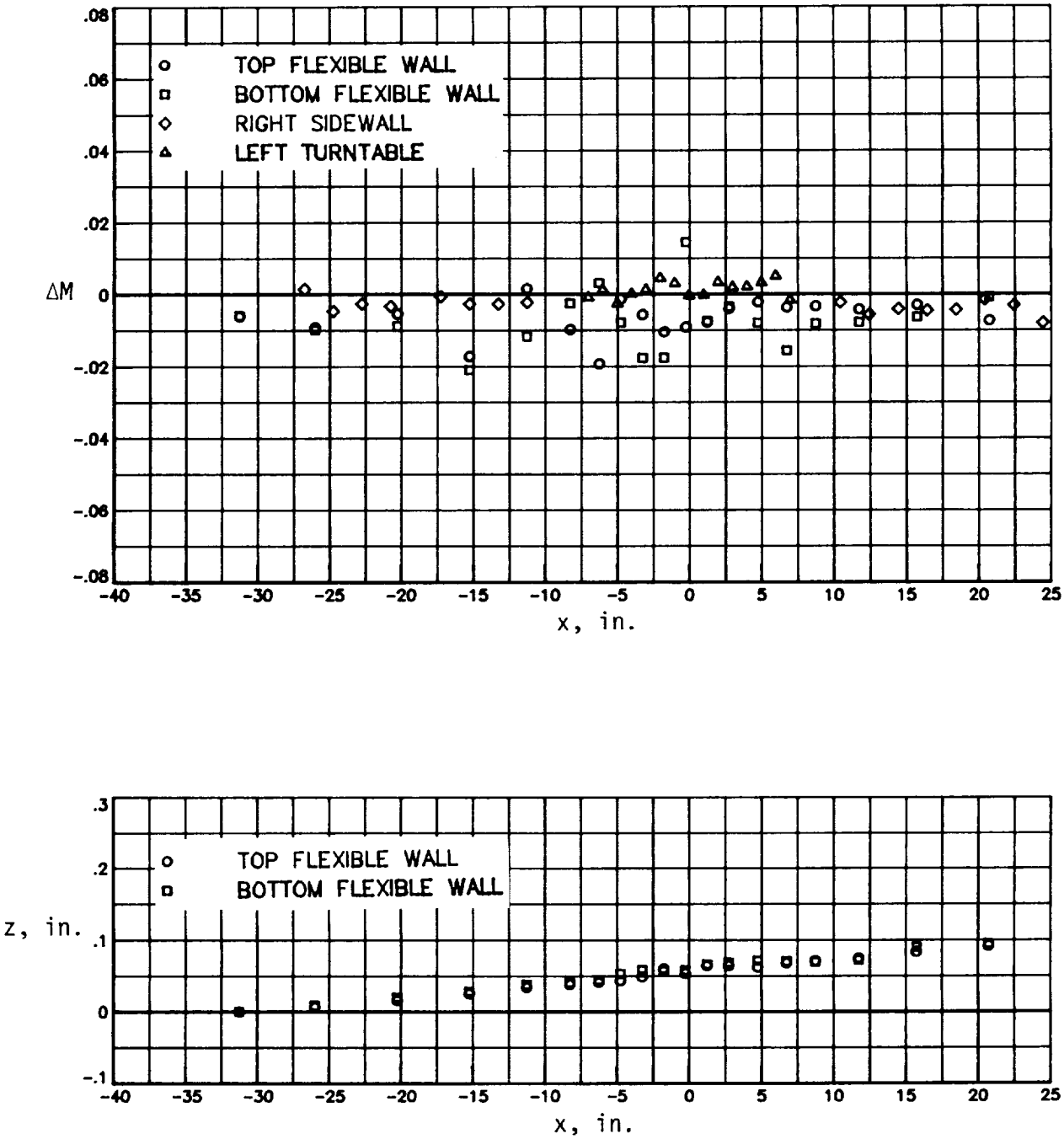

(a) $M_\infty = 0.70$.

Figure 25. Test section flexible wall shape and wall Mach number distribution for $R = 100 \times 10^6$ per foot.

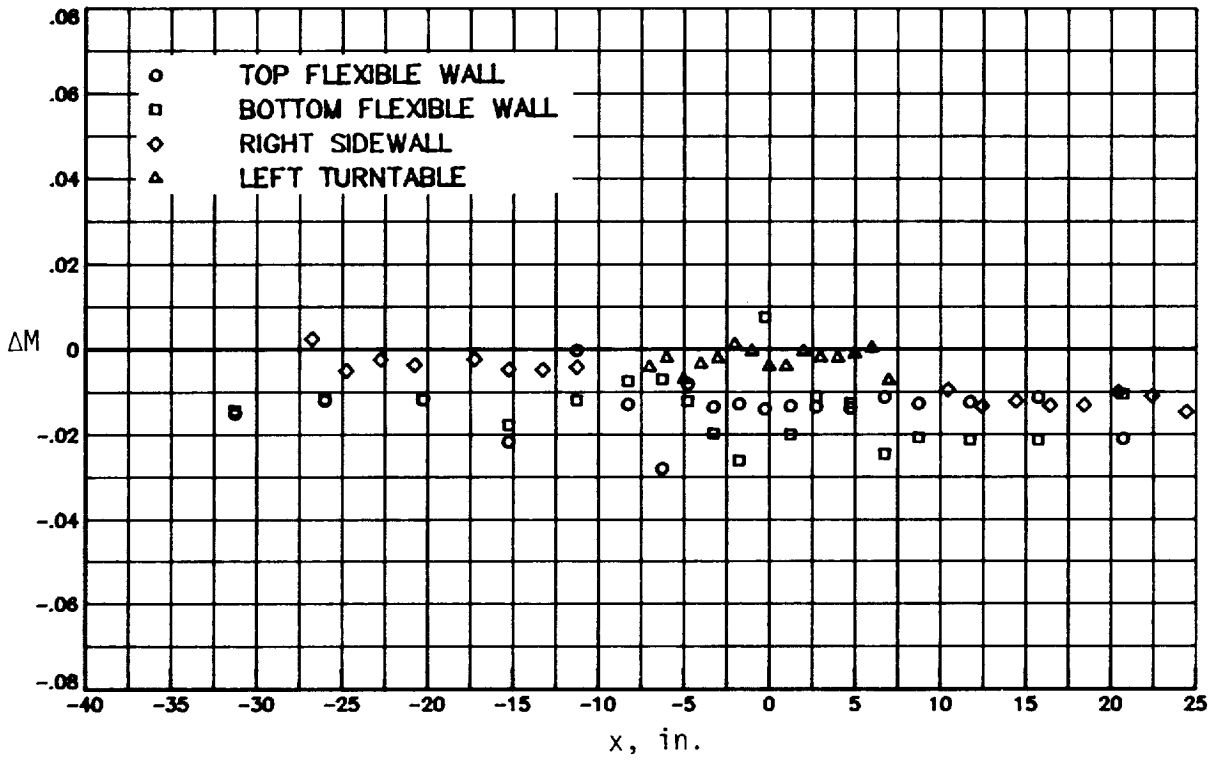

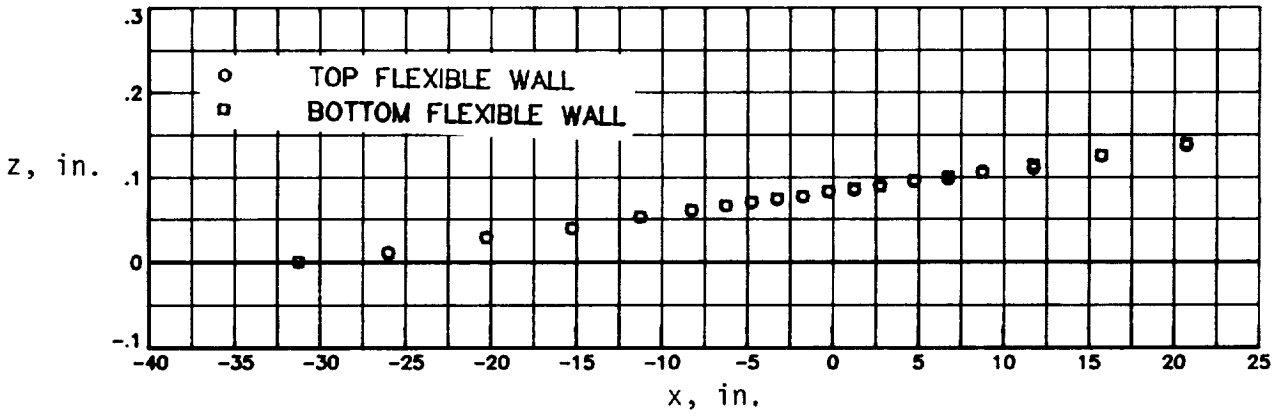

(b) $M_\infty = 0.75$.

Figure 25. Continued.

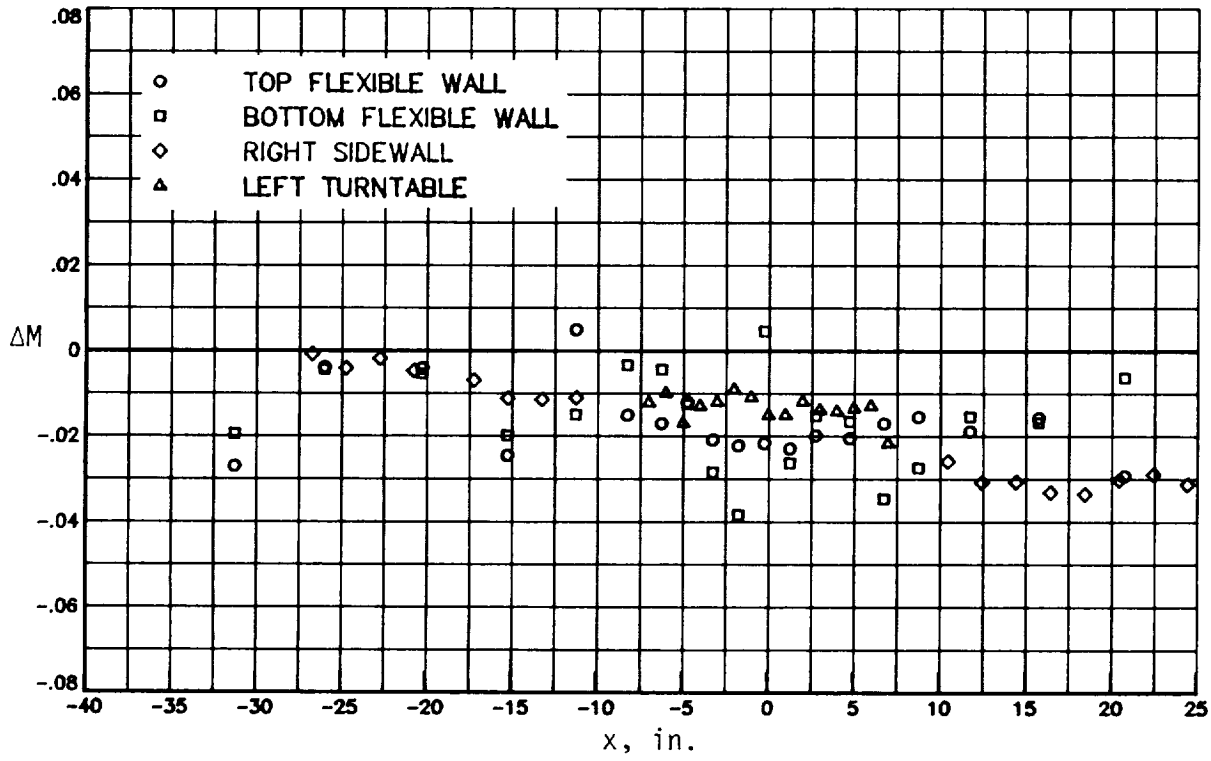

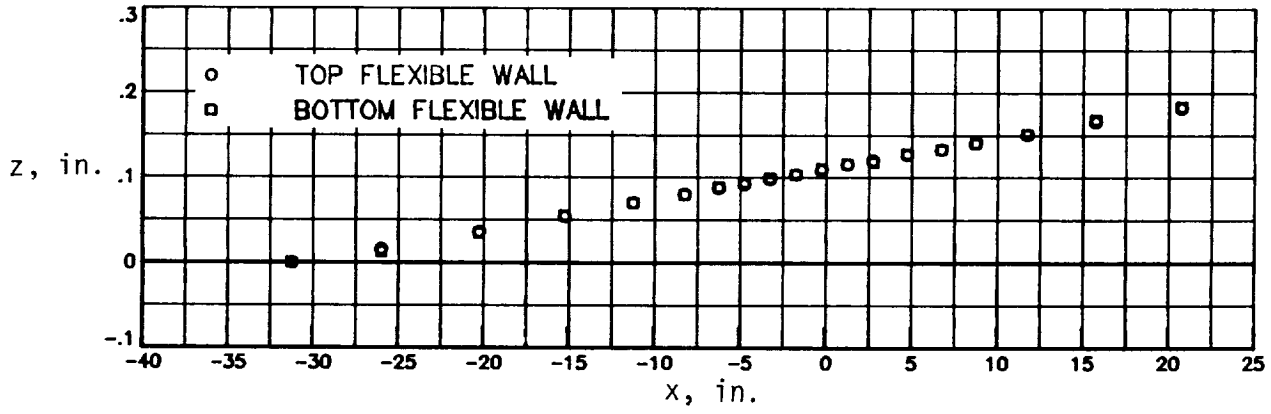

(c) $M_\infty = 0.85$.

Figure 25. Continued.

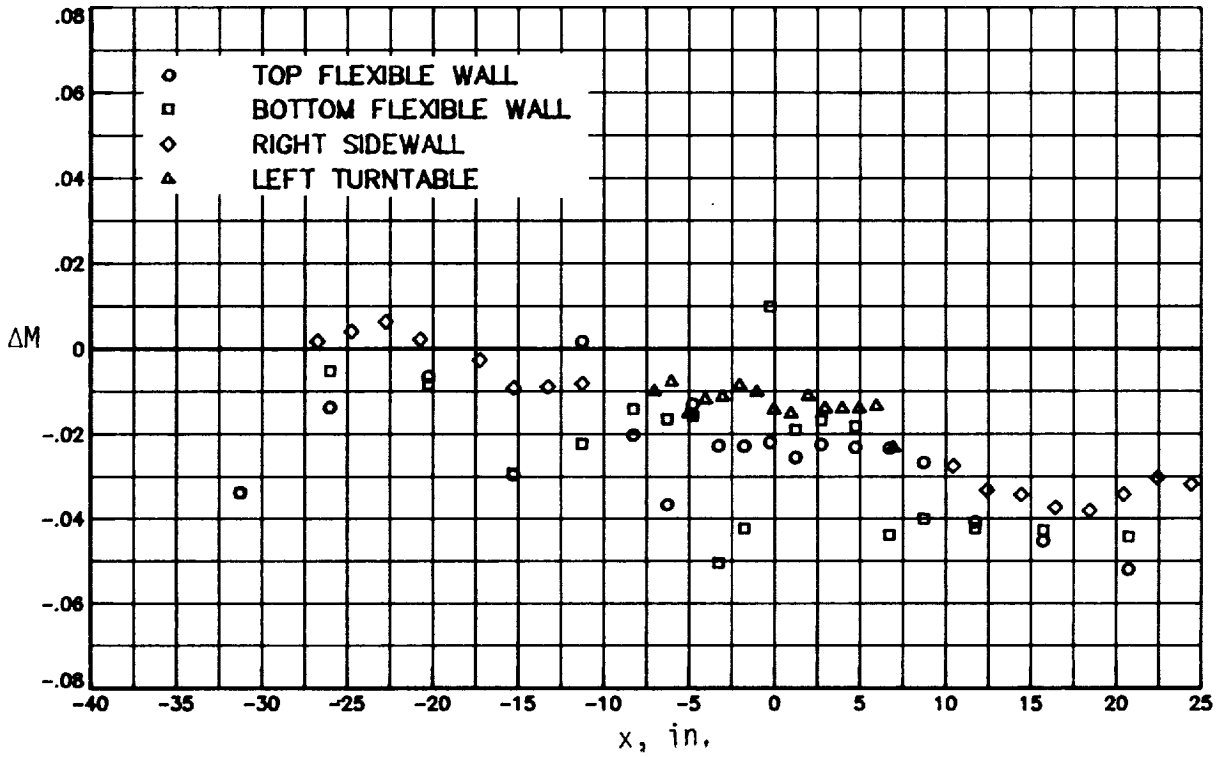

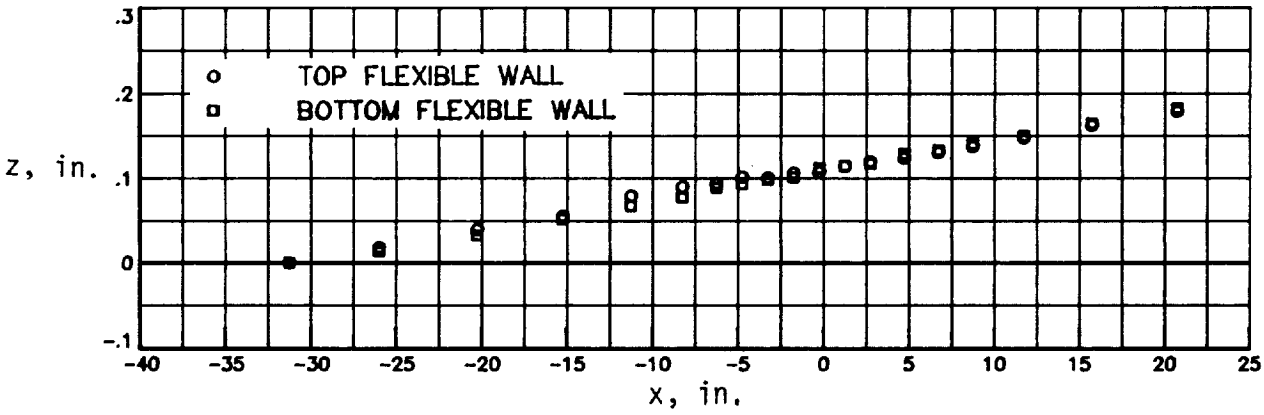

(d) $M_\infty = 0.90$.

Figure 25. Concluded.

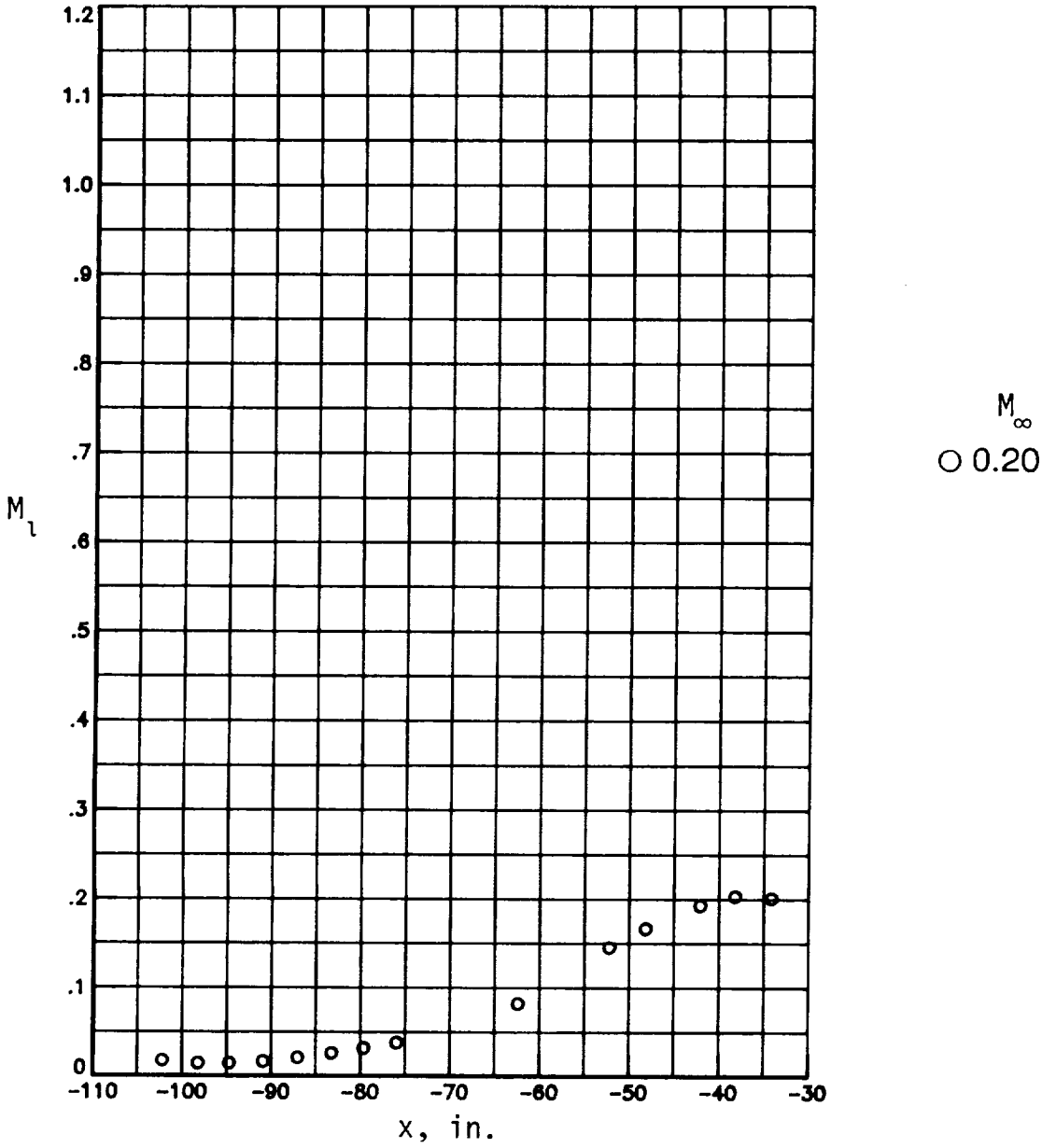

(a) $R = 10 \times 10^6$ per foot.

Figure 26. Local Mach number distributions in contraction section.

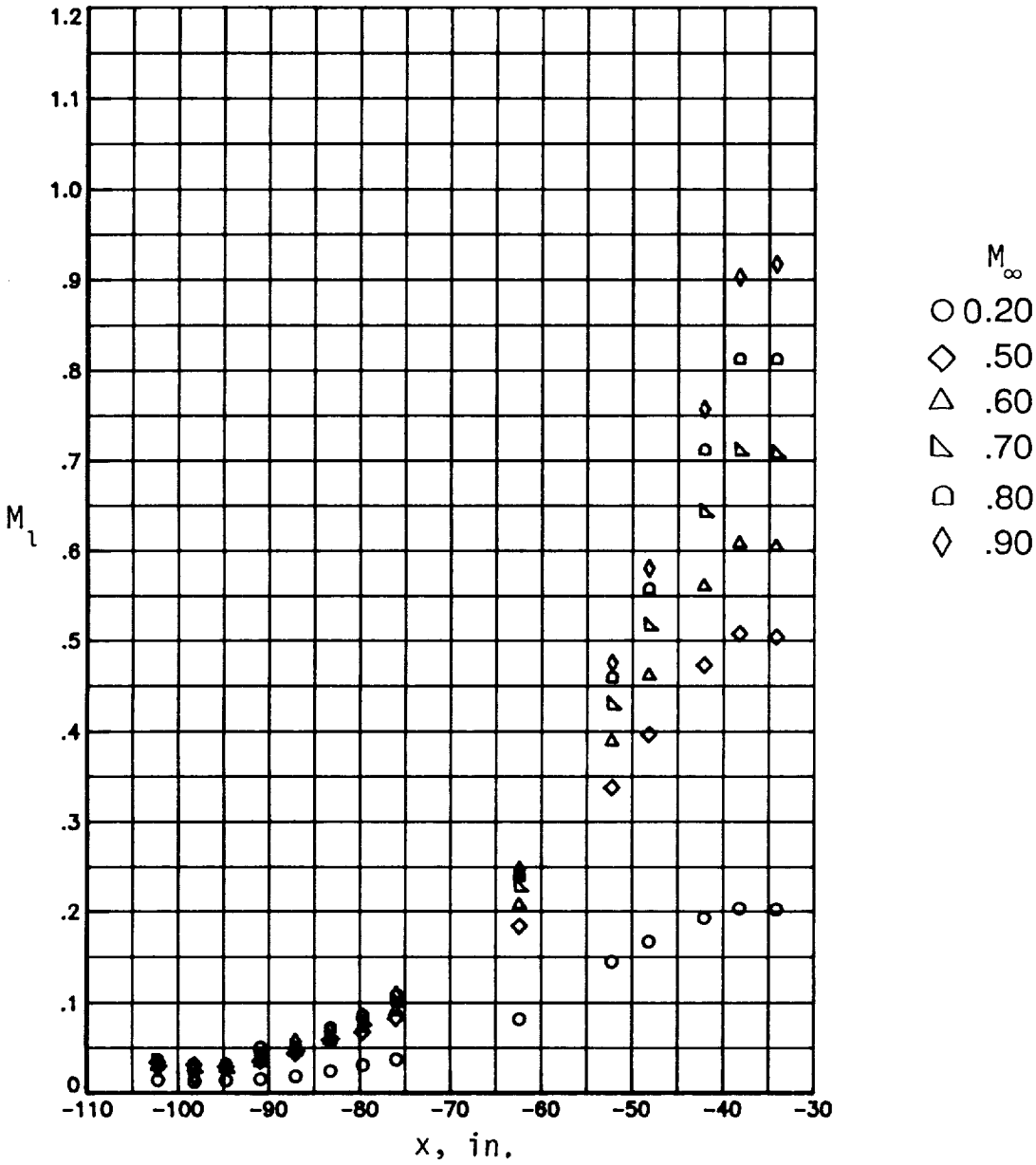

(b) $R = 20 \times 10^6$ per foot.

Figure 26. Continued.

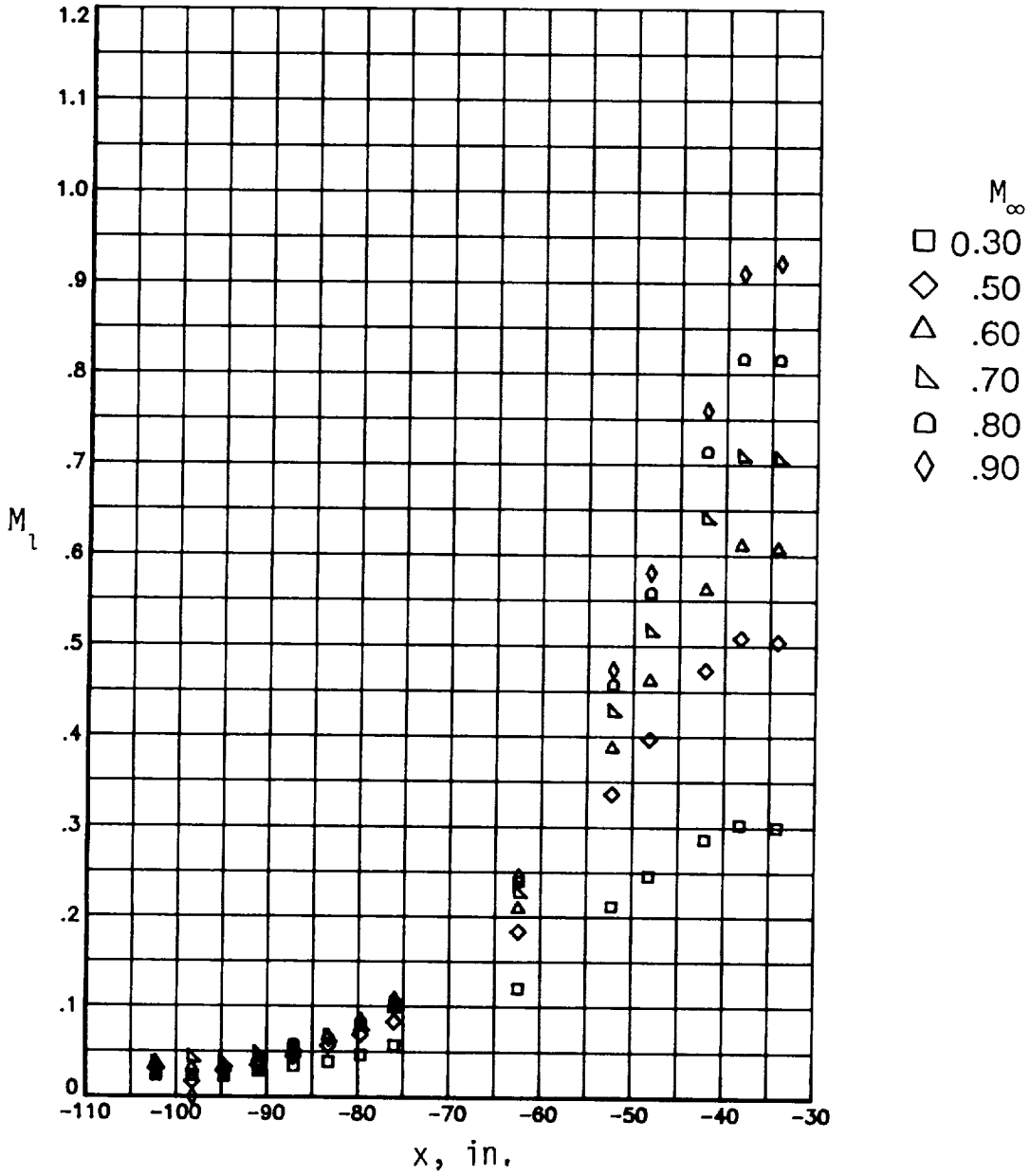

(c) $R = 40 \times 10^6$ per foot.

Figure 26. Continued.

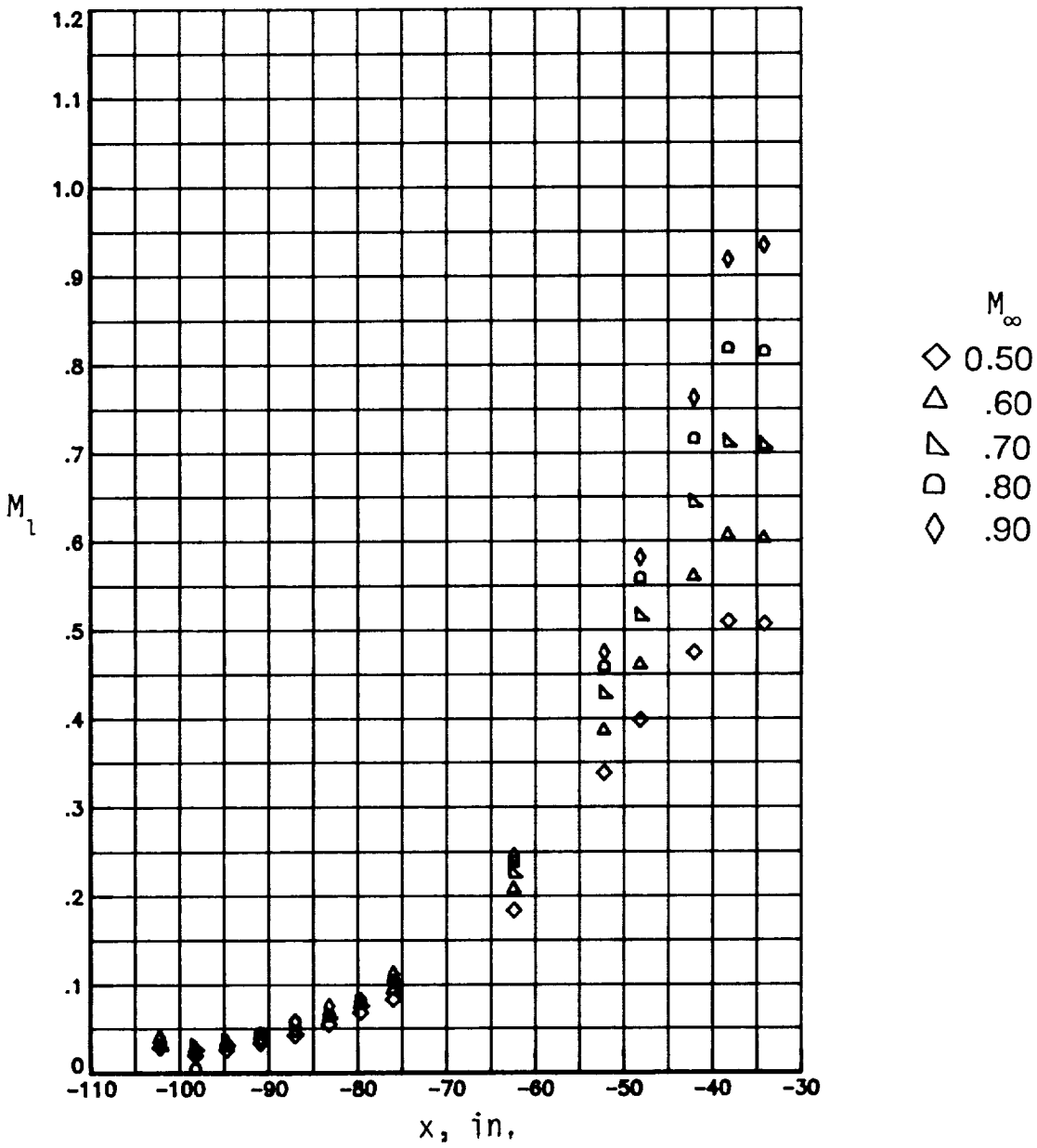

(d) $R = 60 \times 10^6$ per foot.

Figure 26. Continued.

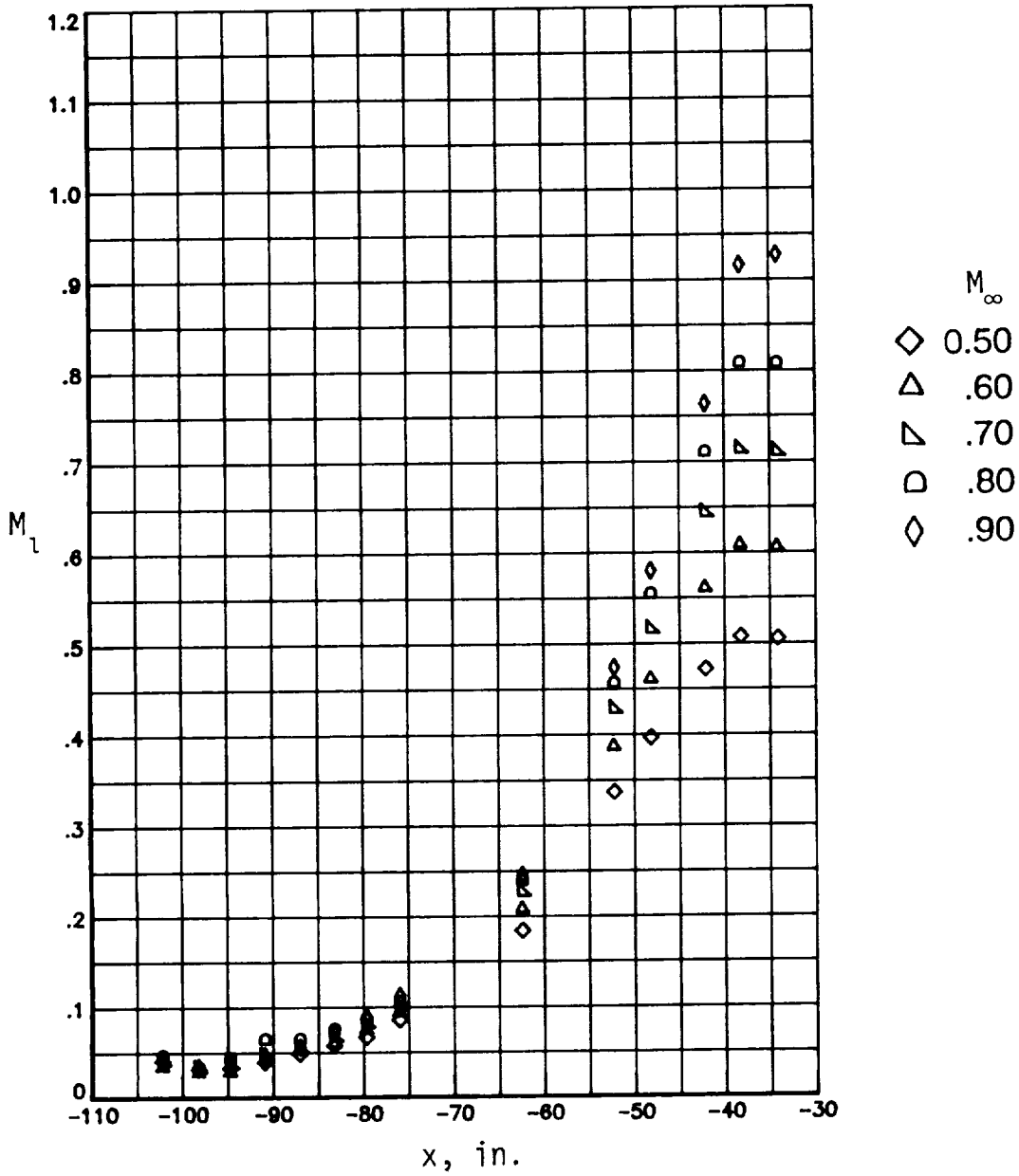

(e) $R = 80 \times 10^6$ per foot.

Figure 26. Continued.

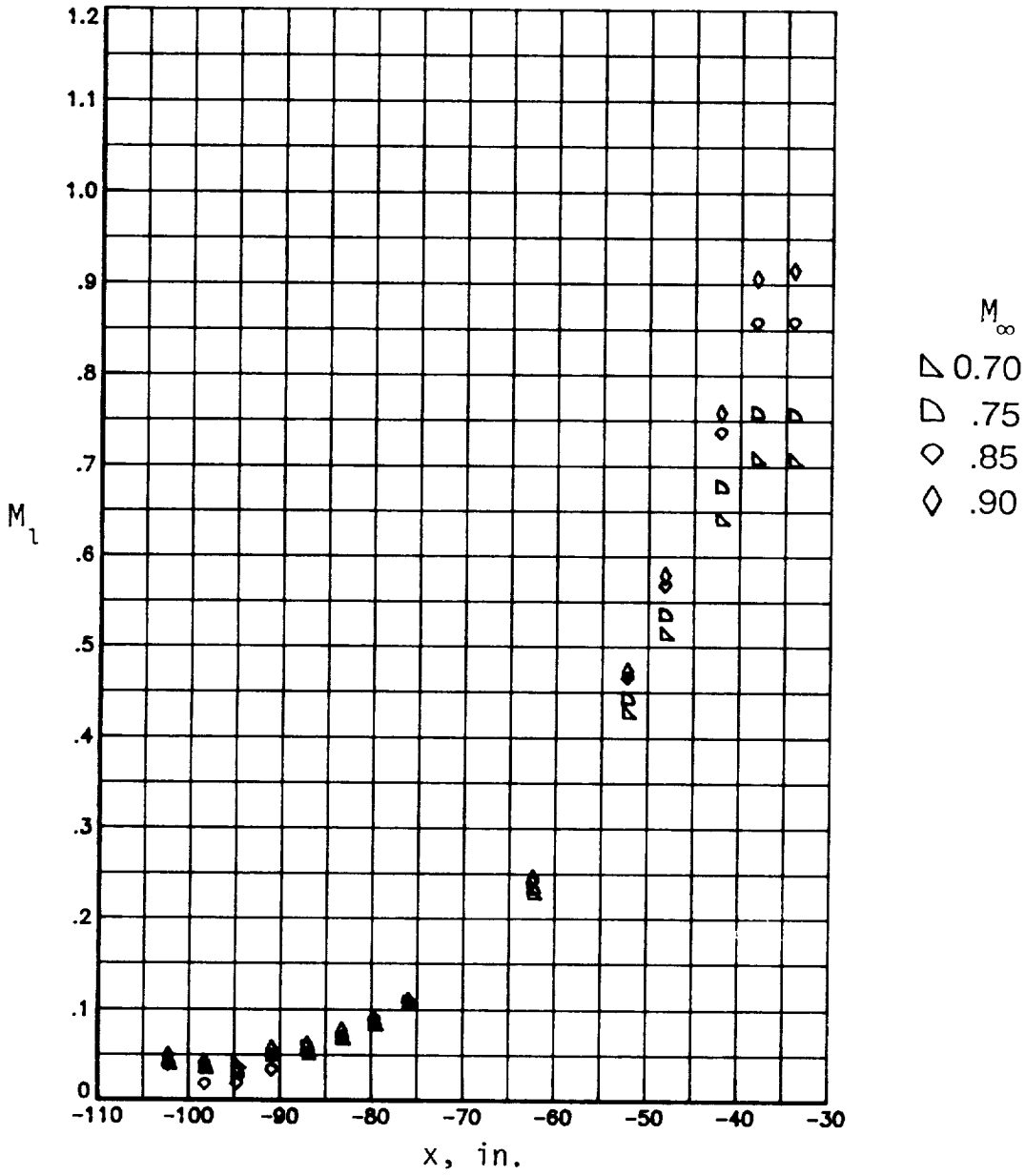

(f) $R = 100 \times 10^6$ per foot.

Figure 26. Concluded.

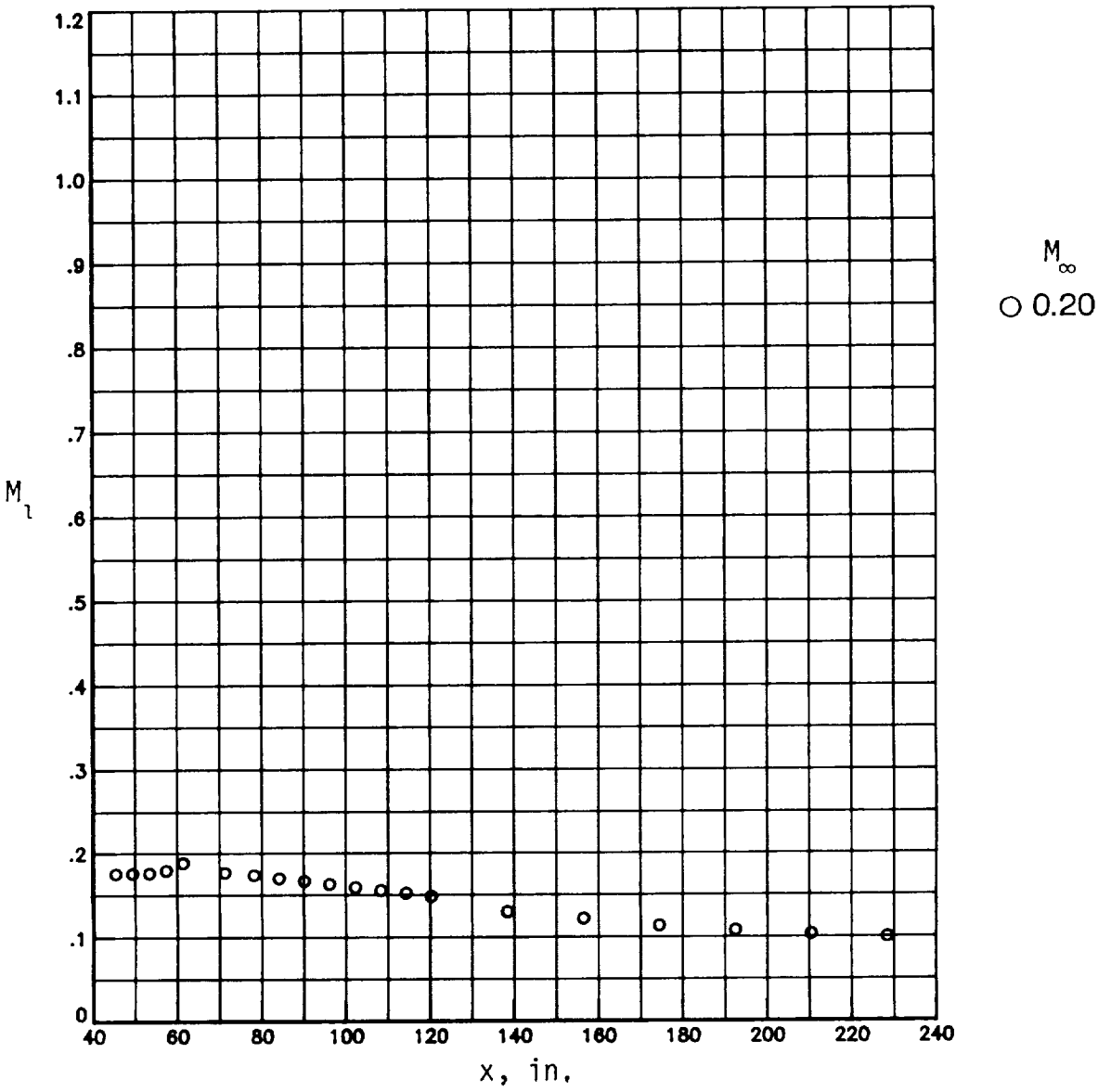

(a) $R = 10 \times 10^6$ per foot.

Figure 27. Local Mach number distributions in high-speed diffuser.

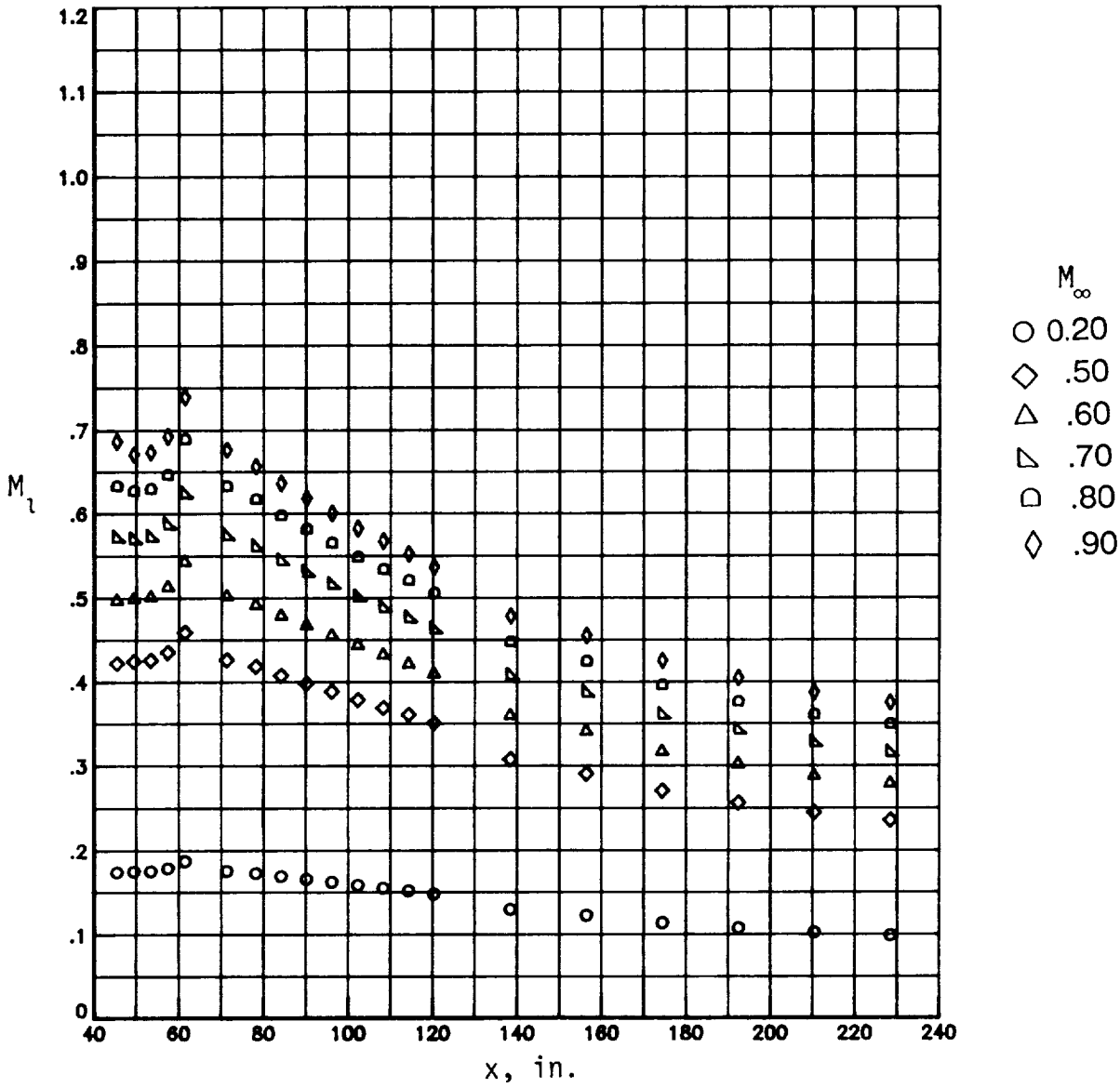

(b) $R = 20 \times 10^6$ per foot.

Figure 27. Continued.

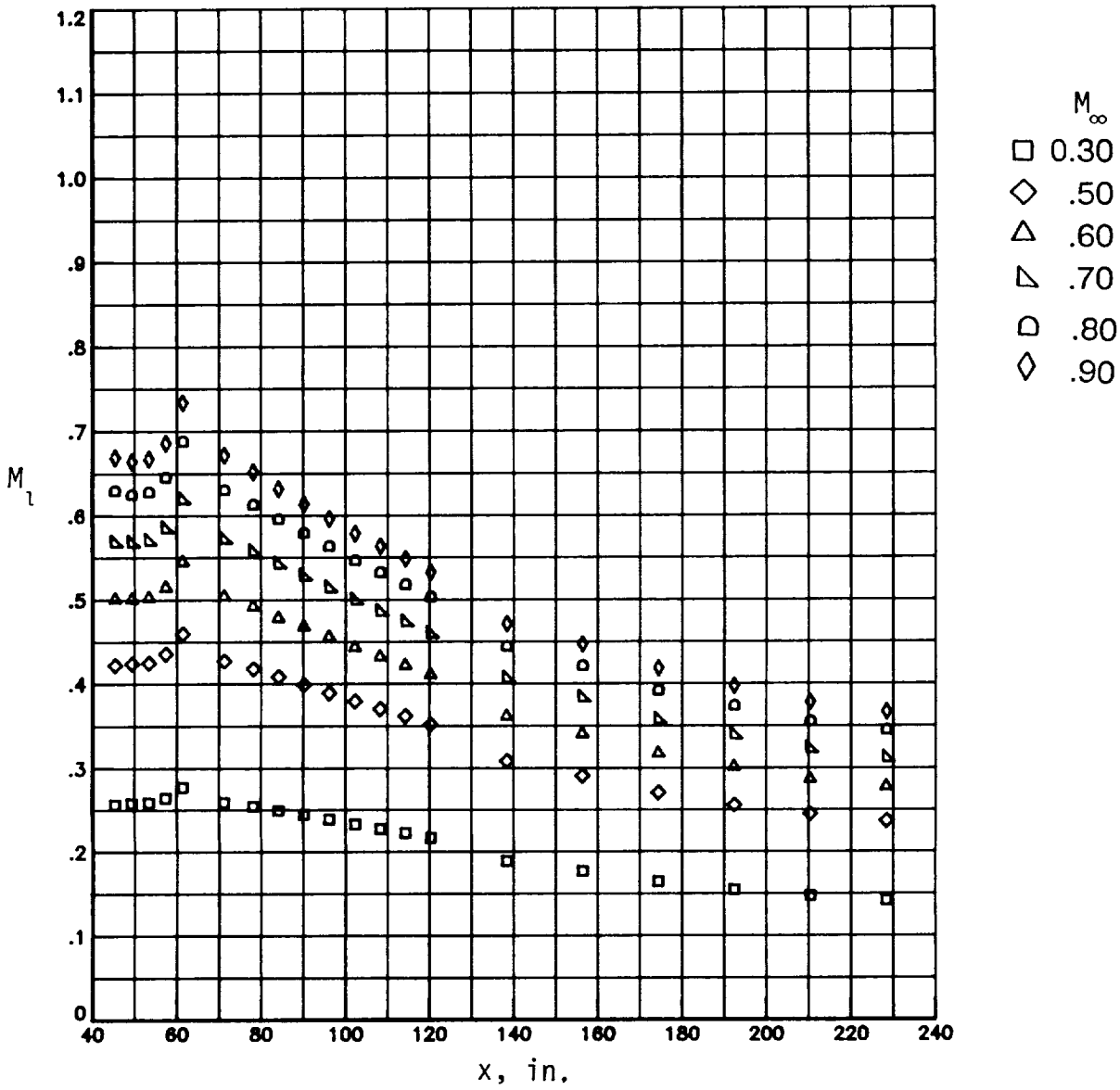

(c) $R = 40 \times 10^6$ per foot.

Figure 27. Continued.

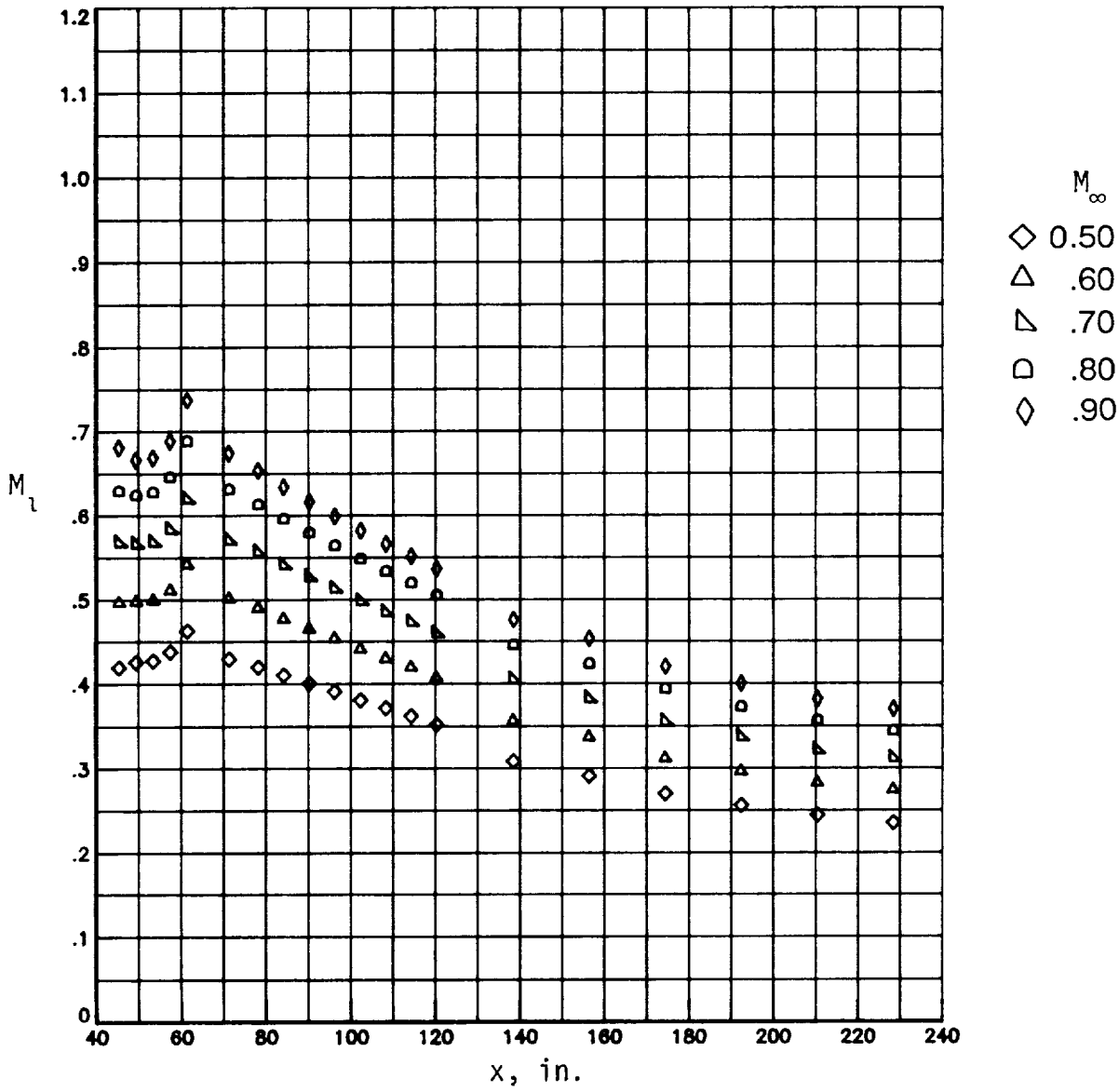

(d) $R = 60 \times 10^6$ per foot.

Figure 27. Continued.

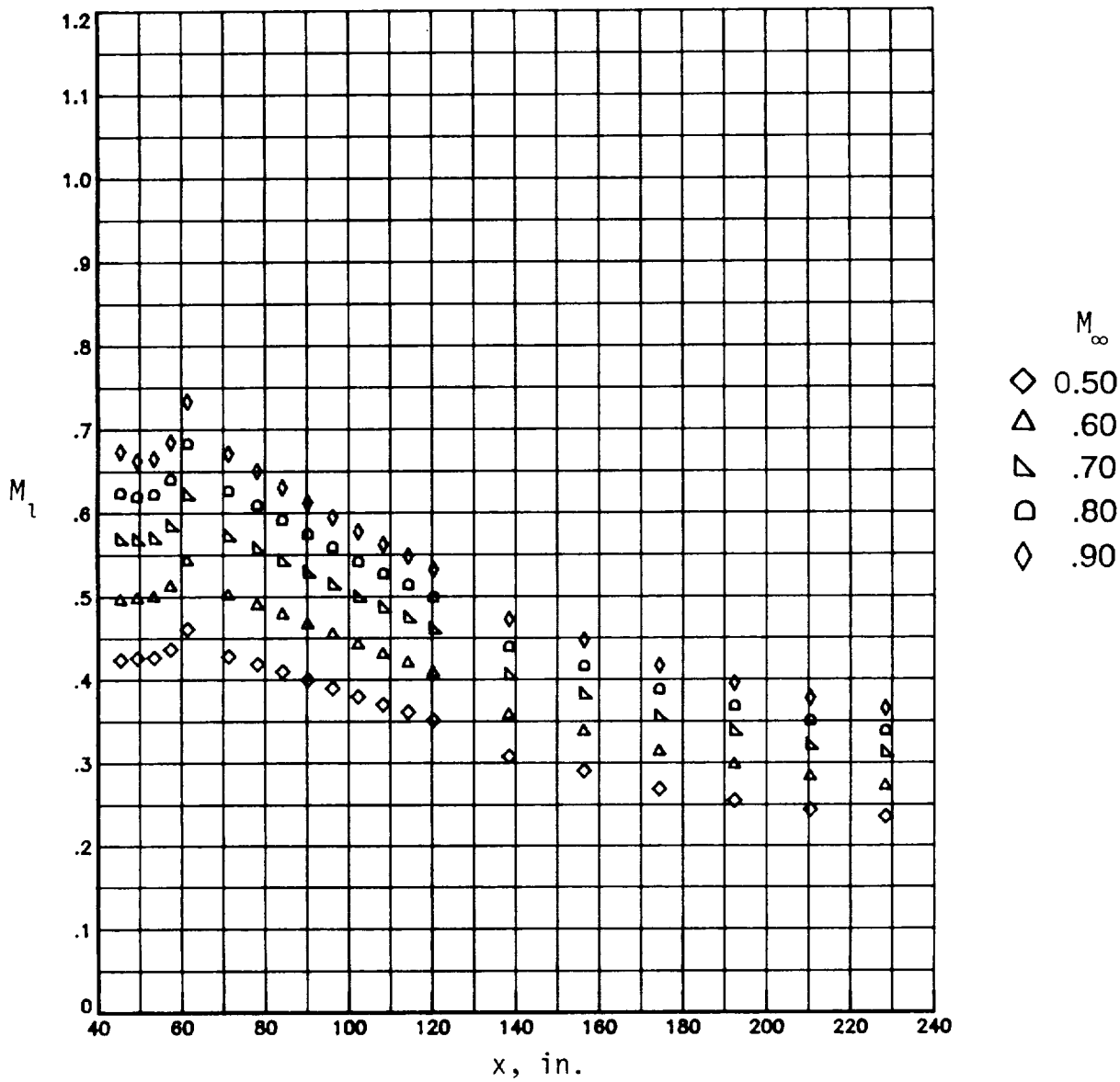

(e) $R = 80 \times 10^6$ per foot.

Figure 27. Continued.

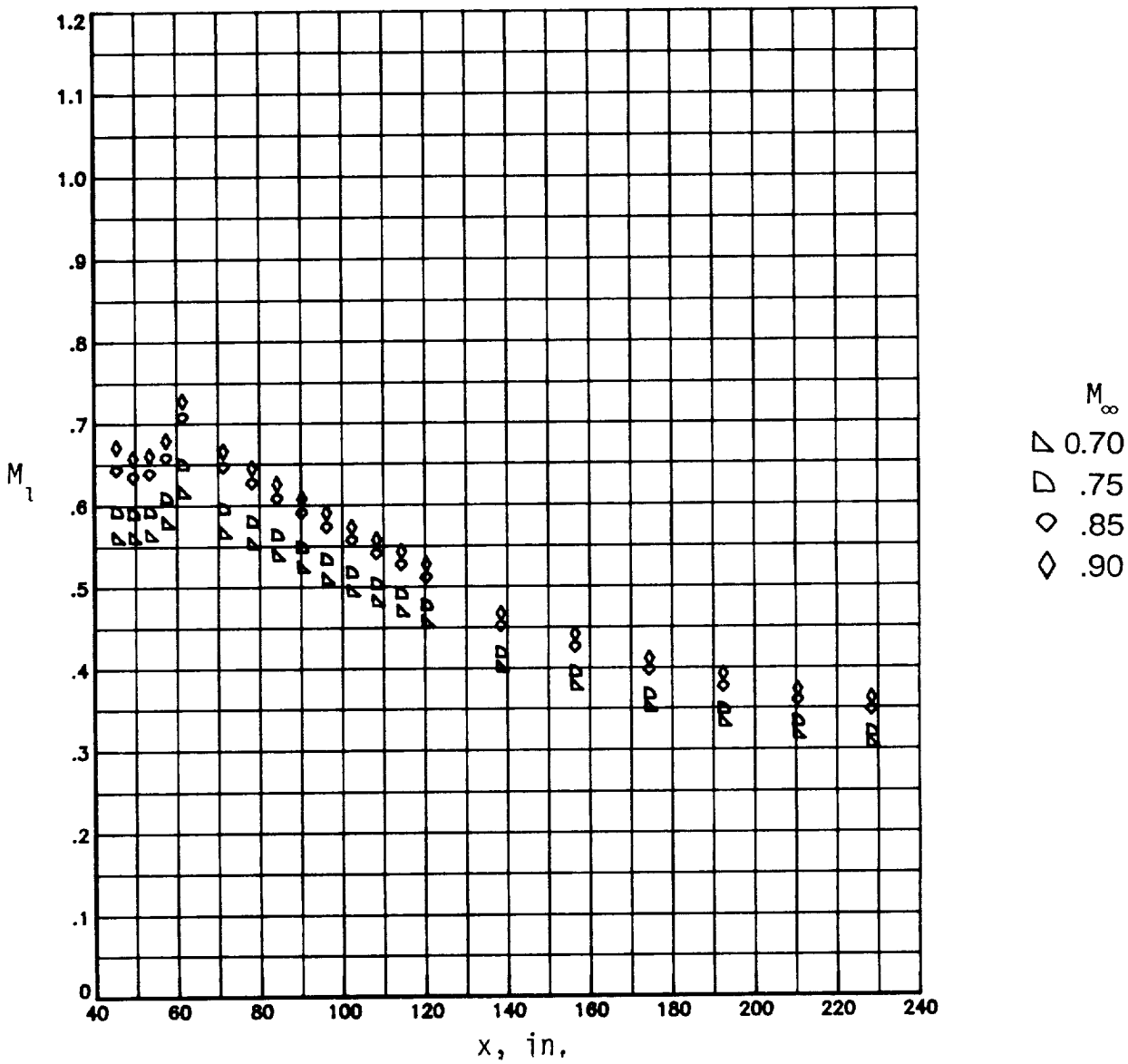

(f) $R = 100 \times 10^6$ per foot.

Figure 27. Concluded.

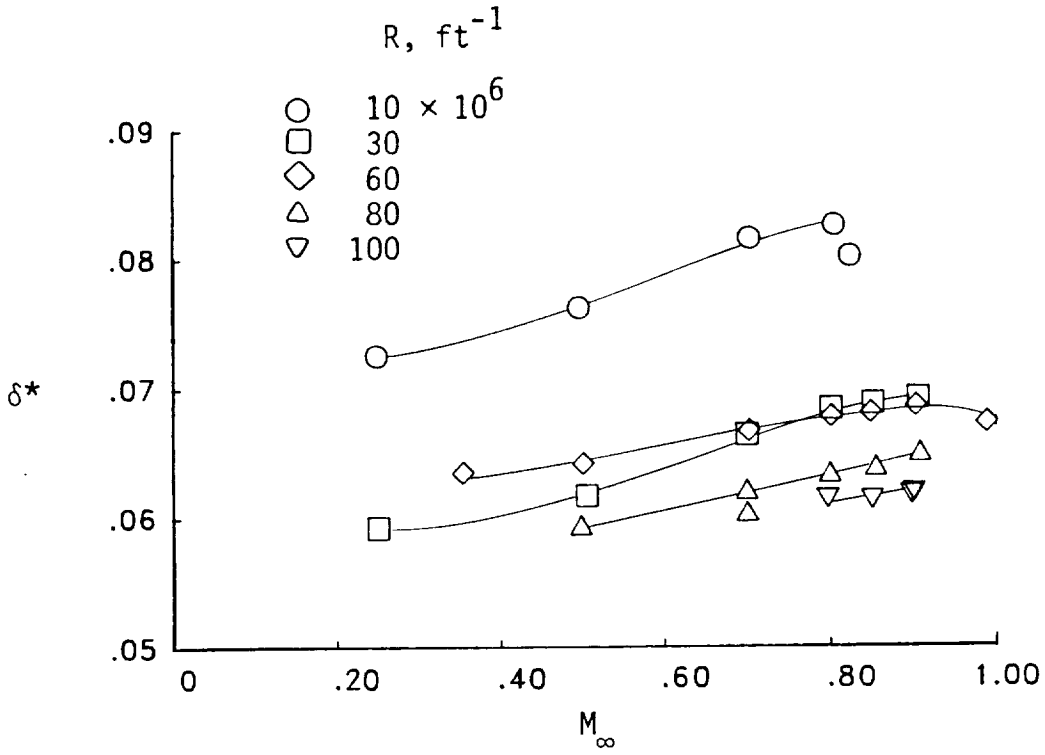

(a) Displacement thickness.

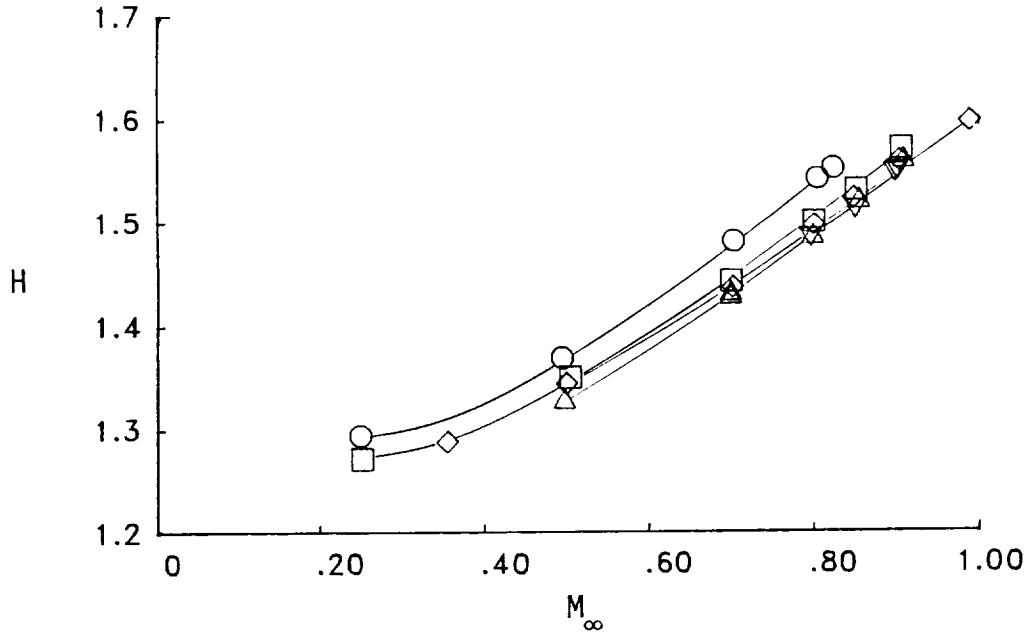

(b) Shape factor.

Figure 28. Sidewall boundary-layer characteristics at station −1.25 on right sidewall.

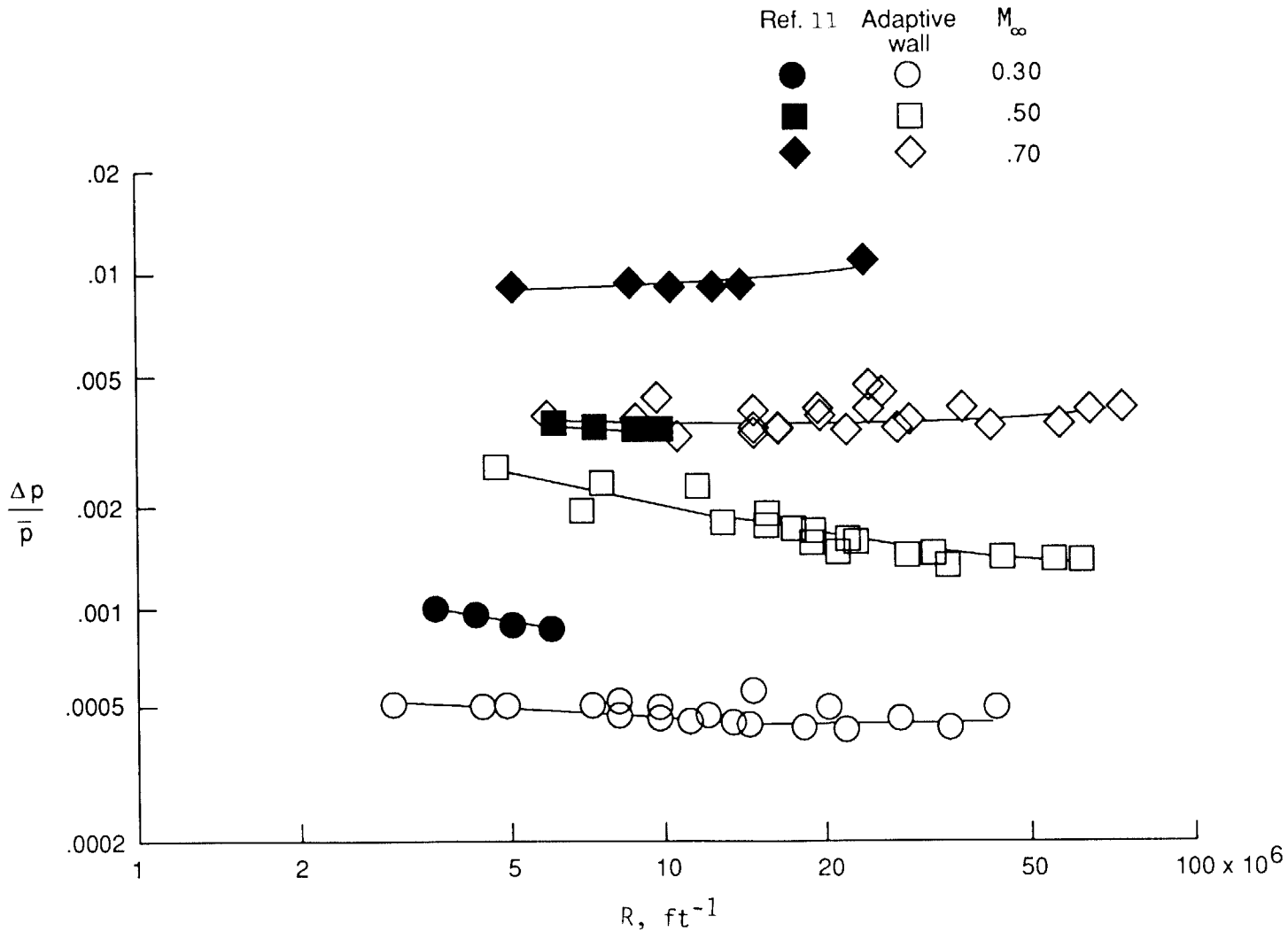

Figure 29. Comparison of sidewall fluctuating pressures in slotted test section (ref. 11) and in adaptive wall test section.

NASA
National Aeronautics and Space Administration

Report Documentation Page

1. Report No.	2. Government Accession No.	3. Recipient's Catalog No.
NASA TP-3049		

4. Title and Subtitle	5. Report Date
Calibration of the 13- by 13-Inch Adaptive Wall Test Section for the Langley 0.3-Meter Transonic Cryogenic Tunnel	December 1990
	6. Performing Organization Code
7. Author(s)	8. Performing Organization Report No.
Raymond E. Mineck and Acquilla S. Hill	L-16787
9. Performing Organization Name and Address	10. Work Unit No.
NASA Langley Research Center Hampton, VA 23665-5225	505-61-21-03
	11. Contract or Grant No.
12. Sponsoring Agency Name and Address	13. Type of Report and Period Covered
National Aeronautics and Space Administration Washington, DC 20546-0001	Technical Paper
	14. Sponsoring Agency Code

15. Supplementary Notes

16. Abstract

A 13- by 13-in. adaptive solid-wall test section has been installed in the circuit of the Langley 0.3-Meter Transonic Cryogenic Tunnel. This new test section is configured for two-dimensional airfoil testing. The top and bottom walls are flexible and movable, whereas the sidewalls are rigid and fixed. The wall adaptation strategy employed requires the test section wall shapes associated with nearly uniform test section Mach number distributions. Calibration tests with the test section empty were conducted with the top and bottom walls linearly diverged to approach a nearly uniform Mach number distribution. Pressure distributions were measured in the contraction section, the test section, and the high-speed diffuser at Mach numbers from 0.20 to 0.95 and Reynolds numbers from 10×10^6 to 100×10^6 per foot.

17. Key Words (Suggested by Authors(s))

Cryogenic tunnels
Two-dimensional test sections
Adaptive wall test sections
Wind-tunnel calibration

18. Distribution Statement

Unclassified—Unlimited

Subject Category 09

19. Security Classif. (of this report)	20. Security Classif. (of this page)	21. No. of Pages	22. Price
Unclassified	Unclassified	109	A06